Physical forces and mechanical waves during tissue growth

Xavier Serra Picamal

Tesi doctoral

Physical forces and mechanical waves during tissue growth

Memòria presentada per

Xavier Serra Picamal

Per optar al grau de Doctor

Barcelona, gener de 2013

Treball dirigit pel Dr. Xavier Trepat i Guixer

Tesi doctoral

Physical forces and mechanical waves during tissue growth

Memòria presentada per

Xavier Serra Picamal

Per optar al grau de Doctor

Barcelona, gener de 2013

–

El Dr. Xavier Trepat i Guixer, del Departament de Ciències Fisiològiques I de la Universitat de Barcelona

CERTIFICA

Que aquest treball, titulat "Physical forces and mechanical waves during tissue growth", presentat per Xavier Serra Picamal per optar al grau de Doctor en Biomedicina, ha estat realitzat sota la seva direcció

Dr. Xavier Trepat i Guixer

Professor associat
Departament de Ciències Fisiològiques I
Universitat de Barcelona

Group leader / ICREA Research Professor
Integrative cell and tissue dynamics
Institut de Bioenginyeria de Catalunya (IBEC)

Barcelona, gener de 2013

UNIVERSITAT DE BARCELONA

Unitat de Biofísica i Bioenginyeria
Departament de Ciències Fisiològiques I
Facultat de Medicina
Casanova 143
08036 Barcelona. Spain
Tel. (34) 93 402 0265

INFORME DEL DIRECTOR

A qui correspongui,

Els articles presentats pel doctorand Xavier Serra Picamal en la tesi doctoral "Physical forces and mechanical waves during tissue growth" en el format de tesi com a compendi de publicacions han estat publicats a les revistes ***Nature Materials*** i ***Nature Physics***. Els factors d'impacte de cadascuna d'elles de l'any 2011 es mostren a continuació:

	Factor d'impacte[1]
Nature Materials	32.842
Nature Physics	18.967

Nature Materials és la revista amb el factor d'impacte més elevat en l'àmbit de la física aplicada (1a sobre 125 revistes en el camp) i *Nature Physics* la tercera revista amb el factor d'impacte més elevat en l'àmbit de la física multidisciplinar (3a sobre 84).

En el primer article[2], el doctorand va mesurar les forces de tracció i esforços en cèl·lules epitelials, va quantificar l'alçada de les cèl·lules (Suplement 4 de l'article) i va estudiar la morfologia de les cèl·lules a alta resolució durant la migració cel·lular col·lectiva (Suplement 7 de l'article). En el segon article[3], el doctorand va dissenyar i realitzar tots els experiments de l'estudi, va analitzar les dades, i va participar en la discussió i interpretació dels resultats i la redacció de l'article. En cap cas cap dels altres coautors dels articles ha utilitzat els treballs per a la realització d'una tesi doctoral.

A Barcelona, 13 de Gener de 2013,

Xavier Trepat Guixer, Director de la tesi doctoral

---

[1] Segons el document "*2011 Journal Citation Report*", Science Edition (Thomson Reuters, 2012) .
[2] *Collective cell guidance by cooperative intercellular forces.* Tambe DT, Hardin CC, Angelini TE, Rajendran K, Park CY, Serra-Picamal X, Zhou EH, Zaman MH, Butler JP, Weitz DA, Fredberg JJ & Trepat X. **Nature Materials** 10, 469-475 (2011).
[3] *Mechanical waves during tissue expansion.* Serra-Picamal X, Conte V, Vincent R, Anon E, Tambe DT, Bazallieres E, Butler JP, Fredberg JJ & Trepat X. **Nature Physics** 8, 628-634 (2012).

Agraïments

Aquesta tesi ha estat possible gràcies al suport de moltes persones que m'han ajudat professionalment, intel·lectualment i personalment, al llarg d'aquests quatre anys. A tots ells, el meu agraïment més sincer, i en particular a:

en Xavi, el meu director de tesi, per l'entusiasme, l'esforç i la confiança que sempre transmet.

en Daniel Navajas i en Ramon Farré, de la Unitat de Biofísica i Bioenginyeria.

en Jeff Fredberg, de la Harvard School of Public Health.

tots els membres del laboratori de l'IBEC, i molt especialment a l'Ester, l'Agustí, la Laura, la Marina, en Simon, l'Elsa, en Romaric i en Vito, per les estones passades, algunes divertides i d'altres sacrificades, durant el temps que hem treballat junts.

en Raimon, l'Alba, la Irene i en Tomàs, per l'ajuda al laboratori de la UBB.

en Peter Yingxiao Wang i en Wagner, per haver-me acollit i ensenyat durant l'estada al laboratori de Molecular Engineering and Live Cell Imaging a la Universitat d'Illinois a Urbana-Champaign.

...

... als meus pares, en Manel i la Rosa Maria, a l'Anna, a l'àvia Marina

i a la Marina,

de qui tant aprenc, i a qui dedico aquesta tesi.

Nothing in life is to be feared, it is only to be understood. Now is the time to understand more, so that we may fear less

Marie Skłodowska-Curie

But nature is always more subtle, more intricate, more elegant than what we are able to imagine

Carl Sagan

Index

Chapter 1 Introduction

1.1 Cellular biomechanics

Eukaryotic cells are the building blocks of higher organisms. They are formed by a variety of organelles and structures that self-assemble to permit proper cell function. Whether isolated or as a part of a multicellular tissue, cell survival is based on the ability to integrate and respond to environmental pressures, including different forms of forces (compression, tension, hydrostatic pressure…) and other mechanical inputs. There is clear evidence that forces and mechanics are involved and eventually regulate important processes such as cell proliferation, division, adhesion and migration (Vogel and Sheetz, 2006; DuFort et al., 2011; Fink et al., 2011). Perhaps the most clear evidence of this is the observation that stem cells can be directed to specific cell fates depending on the mechanical properties of the substrate on which they are grown (Engler et al., 2006). Consequently, studying cells from a mechanical point of view has emerged as a promising field to understand such processes. In this section I will first describe the structural determinants of the mechanical properties of the cell (cytoskeleton) and the structures used to provide contact to their environment (cell junctions). I will later focus on the process by which cells sense and respond to mechanical cues, and finally I will describe the main methods used to study mechanical properties of adherent cells.

1.1.1 Overview of the cytoskeleton

The cytoskeleton provides structural support to the cell, establishing and maintaining its shape. It is fundamental in key cellular processes such as cell division, migration, and intracellular transport of organelles, and consists of three different types of filaments: actin filaments, microtubules, and intermediate filaments.

Actin filaments

Actin filaments (or microfilaments) are two-stranded helical fibers formed by polymerization of monomeric globular actin (G-actin). They are flexible structures, of about 6 nm in diameter and up to several micrometers in length (Figure 1.1). Microfilaments have a polar configuration, due to the fact that all the G-actin monomers that form the microfilament have the same orientation. This polarity creates a different growth rate in the two ends of the filament, with the plus end (or barbed end) with higher polymerization rates than the minus end (or pointed end). Actin

filaments maintain a steady-state length by releasing monomers from the minus end at the same rate as new monomers are added at the plus end. Actin filaments are organized either into bundles or networks. Bundles are parallel arrays of actin filaments, whereas networks are formed by crosslinking of actin filaments in orthogonal arrays that form three-dimensional meshworks. The formation of bundles or networks depends on actin cross-linking proteins, which have two actin-binding sites allowing them to crosslink the actin filaments. Depending on the properties of the crosslinking protein, networks or bundles are formed.

Several intracellular structures with different functions are formed by microfilaments. At the cell periphery, microfilaments associate to the plasma membrane and provide structural support to the cell, determining its shape. At the cell basal domain, thick contractile bundles of approximately 10-30 actin filaments are integrated to give rise to stress fibers (Pellegrin and Mellor, 2007). These structures connect either two focal adhesions of the same cell or of two adjacent cells (Follonier et al., 2008), thereby providing mechanical coupling between them, and play an important role for cell contraction. Protrusions at the cell surface are also based on actin filaments, and some of them such as lamellipodia and filopodia are particularly relevant for cell migration. Lamellipodia are broad, sheet like projections of the membrane at the leading edge of the migrating cell. They are formed by ARP2/3 mediated actin branching, which pushes the cell membrane forward (Pollard and Borisy, 2003). Filopodia are thin projections of the plasma membrane, composed of a bundle of actin filaments, that senses the extracellular environment and plays a prominent role in cell guidance (Nemethova et al., 2008).

Actin is highly important for force generation during cell adhesion, spreading, or migration. Force can be generated by two mechanisms: either by simple polymerization (as in the lamellipodia) or through coupling to the motor protein myosin (as in stress fibers). In this latter case, anti-parallel overlapping filaments are bound by myosin, which mediates actin fibers sliding relative to one another in an ATP-dependent manner (Alberts, 2002; Carey et al., 2011).

Microtubules

Microtubules are long, stiff, and hollow cylinders of 25 nm diameter, made of tubulin (Figure 1.1). Each tubulin subunit is an heterodimer formed by α- and β-tubulin, which are bound by noncovalent bonds. Many adjacent subunits with the same orientation form a protofilament, and 13 parallel protofilaments associate laterally to form a microtubule (Alberts, 2002). In contrast to actin filaments, which nucleate usually at the plasma membrane, microtubule nucleation occurs primarily at the center of the cell, in structures known as microtubule-organizing centers (MTOCs). In eukaryotic cells, there is often a single MTOC, called the centrosome, located near the nucleus. Microtubules emanate from there in an astral conformation, being a component of the mitotic spindle that segregates the chromosomes and orients the cleavage plane during cell division (Desai and Mitchison, 1997). Additionally, MTOCs can be found at the base of eukaryotic cells with a cilium or flagellum (such as trachea or sperm cells respectively), in which case the MTOCs are called basal bodies. Microtubules that originate in these structures give structural support to cilia and flagella. The movement

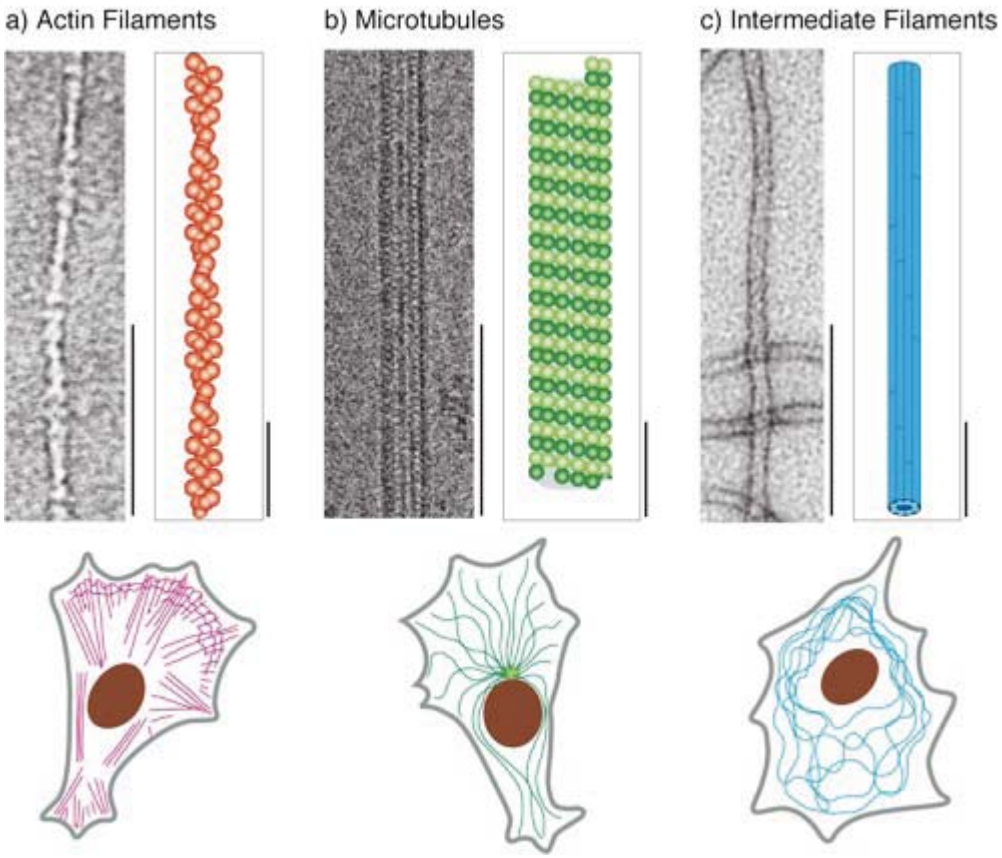

Figure 1.1. Major components of the cytoskeleton. Electron microscopy image (left), structure (right), and distribution in the cell (bottom) of actin filaments, microtubules and intermediate filaments. Electron microscopy scale bars = 100 nm;Structure scale bars = 25 nm. Adapted from (Alberts, 2002).

of these structures is achieved by the sliding of microtubule doublets relative to one another, powered by the motor activity of dynein.

Intermediate filaments

Intermediate filaments are ropelike fibers with an approximate diameter of 10 nm. Their basic structure consists on coiled-coil dimers that associate with a second dimer in an antiparallel fashion to form tetramers. Equivalently to actin or tubulin subunits of microfilaments or microtubules (Alberts, 2002), these tetramers pack together to form the filament (Figure 1.1). Interestingly, there is not a single peptide that generates the tetramers. Instead, different families of proteins, encoded by more than 60 different genes, give rise to different intermediate filaments (Herrmann et al., 2007). Some examples are keratins (present in epithelial cells), vimentin (present in mesenchymal cells), or lamins (located at the interior part of the nuclear envelope). Due to their rope-like structure, they have the capability to bend easily, but they are difficult to break. It has been demonstrated that single fibers can bear huge deformations, achieving up to 3.6-fold increase in length when laterally displaced by an Atomic Force Microscopy tip (Kreplak et al., 2005). These results have been complemented with experiments performed on stretched tissues that also demonstrated that the intermediate filament network in keratinocytes can survive with little or no damage to uniaxial strains up to 100 % (Fudge et al., 2008).

1.1.2 Cell adhesion

In multicellular organisms, cells need to interact with different kind of structures and environments to perform their function. Inside connective tissue, for instance, cells such as fibroblast are sparsely distributed and attach mainly to the extracellular matrix, but do not establish direct attachments with other cells. In epithelial tissues, however, on top of attaching to the basal extracellular matrix, cells also tightly bind together, forming sheets that act as a controlled barrier between the external environment and the organ they are covering. The specialized structures that cells use to attach to their environment are called cell adhesions. Two types of cell adhesions can be distinguished: those that link cells to the extracellular matrix and those that link cells together (Figure 1.2).

Cell adhesion to the extracellular matrix

Cells attach to the extracellular matrix through two types of junctions: focal adhesions and hemidesmosomes. Both types have in common the presence of integrins, a family of hetero-dimeric transmembrane proteins formed by different types of α and β subunits. The extracellular domain of integrins contains a ligand-binding region to different types of extracellular matrix ligands, and the intracellular domain interacts with the cytoskeleton and signaling effectors (Luo et al., 2007; Campbell and Humphries, 2011). Focal adhesions link the extracellular matrix to the actin cytoskeleton, whereas hemidesmosomes establish the link to intermediate filaments (mainly keratin) (Lodish et al., 2007).

In focal adhesions, integrins cluster and associate to actin filaments through the β subunit and a large number of adapter proteins (Lodish et al., 2007) such as Focal Adhesion Kinase (FAK), paxillin, vinculin or talin. Focal adhesions assemble into oval structures and provide the anchoring points for the actin filaments, which generate the cellular forces required for attachment, spreading, or migration. These forces are transmitted to the substrate and are commonly known as traction forces. Integrins integrate and transmit mechanochemical information about the extracellular composition via outside-in signaling, which is important for cell migration or spreading. Moreover, intracellular signals induce changes in integrin conformation and attachment to the extracellular matrix, via inside-out signaling (Arnaout et al., 2005). These signaling mechanisms permit focal adhesions to adapt to their specific extracellular environment. Indeed, it has been shown that focal adhesions are larger and more stable in stiff substrates (Pelham and Wang, 1997; Engler et al., 2004), and that external mechanical forces induce the assembly of focal adhesions by mediation of the small GTPase protein Rho (Riveline et al., 2001).

Cell-cell adhesion

Cells within tissues connect to the neighboring cells by multiprotein complexes to maintain tissue integrity and to migrate as a cohesive group when needed. There are four main types of cell-cell adhesions complexes: tight junctions, adherens junctions, desmosomes, and gap junctions. The first three types of junctions provide structural support and allow mechanical coupling between cells, while gap junctions are

transmembrane channels that connect the cytoplasm of adjacent cells, homogenizing biochemical conditions in communicating cells.

Tight junctions are the most apical cell-cell junctions. They act as a barrier preventing the transit of molecules and ions between cells and also to impede the diffusion of membrane proteins between the apical and the basolateral surface of the cell. They are formed by a network of a long row of transmembrane adhesion proteins (mainly occludin and claudin) that interact in the extracellular space. In their intracellular compartment, they interact with scaffolding proteins that link them to the actin cytoskeleton.

Adherens junctions and desmosomes are the cell-cell junctions' elements that provide mechanical coupling between cells. Analogously to integrins in focal adhesions and hemidesmosomes, proteins from the cadherin family form adherens junctions (connecting to actin cytoskeleton) and desmosomes (connecting to intermediate filaments). Cadherins are a large family of transmembrane adhesion proteins that interact in a calcium-dependent manner to form homodimers (Green et al., 2010). E-cadherin (present on epithelial cells), N-cadherin (on nerve cells) or P-cadherin (on placenta cells or epidermis) are some of its members. Cadherin linkage to the cytoskeleton depends on accessory proteins: in adherens junctions, proteins of the catenin family (such as α-catenin, β-catenin or p120-catenin) mediate the interaction to

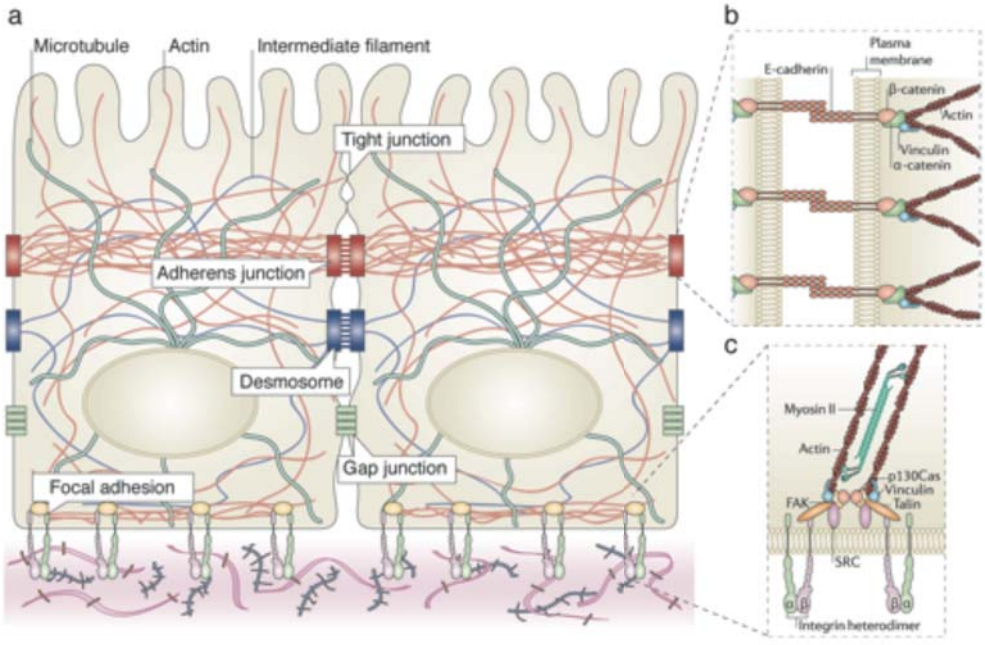

Figure 1.2. Cell-cell junctions. (a) Distribution of the main cell-cell junctions and the cell cytoskeleton in epithelial cells. **(b)** Adherens junctions and **(c)** focal adhesion structure. Adapted from (DuFort et al., 2011).

actin cytoskeleton (Drees et al., 2005; Yamada et al., 2005). In desmosomes, plakoglobin, plakophilin or desmoplakin mediate the interaction to intermediate filaments (Bass-Zubek et al., 2009). In epithelia, adherens junctions give rise to a continuous adhesion belt, with actin bundles forming a transcellular network that embraces many cells. This network is fundamental in order to coordinate collective morphogenetic processes such as epithelial folding into tubes or vesicles (Martin et al., 2010).

1.1.3 Mechanotransduction

As mentioned earlier, the mechanical environment in which the cells are located has direct impact on their function. The process by which cells translate mechanical stimuli into biochemical signals is known as mechanotransduction, and it modulates fundamental cell functions such as proliferation, migration, differentiation, or apoptosis (DuFort et al., 2011). Mechanotransduction can be divided in two different phases: reception of mechanical signals, or *mechanoreception*, and cellular response to these mechanical signals, or *mechanoresponse*.

Mechanoreception

Mechanoreceptors are usually located at the cell membrane or in its adjacent structures, where they integrate the extracellular mechanical signals and transmit them from the outside of the cell to the inside. The mechanisms by which a force can be sensed by the cell include exposure of cryptic peptide sequences upon mechanical force, stretch-sensitive ion channels, and receptor-ligand interactions that strengthen if strained (Figure 1.3) (Vogel and Sheetz, 2006).

Mechanoreceptors can be found in integrin-based focal adhesion complexes, which act as mechanical sensors between the extracellular matrix and the cell cytoskeleton. At a molecular level, stretching a single molecule of talin, for example, has been shown to expose vinculin binding sites (del Rio et al., 2009). Cell-cell junctions also have the capability to probe the mechanical state of the neighboring cells. In particular, it has been demonstrated that the adherens junction complex has the capability to act as a mechanosensor that can probe the mechanical state of the adjacent cells and induce a proportional change in the mechanics of the cell-cell junction (le Duc et al., 2010). This has been shown by allowing E-cadherin coated magnetic beads to adhere to cell surface

and applying an oscillatory magnetic field to twist the beads, thereby applying forces at the sites of adhesion. The authors observed an increase in stiffness in the adhesion site when applying a shear stress, which did not occur when E-cadherin adhesion was blocked using an E-cadherin antibody or when the mechanical link to the actin cytoskeleton was disrupted using latrunculin B or cycochalasin D (actin polymerization inhibitors), or blebbistatin (myosin II inhibitor) (le Duc et al., 2010). The molecular mechanisms by which adherens junctions act as mechanoreceptors are starting to be elucidated. It has been recently shown that α-catenin also exposes vinculin binding sites

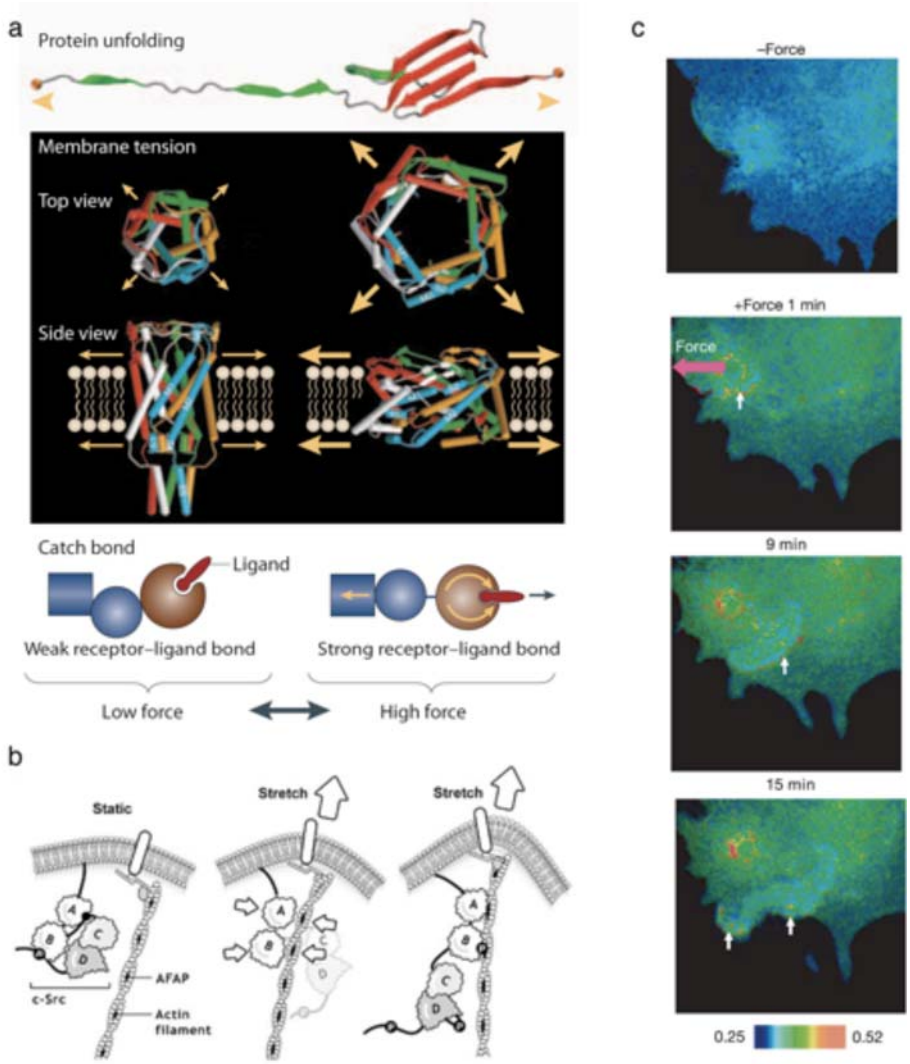

Figure 1.3. Mechanotransduction. (a) Mechanisms of force sensing. Top: Protein unfolding can result in a gain or loss of binding sites, increased separation between protein domains, or gain or loss of enzyme function. Middle: Membrane tension can induce opening of ion channels. Bottom: Forces can stabilize receptor–ligand bond interactions. Adapted from (Vogel and Sheetz, 2006). **(b)** Suggested model of mechanical-induced Src activation: Membrane stretch induces deformation of the cytoskeleton and a binding region of AFAP is presented to c-Src, which changes configuration and is activated. Adapted from (Han et al., 2004). **(c)** Mechanical stimulation induces a directional wave of Src activation away from the site of mechanical stimulation. Adapted from (Wang et al., 2005).

when cadherins are subject to tension, inducing junctional development (Yonemura et al., 2010). Other proteins and pathways are also thought to be involved in this process (Leckband et al., 2011).

Mechanoresponse

Ultimately, cells respond to the sensed mechanical signal by, for instance, migrating, differentiating, or dividing. The response can be driven by cell elements and pathways that need not to be different than the well-established biochemical pathways. Therefore, biochemical signaling cascades driven by phosphorylation, ions influx, induction of gene or protein expression, or reorganization of the cytoskeleton might be involved in the cellular response (Vogel and Sheetz, 2006).

Wang et al. (Wang et al., 2005) provided an illustrative example of the activation of a signaling cascade by mechanical stimuli. They used a Fluorescence Resonance Energy Transfer biosensor that reported the activation of the signaling tyrosine kinase protein Src, which was previously known to be activated upon mechanical stimulus, probably mediated by Actin-filament associated protein (AFAP) (Liu et al., 1996; Han et al., 2004). Pulling of fibronectin-coated beads attached to the cell surface using laser-tweezers, they observed a wave of Src activation that propagated along the plasma membrane (Figure 1.3).

1.1.4 Methods for studying cell mechanics of adherent cells

Several techniques have been developed in order to measure the mechanical properties of molecules, cells and tissues. These techniques require very high precision, since they need to resolve distances in the micrometer scale and, more importantly, forces as low as a few piconewtons. In this section, I will describe a particular subset of techniques used to measure the forces that cells apply on the substrate they are attached to, namely cell traction forces. These techniques include thin elastomeric membranes, microfabricated post array detectors, and traction microscopy.

Thin silicone membrane

The first description of the traction forces that isolated cells generated on the substrate was performed by Harris et al., (Harris et al., 1980; Harris et al., 1981) by culturing cells on thin polydimethyl siloxane (PDMS) membranes. As cells spreaded on the substrates, they pulled the rubber sheet centripetally, producing wrinkles (Figure 1.4) that could be easily observed under the microscope. Compressive forces in the nanonewton range have been measured using this method by considering the stiffness of the substratum and the extent of wrinkling (Burton et al., 1999). However, it is difficult to convert the pattern of wrinkles to maps of traction forces (Beningo and Wang, 2002).

Microfabricated Post Array Detector

Quantitative sub-cellular traction force measurements have been possible by seeding cells on top of an array of microfabricated posts made on PDMS (Tan et al., 2003). A single cell embraces multiple posts, and each post acts as an independent force-sensing

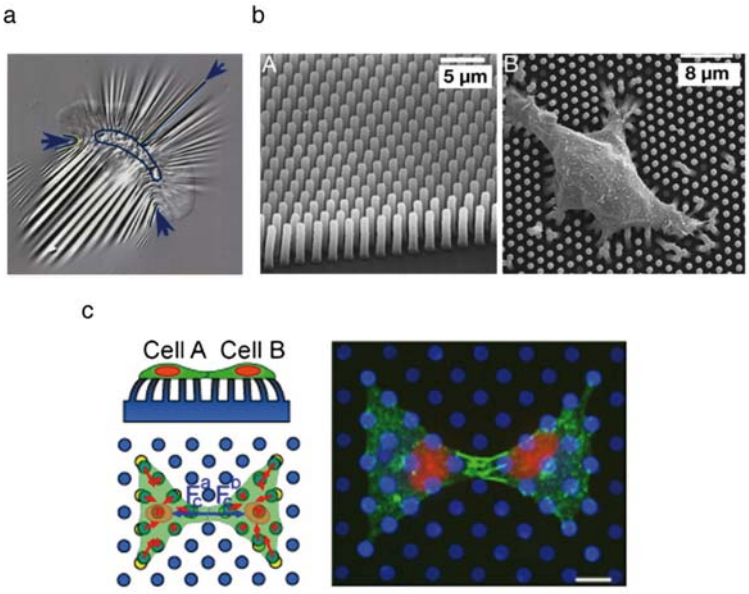

Figure 1.4. Thin silicone membrane and microfacticated post array detector for cell traction force quantification. (a) Fish keratinocyte migrating on a thin silicone sheet (Burton et al., 1999). **(b)** Scanning electron micrograph images of a PDMS post microarrray (left) and of an individual cell lying on it (right) (Du Roure et al., 2005). **(c)** Side view (top left) and top view (bottom left) for the measurement method of traction forces and intercellular tugging force in a pair of contacting cells by a microfabricated post array. The net force includes both traction forces (red arrows) and the intercellular tugging force (blue arrows). Immunofluorescence (right) of contacting cells constrained in a bowtie pattern by microcontact printing of fibronectin (cyan) and forming strong cell-cell adherens junctions (ß-catenin, green) (Liu et al., 2010).

unit of the traction forces exerted by the cell (Figure 1.4). The deflection of each post is measured with an optical microscope, and the traction forces are calculated by multiplying the spring constant of the post by the distance between the deflected and the theoretical relaxed position of each post. In order to obtain a good spatial resolution, dense arrays of micropillars (2 μm center-to-center spacing in between 1 μm diameter pillars) have been used to measure traction forces on both single and groups of cells (Du Roure et al., 2005; Saez et al., 2010). Moreover, this approach allows the possibility to apply localized mechanical forces and examine the changes in traction force after force application. This has been achieved by embedding magnetic nano-wires inside the posts (Sniadecki et al., 2007) or by encapsulating magnetic particles into the pillars (le Digabel et al., 2011). On the other hand, this method has been adapted to quantitatively measure cell-cell forces (Liu et al., 2010) by seeding cell doublets and measuring the force imbalance precisely at cell-cell junctions (Figure 1.4): intercellular tugging force is equal in magnitude and opposite in direction to the measured net traction forces reported on the microneedle assay (Liu et al., 2010).

Traction Force Microscopy

Traction Force Microscopy (TFM) allows the measurement of cell traction forces in a continuum substrate. To do so, it is based on Newton's third law: the force that the cell is applying on the substrate is equal in magnitude and directed in opposite direction to the force that the substrate is applying to the cell. Since it is not possible to measure the forces directly, the cell tractions are obtained from the deformation that they produce on the substrate.

TFM involves three major steps. The first one consists on fabricating a soft, elastic substrate over which cells are cultured and that contains fluorescent markers. The second step requires a quantification of gel deformation due to the force generated by the cell. This is achieved by comparing two images of the fluorescent markers, one under force loading conditions ("Force Loaded" image, or FL, with the cells generating forces) and the other one with the gel relaxed ("Null Force" image, or NF), usually taken after trypsinizing the cells at the end of the experiment. The final step involves computing the actual traction forces from the measured deformation of the gel (Wang and Lin, 2007) (Figure 1.4). Since FL images at different time points can be acquired and compared independently to the NF image, TFM allows the dynamic study of the forces generated by the cells as they migrate or as they respond to a specific drug or stimulus.

Polyacrylamide gels are used as the standard substrate for traction microscopy experiments because they offer several advantages in comparison with other substrates (Kandow et al., 2007): they are elastic, their stiffness can be adjusted by changing the proportion of acrylamide and bis-acrylamide monomers (Young's Moduls can be tuned from 1.2 to 100 kPa), they are transparent, easy to prepare, and mechanically stable. Since they are inert, they need to be coated with a protein of the extra-cellular matrix (such as collagen), allowing the cells to attach. Polyacrylamide gels used for traction microscopy are usually around 100 μm in height (Kandow et al., 2007).

Several methods have been developed to determine the displacement field of the substrate due to the forces exerted by the cell. In a first approach, the displacement of each bead relative to its undisturbed position was computed (Dembo and Wang, 1999). Butler et al., used another approach, based on particle image velocimetry (PIV), consisting on comparing sub-regions (called interrogation windows) on the FL and the NF images and computing their cross-correlation (Butler et al., 2002). A different approach, developed by Yang et al. (Yang et al., 2006), identified the actual displacement of each bead by analyzing the elongation and rotation between pairs of beads between the two images. Sabass et al. (Sabass et al., 2008) implemented a new approach to achieve higher resolution of the displacement field by combining PIV with particle tracking velocimetry (PTV), which directly monitors the movement of each bead. The approach requires the use of fluorescent markers in two different colors. The displacement is obtained by comparing the FL and the NF images firstly with a standard PIV routine to coarsely determine gel deformation and, using this result, applying PTV to identify the displacement of each bead (Sabass et al., 2008; Wang and Li, 2010).

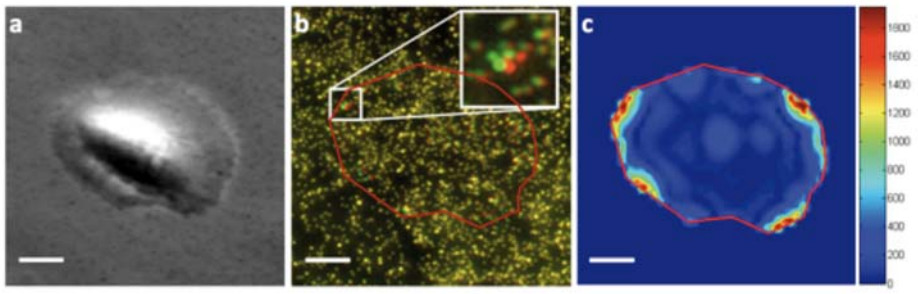

Figure 1.5. Traction Force Microscopy. (a) Phase contrast image of MCF-10A cell on top of a collagen-coated polyacrylamide gel. **(b)** Overlay of fluorescent markers images taken with (red, FL image) or without (green, NF image) the cell. Yellow color beads indicate no displacement between the two images. The magnified region shows a region were there is displacement of the fluorescent markers due to cell traction force. **(c)** Traction forces (in Pascal) exerted by the cell. Force direction is centripetal. Scale bar = 10 μm. From (Serra-Picamal and Trepat).

Determining traction forces from the estimated displacement field has been also tackled by different methods. Dembo and Wang (Dembo and Wang, 1999) developed the first approach to do so, by solving a regularized inverse problem. This method is computationally intensive. For this reason, Butler et al. (Butler et al., 2002) implemented a new approach by performing the computation of traction forces on the Fourier domain, which reduced the computation time. Finally, Yang et al. (Yang et al., 2006) used 3D finite element method (FEM), incorporating the effects of finite substrate thickness. In all the cases, the computed traction fields give information about the magnitude, the distribution and the direction of traction forces exerted by the adherent cell (Figure 1.5).

Since it was firstly developed (Dembo and Wang, 1999), several variants of traction force microscopy have been implemented in order to obtain the traction forces that cells exert in different conditions. Traction force microscopy was rapidly combined with cell micropatterning in order to quantify cell traction forces in physically constrained cells (Wang et al., 2002; Li et al., 2008). On the other hand, Das et al. (Das et al., 2008) used an ultrasoft PDMS as a cell substrate and integrated it in a microfluidic platform, allowing measurements of traction forces under flow conditions. A novel approach was also implemented by Polio et al. (Polio et al., 2012) by generating polyacrylamide gels with fluorescent 1 μm markers placed in a regularized array. Since the position of each marker is known in advance, its displacement can be easily computed without the need of removing the cells at the end of the experiment. All the methods described above have restricted the measurement of traction forces to two-dimensions, tangential to the substrate surface (Txy). However, several studies have also quantified cell traction forces in the vertical direction (Tz) by obtaining the displacement of the fluorescent markers in three dimensions (Hur et al., 2009; Maskarinec et al., 2009; Delanoë-Ayari et al., 2010), showing that vertical forces are of the same order of magnitude of the horizontal forces. Finally, traction force microscopy has also been used to determine the forces of cell colonies (Wang and Li, 2009). Li et al. (Li et al., 2009) confined fibroblast in cell islands and showed that, in multicellular groups, traction forces were located at the edges of the cell island. Traction force microscopy was also used in order to measure forces of large colonies of migrating epithelial cells (Trepat et al., 2009). In this case, a new algorithm was developed in order to take into consideration the polyacrylamide gel finite thickness.

1.2 Cell Migration

Cell migration is a central process in the formation and homeostasis of multicellular organisms. Tissue formation during embryonic development, wound healing, or the immune response, involves the precise and coordinated migration of cells to specific locations. Moreover, deregulated cell migration is also critical in pathological conditions: during metastasis, cancer cells migrate from the primary tumor to distant tissues, where they eventually generate secondary tumors. Two main categories of cell migration have been described: single cell migration, in which cells move individually, or collective cell migration, in which cells move as cohesive multicellular units.

1.2.1 Single cell migration

Single cell migration is the process by which isolated cells move through or along tissues in the body to a specific position. Two principal modes of single cell migration have been described. In the first mode, cells move via formation of blebbs, driven by protrusions of actin to the anterior part of the cell and supported by actomyosin contraction at the trailing edge. This mode does not require formation of focal adhesions or stress fibers, and is known as amoeboid migration. Some examples of cell migration driven by blebbing include leucocyte migration in three-dimensional environments (Lämmermann et al., 2008) or some forms of cancer cell invasion (Wolf et al., 2003).

The second mode of cell migration is known as mesenchymal migration, and is the most studied and prevalent mechanism. It is based on a cyclic process involving four steps, which include cell polarization and protrusion, adhesion, contraction and release at the cell rear (Figure 1.6). This cycle is repeated continuously as the cell migrates. The different steps can be precisely coordinated producing a smooth, persistent migration (as in keratinocytes), or much more discontinuous and give rise to a more disordered migration (as in fibroblasts). The four steps are separately described below.

1) Polarization and membrane protrusion.

Isolated cells move spontaneously or in response to external physical or chemical signals, which are transmitted and integrated via signaling cascades to the cell interior. In every case, cells must acquire a polarized configuration for proper migration,

defining a differentiated leading and trailing edge. The membrane at the leading edge is pushed forward by polymerization of actin filaments, either in lamellipodia or filopodia. In the case of lamellipodia, actin filaments polymerize forming a branched dendritic network, mediated principally by the Arp2/3 protein complex (Pollard et al., 2000). External signals result in the activation of the Arp2/3 complex near the plasma membrane, inducing its binding to a formed actin filament and providing a nucleation site for a new actin branch. Each new filament grows rapidly and pushes the membrane forward (Figure 1.7). The regulation of this process involves a set of different types of proteins, including 1) Monomer-binding proteins, such as profilin, which bind to actin momoners preventing self-nucleation and targeting monomers to the barbed end, 2) Capping proteins, which terminate filament elongation, controlling the localization of membrane protrusion and limiting the length of the growing branches, creating shorter and stiffer filaments and 3) proteins that assist disassembly of old filaments, such as cofilin, which maintain a pool of monomeric actin to be used at the growing filaments (Pollard et al., 2000; Pollard and Borisy, 2003; Ridley et al., 2003). It must be noted that the actual pushing of the membrane is believed not to occur by the elongation of the actin filament *per se* but by a mechanism described as the elastic Brownian ratchet model, in which the random bending of the actin filament provides space for actin monomers to squeeze in, and this generates an elastic energy that is stored in the bent filament which then pushes the membrane forward (Kaksonen et al., 2006). For

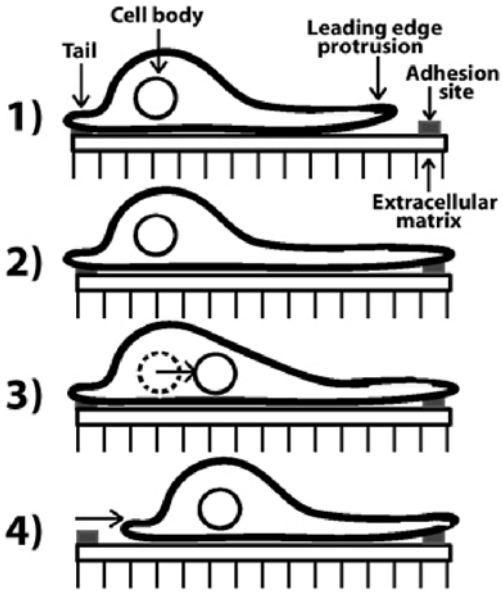

Figure 1.6. Four-step cycle in cell migration. The cycle begins with the protrusion of the leading edge driven by actin polymerization. The extended cell forms new attachments and then contracts against this attachment to break tail adhesions and translate forward. From (Mofrad and Kamm, 2006).

successful protrusion, newly polymerized actin filaments need to be linked to the cell-substrate adhesions, which immobilize the actin filaments. In the absence of these bonds, the newly assembled actin, with the action of myosin motors, drives the filament rearward, generating a retrograde flow at the leading edge. It is hypothesized that these links between the actin filaments and the extra-cellular matrix are locally variable and potentially regulatable. This suggests the idea that a local mechanism, described as a molecular clutch, allows a tunable balance between myosin or polymerization-driven retrograde flow (clutch disengaged) and leading edge protrusion (clutch engaged) (Chan and Odde, 2008; Giannone et al., 2009; Gardel et al., 2010).

Proteins of the Rho family of GTPases have a pivotal role in regulating actin dynamics and, as a consequence, they are key regulators of cell protrusion. They act as molecular switches, bound to GTP (guanosine triphosphate) in its activated state, and inactive when, by GTP hydrolysis, they are bound to GDP (guanosine diphosphate) (Ridley et al., 2003). Guanine nucleotide exchange factors (GEFs) control the release of GDP and its replacement by GTP, and GTPase-activating proteins (GAPs) control the ability of the GTPases to hydrolyze GTP to GDP. They integrate external signals and activate the Arp2/3 complex by a signaling cascade that involves proteins of the WASPs (Wiskott-Aldrich syndrome proteins) or WAVE (WASP family verprolin homologous) family. The most studied members of the Rho family are Rac1, Cdc42 and RhoA, which localize at the leading edge of migrating cells (Kraynov et al., 2000; Nalbant et al.,

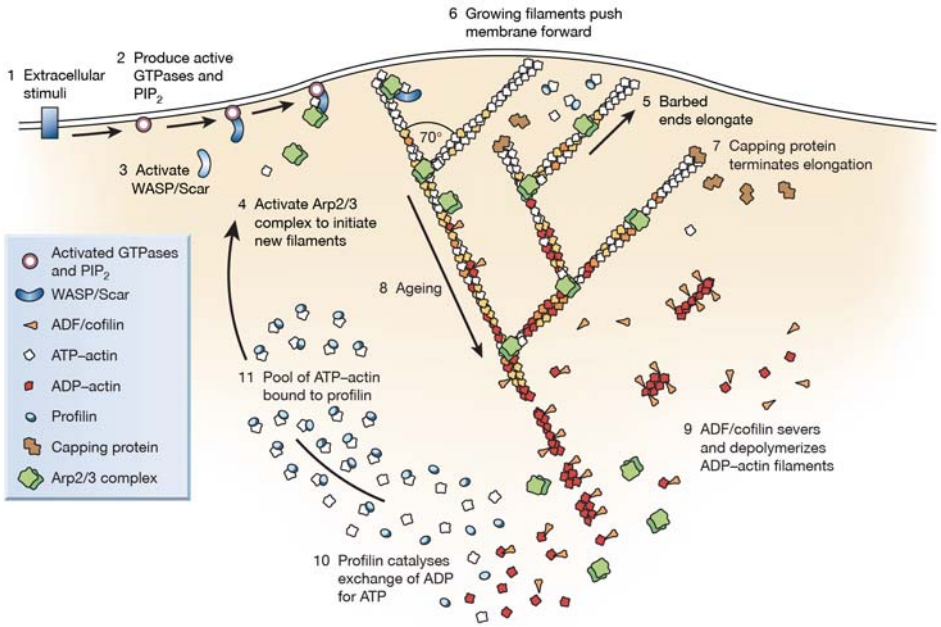

Figure 1.7. The dendritic-nucleation model for protrusion of lamellipodia. From (Pollard, 2003).

2004; Pertz et al., 2006). It has been shown that Rac1 activation using photoactivatable Rac1 is sufficient to induce lamellipodium extension (Wu et al., 2009). Interestingly, the different proteins are regulated with a distinctive spatiotemporal coordination (Machacek et al., 2009): RhoA is activated in synchrony with protrusion and is confined in a band within 2 μm from the leading edge. Cdc42 and Rac1 are activated with a 40 seconds delay relative to protrusion, and their activation is initiated 1.8 μm away from the leading edge, suggesting that their primary role may be in the regulation of adhesion dynamics.

2) Formation of adhesion complexes

Protrusion at the cell edge is tightly coordinated with formation of new adhesion complexes, which are the points of molecular interaction between the cell and the substrate. As described in section 1.1.2, integrins mediate the attachment of the cell to the extracellular matrix. The initial anchorage complexes are known as nascent adhesions, and they are smaller than 0,25 μm (Choi et al., 2008). The newly formed adhesions can either disassemble (adhesion turnover) or grow into more mature adhesions, recruiting more integrins and other proteins (such as α-actinin and talin) and establish a link between integrins and the actin cytoskeleton. The nascent adhesions stimulated to continue the maturation process grow to form focal complexes, which are approximately 0,5 μm. Similarly, a fraction of the focal complexes disassemble and the rest gives rise to focal adhesions (1 - 5 μm long). Finally, some of the focal adhesions mature and form fibrillar adhesions (> 5 μm). Paxillin, talin, FAK, or tensin are incrementally found as the new structures form (Figure 1.8) (Gardel et al., 2010). External forces or myosin II-mediated contractility are mechanotranduced and

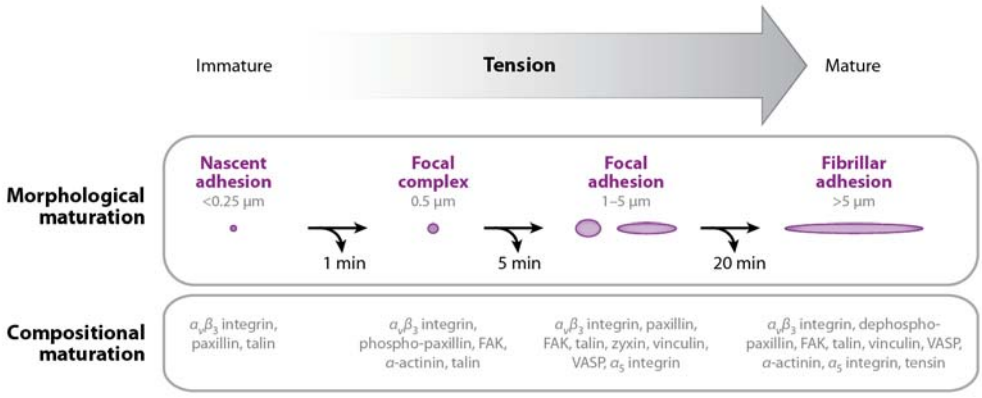

Figure 1.8. Phases of adhesion maturation. Above, morphological maturation phases of adhesion maturation, showing adhesion shape and size as it matures. Below, protein composition of the forming adhesion (Gardel et al., 2010).

stimulate the progression of the initial nascent adhesions to latter stages of adhesion maturation (Gardel et al., 2010).

3) Contraction

The newly formed cell substrate adhesions serve as traction force generation sites to allow cell contraction, which enables cell body translocation. The forces transmitted to the adhesion sites are generated by the interaction of myosin II with the actin cytoskeleton. Myosin contractility is stimulated by phosphorylation of its regulatory light chain (myosin light chain), which is either positively regulated by MLC kinase or Rho kinase or negatively regulated by MLC phosphatase.

It must be noted that the generated traction forces are globally balanced and that the net traction to move the cell is effectively zero (Liu et al., 2010; Trepat et al., 2012). Indeed, traction forces are transmitted to the adhesion sites at the leading edge and at the cell rear, and have in average equal magnitude but opposite, centripetal directions. The magnitude of the measured traction forces does not necessarily determine cell migration speed. By studying traction forces and actin flow in fish keratinocytes it has been hypothesized that the adhesions transmit forces to the substratum either by a slipping or a gripping mechanism (Fournier et al., 2010). Adhesions at the cell front produce forces independent of the velocity of the adjacent actin filaments (gripping adhesions), whereas adhesions at the back exhibit frictional slippage and are dependent on the motion of the actin filaments (slipping adhesions) (Fournier et al., 2010).

Based on the importance of traction force in cell migration, many studies have compared traction force generation between normal and cancer cells or among cancer cells that exhibit different metastatic potential. Munevar et al. (Munevar et al., 2001) compared cell migration properties and traction forces between normal NIH 3T3 fibroblasts and oncogenic, H-ras transformed 3T3 fibroblast. Cell migration in transformed fibroblast was in average enhanced compared to the normal ones (0,31 μm/min vs. 0,19 μm/min), although the directionality of the movement was reduced. Interestingly, tractions were also reduced in transformed cells (Average traction stress = 997 Pa vs. 3030 Pa in normal cells). Similarly, Indra et al. (Indra et al., 2011) studied traction force generation in murine breast cancer cells derived from primary tumor with increasing metastatic capacity, reporting that metastatic potential was inversely correlated with traction force generation. However, other studies have found opposite

results, reporting higher traction forces in metastatic breast, prostate and lung cancer cells compared to the non-metastatic counterparts (Kraning-Rush et al., 2012). It must be noted that inhibition of myosin II (and, therefore, of cell contractility), does not prevent cells to migrate (Fournier et al., 2010; Matsubayashi et al., 2011). It has been suggested that under this circumstance, the relatively weak forces generated by the actin assembly at the front protrusions are thought to make possible cell migration, since cells are weakly attached to the substrate. For all these reasons, the relationship among adhesion, traction, and cell migration is still under active investigation.

4) Release

For productive advance of the cell body, contraction must be coupled to release of the adhesions at the cell rear. Adhesions can disassemble by the mechanical stress generated by actomyosin fiber contraction, by cytosolic protein dissociation driven by phosphatases or kinases or by extracellular disruption driven by matrix proteases (Kirfel et al., 2004). While some of the rear adhesions are completely disassembled, in some cases there is a polarized remodeling, consisting on a continuous loss of adhesions at the back and recruitment of new integrins at the front of the adhesion. In this case, the adhesions seem to be sliding on the direction of the cell movement (Ballestrem et al., 2001). The contractile machinery is essential for proper de-adhesion; fibroblast deficient in myosin IIA show compromised adhesion disassembly, with impaired retraction resulting in extended tails (Vicente-Manzanares et al., 2007). Similarly, monocytes with inhibited Rho kinase show also an elongated morphology and impaired rear-end detachment (Worthylake et al., 2001).

Cell guidance

A fundamental issue for proper migration is cellular guidance, by which cells are directed in order to reach the specific location where they have to develop its specific role. Cell migration direction can be defined by different kinds of stimulus. The most studied guidance mechanism is chemotaxis, by which cell migration direction is affected by a chemical gradient in a way that results in net motility up a chemoattractant gradient or down a chemorepellent gradient (Eisenbach and Lengeler, 2004). Neutrophils are one of the most used models for eukaryotic chemotaxis. They are capable of detecting small differences in chemoattractant concentration across their surface and translate these differences into a much larger intracellular biochemical

gradient that polarizes the cell and orients cell migration direction (Dianqing, 2005). It has been shown that gradient sensing does not depend on a single molecular mechanism: about 50 different molecules have been identified to act as chemokines in neutrophils, which are detected by G-protein-coupled receptors (Vorotnikov, 2011). The most relevant intracellular effector is phosphatidylinositol-3,4,5-trisphosphate (PIP_3). Interestingly, neither the distribution of chemoattractant receptor nor the distribution of G-protein activation becomes substantially polarized. Instead, the downstream effector PIP_3 localizes at the edge of the cell exposed to the highest concentration of chemoattractant and functions as a strong amplifier, sensitizer, and director of chemoattraction, structuring the actin-filament system required for cell migration (Van Haastert and Devreotes, 2004). The upstream components remain homogeneously distributed along the membrane, permitting the cell to respond rapidly to changes in external gradient. It must be noted that the chemoattractant does not necessarily need to be a soluble molecule; it can also be bound to the substrate. In this case, the guidance is known as haptotaxis (Vorotnikov, 2011).

Mechanical cues have also been found to be capable of directing cell movement. Endothelial cells under shear stress, for instance, have been shown to align and migrate in the direction of the flow (Lin and Helmke, 2008; Wojciak-Stothard, 2011). On the other hand, it has also been reported that some cells migrate to regions with stiffer substrates, a process termed durotaxis and firstly reported in fibroblast (Lo et al., 2000). Isenberg et al., (Isenberg et al., 2009) showed that smooth muscle cells also exhibited durotaxis, which was enhanced as the magnitude of the stiffness gradient increased. A posterior study by Trichet et al. (Trichet et al., 2012) has showed similar results in fibroblasts, defining also a range of rigidities that cells can sense and respond to.

1.2.2 Collective cell migration

Collective cell migration is the prevailing mode of migration during development, wound healing, and in some forms of cancer metastases. During collective cell migration, cells remain physically and functionally connected as they move, maintaining tissue integrity and allowing direct signaling (either chemical or mechanical) between cells. Collective cell migration must be distinguished from other types of multicellular position changes, including embolic transport (passive movements of cell groups in body fluids), expansive growth (which refers to the proliferation-driven multicellular

growth usually associated to spherical neoplastic lesions), or cell intercalation (which refers to cellular rearrangements in a tissue to make it narrower and more elongated) (Friedl and Gilmour, 2009). For cohesive and productive collective cell migration, emerging properties such as multicellular polarity, collective guidance, and supracellular actin organization often appear, which are obviously absent in the case of single cell migration.

Epithelial to mesenchymal transition (EMT) has been traditionally invoked to explain the transition of multicellular collective from a static to a migratory phenotype. EMT is a cellular program that allows a polarized epithelial cell to undergo morphologic, structural, and molecular changes that induce the cell to acquire a mesenchymal phenotype. These changes include cell shape flattening, loss of cell-cell contacts, increased migratory capability, and production of extra-cellular matrix components. Although EMT has been useful to explain the migratory behavior of cells in some situations, it is also acknowledged that incomplete or partial processes of EMT are fundamental when considering many physiological and pathophysiological processes (figure 1.9). In these situations, cells display some characteristics of the mesenchymal phenotype (such as being motile, loss of apicobasal polarity, and generation of cell protrusions) while maintaining some characteristics of the epithelial phenotype (maintaining functional cell-cell junctions and expressing epithelial markers) (Kalluri and Weinberg, 2009; Revenu and Gilmour, 2009; Trepat et al., 2012).

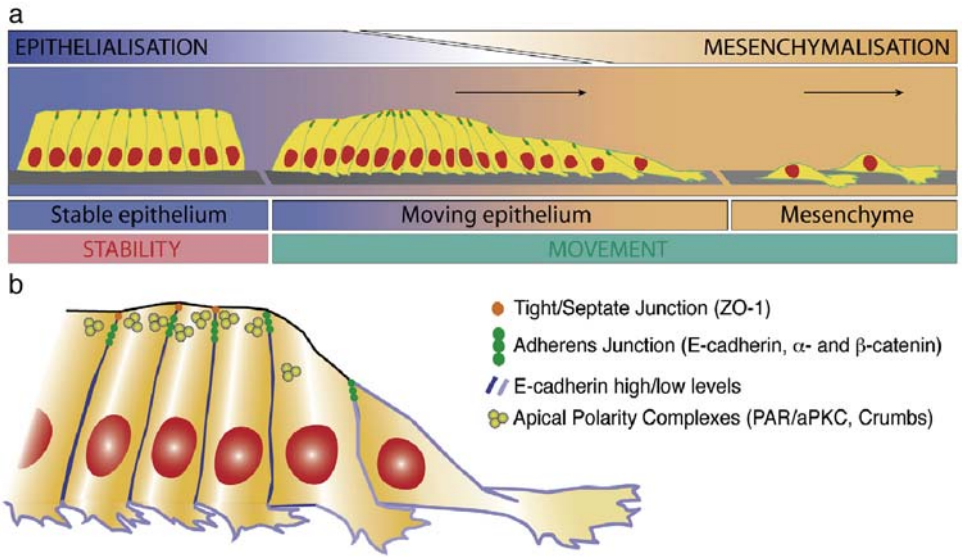

Figure 1.9. Partial EMT. (a) Schematic drawing depicting a static, apico-basally polarized epithelium (left) and two individually migrating cells (right). In between, an intermediate motile state controlled by an equilibrium of epithelial and mesenchymal cues. **(b)** Polarized organization of a collectively migrating group of cells. From (Revenu and Gilmour, 2009).

In this part, I will first describe the main modes of collective cell migration and the relevance of collective cell migration during development, wound healing, and cancer invasion. I will later describe the guidance mechanisms that direct collective cell migration and finally I will focus on the mechanisms of monolayer expansion.

Modes of collective cell migration

Different types of collective cell migration have been described based on the migration mode and the different geometrical structures that cells adopt. The most common ones are described in table 1 and illustrated in figure 1.10.

Collective cell migration in development. During development, cells migrate collectively from the places where they are produced to other places, where they are required to perform specific functions or give rise to new organs. The number of cells and the distances traveled can vary a lot, ranging from a few cells to thousands of cells, and from a few microns to centimeters. The most studied collective migration processes in different

Table 1. Modes of collective cell migration

Mode of migration	Description	Relevant dimensions	Examples
Sheet migration	Simple layer of epithelial or endothelial cells migrating on top of a two-dimensional ECM substrate to cover a surface	2D	Histoblast expansion (Ninov et al., 2010), dorsal closure (Kaltschmidt et al., 2002), wound healing (Anon et al., 2012)
Sprouting	Multicellular projection migrating from a pre-existing structure led by a tip cell to form a functional tree or network	3D	Angiogenesis (Adams and Alitalo, 2007), *Drosophila* tracheal morphogenesis (Affolter and Caussinus, 2008)
Branching	Reiterative process in which a rudimentary epithelial bud extends, bifurcates and differentiates to form a tubular organ	3D	Mammary and salivary gland formation (Larsen et al., 2006), uretral development (Shakya et al., 2005)
Strands	Migration of elongated cell masses, eventually from a cell reservoir, in a particular direction	3D	Cancer invasion (Friedl et al., 2004), Zebrafish lateral line formation (Haas and Gilmour, 2006)
Detached cluster	Migration of a relatively small number of cells through the ECM or other cells	3D	Cancer metastasis (Kawakami et al., 2009), border cell migration (Montell et al., 2012)

organisms during development are described in table 2.

Collective cell migration in regeneration. Collective cell migration is also relevant in wound healing, which has been particularly studied in the case of skin injury. A set of processes occurs immediately after wounding. Initially, a clotting cascade takes place, controlling bleeding and creating a fibrin network that will serve later as a scaffold over which cells will migrate. After an inflammatory response, keratinocytes surrounding the wound promote reepithelization by actively migrating as 2D cell sheets over the provisional matrix. They become flatter, extend filopodia or lamellipodia (Poujade et al., 2007; Friedl and Gilmour, 2009), and secrete laminin-V and collagen IV onto the provisional network to generate an appropriate extracellular matrix for efficient migration. In epithelial cells, two different mechanisms have been identified during the final stage of wound healing. In the first mode, cells are capable of generating a supracellular acto-myosin cable and its contraction in a purse-string manner provides efficient closure (Tamada et al., 2007). The second mode involves cell crawling and extension of dynamic lamellipodia into the wound area (Anon et al., 2012).

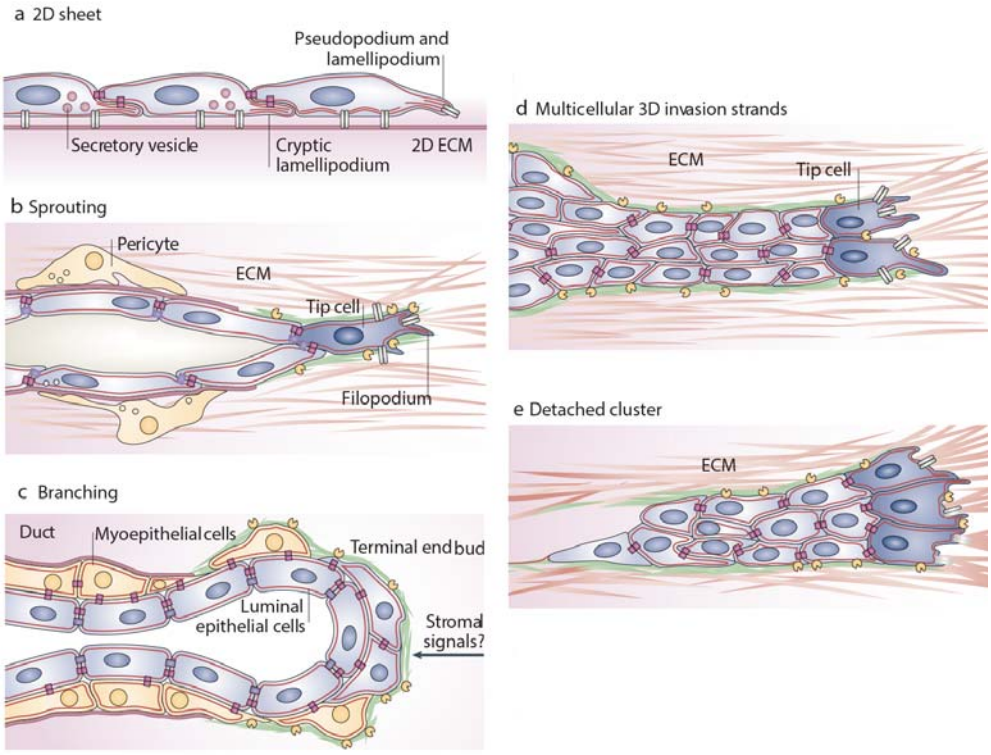

Figure 1.10. Modes of collective cell migration. Cell morphology and cell-cell and cell-extracellular matrix adhesion in different forms of collective migration. **(a)** 2D sheet migration. **(b)** Vascular sprouting. **(c)** Branching morphogenesis. **(d)** Multicellular strand. **(e)** Detached cluster. From (Friedl and Gilmour, 2009).

Collective cell migration in cancer. Cancer cell invasion into the surrounding tissue and the vasculature is the first step in cancer metastasis. Cell invasion has been traditionally thought to occur by mesenchymal, single cell motility, in which isolated cells escape from the primary tumor and move through the matrix by secreting proteases such as MMPs (Sahai, 2005). However, other forms of cell migration have been identified, including amoeboid motility or, especially in cancers of epithelial origin, collective cell migration. Histopathologic observations have revealed invasive sheets (Nabeshima et al., 1999), clusters (Yamamoto et al., 1983; Kawakami et al., 2009), or strands (Friedl et al., 2004) of distinct types of cancer cells surrounding primary tumors. By means of intravital imaging, in which fluorescent cancer cells are observed and followed *in vivo*, collective invasion strands of cells have been also identified in fibrosarcoma cells implanted in the skin of mice (Alexander et al., 2008), being this form of invasion more abundant than single cell invasion (figure 1.11). A useful approach to study this collective behavior of cancer cells has also been the cancer explants *in vitro:* In a study culturing melanoma explants in three-dimensional collagen lattices, Hegerfeldt et al., observed that invasive cell groups developed in approximately 50% of the cultures, maintaining adhesive cell-cell junctions (Hegerfeldt et al., 2002). Moreover, in some cases they identified an accumulation of beta-1 integrin in a subset of cells at the leading edge cell of the migratory cluster, indicating a polarized configuration within the cluster. Interestingly, a later study has demonstrated that leading cells do not necessary need to belong to the same cancer cell type: it has been shown that cancer

Table 2. Collective cell migration during development

Process	Organism	Mode	Description	Reference
Dorsal closure	Drosophila	Sheet	Migration of the lateral epidermal cells, meeting and fusing in the dorsal midline to seal the dorsal side of the embryo	(Solon et al., 2009)
Ventral enclosure	C. Elegans	Sheet	Migration of ventral hypodermal cells, meeting and fusing in the ventral midline to seal the ventral side of the embryo	(Simske and Hardin, 2000)
Lateral line formation	Zebrafish	Strands	Migration of cells caudally and along the flank of the embryo while depositing mechanosensory organs	(Haas and Gilmour, 2006)
Border cell migration	Drosophila	Cluster	Migration of the border cell cluster inside the egg chamber during oogenesis	(Montell et al., 2012)
Gastrulation	Ubiquitous	Sheet migration	Large-scale cell migration events that transform the blastula to the gastrula, with the three cell layers (endoderm, ectoderm and mesoderm) that will give rise to the different organs and tissues.	(Arboleda-Estudillo et al., 2010)
Neural crest migration	Ubiqutous	Strands	Migration of cells from the dorsal part of the neural tube throughout the embryo following well-defined routes to their final locations where they stop and differentiate in a wide range of cell types.	(Druckenbrod and Epstein, 2005; Theveneau and Mayor, 2011)

associated fibroblast recruited by cancer cells can also lead the invasion and generate invasive paths into the stroma (figure 1.11) (Gaggioli et al., 2007).

Finally, angiogenesis is a process mediated by collective cell migration found commonly in development, wound healing and cancer. It involves the formation of new blood vessels from pre-existing ones, and gives rise to the vascular system during development, regenerates it in case of injury or, in cancer, creates a capillary structure that is capable of supplying nutrients to tumor cells. It consists on the activation of endothelial cells in pre-existing blood vessels stimulated by growth factors and subsequent release of proteases that degrade the basement membrane. The sprout is driven by a clear differentiated non-proliferative tip cell that extends filopodia into the surrounding tissue, senses the environment and generates the required forces in order to migrate (Friedl and Gilmour, 2009). Proliferation is important in the cells behind this tip cell, providing the required number of cell to form a proper loop and a functional vessel.

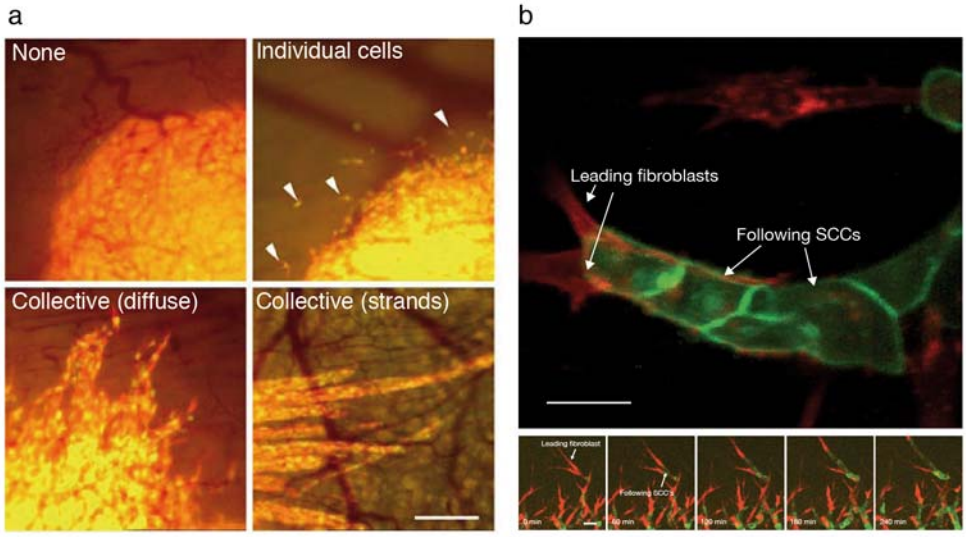

Figure 1.11. Collective cell migration in cancer. **(a)** Invasion modes of HT-1080 fibrosarcoma cells as seen by intravital imaging microscopy, including lack of invasion (top left), single cell dissemination (top right) and diffuse or strand-like collective invasion (lower panels), scale bar = 250 μm. From (Alexander et al., 2008). **(b)** Top: Squamous cell carcinoma cells (green) led by cancer associated fibroblasts (red) invading into naïve matrix, scale bar = 20 μm. Bottom: representative images of the same process at 60 min intervals, scale bar = 40 μm. From (Gaggioli et al., 2007).

Mechanisms of collective cell migration

While collective cell migration occurs in many physiological and pathophysiological processes, the mechanisms that allow for this mode of cell migration are still under active investigation. The principal questions that need to be addressed include signaling (what are the genes and proteins required for collective cell migration?), cell guidance (how are cells coordinated and guided to perform the requested migration?) and forces (what are the forces required to move a group of cells and who is responsible for generating them?). Deciphering how these mechanisms are regulated in model systems might shed light on understanding how they are deregulated in disease. To investigate them in a systematic manner, many studies have used the migration of cells in a monolayer *in vitro* as a model, since they can be easily prepared, manipulated and imaged.

In order to provide an analysis of the regulatory mechanisms behind collective cell migration, some studies have knocked down an array of genes to identify those regulating collective cell migration. Simpson et al., (Simpson et al., 2008) performed a small interfering RNA (siRNA) screen in MCF-10A epithelial cells in a wound healing model targeting 1.081 human genes, ultimately identifying 66 high confidence genes that, when downregulated, either accelerated or impaired collective migration. Downregulation of genes encoding for proteins such as cadherin 3, catenin, or WASP accelerated migration. Inversely, downregulation of genes encoding for proteins such as actin, integrin, talin, or vimentin impaired migration. A similar study was done in endothelial cells (Vitorino and Meyer, 2008), identifying 91 migration regulators genes which could be categorized into three different bins: cell motility regulators, which drive random motility, directed migration regulators, which are mandatory for proper

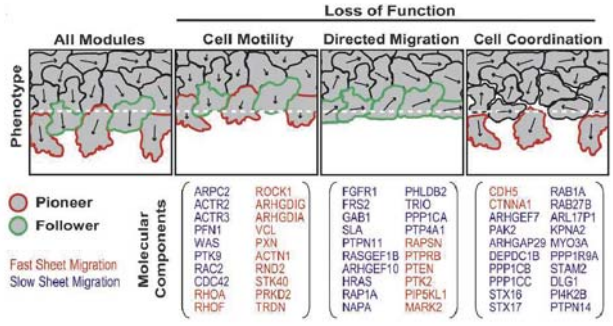

Figure 1.12. Modular control of endothelial sheet migration. Sheet migration defects when specific proteins of different functional modules are perturbed. Genes for each module are listed as examples. From (Vitorino and Meyer, 2008).

migration direction, and regulators of cell-cell coordination, which reorient randomly migrating cells inside the sheet when boundary cells begin to migrate (Figure 1.12).

On top of identifying genes that regulate collective cell migration, a sequence of events at the level of post-translational modifications of proteins have been reported to occur and regulate cell migration after wounding. Matsubayashi et al (Matsubayashi et al., 2004) reported two waves of ERK map kinase activation that propagated into Madin Darby Canine Kidney (MDCK) cell sheets after wounding that were initiated at the site of injury. The first wave propagated within the first 10 minutes after wounding; the second wave was slower and lasted at least during 4 hours after wounding (Figure 1.13). ERK inhibition impaired cell sheet migration, and actin cytoskeleton disruption suppressed its activation. Interestingly, further investigation showed that the initial, fast wave was due to the generation of reactive oxygen species (ROS) at the wound interface following injury: triggering collective cell migration by removing a polydimethylsiloxane (PDMS) barrier without causing cell injury induced only the second wave of ERK activation (Nikolic et al., 2006).

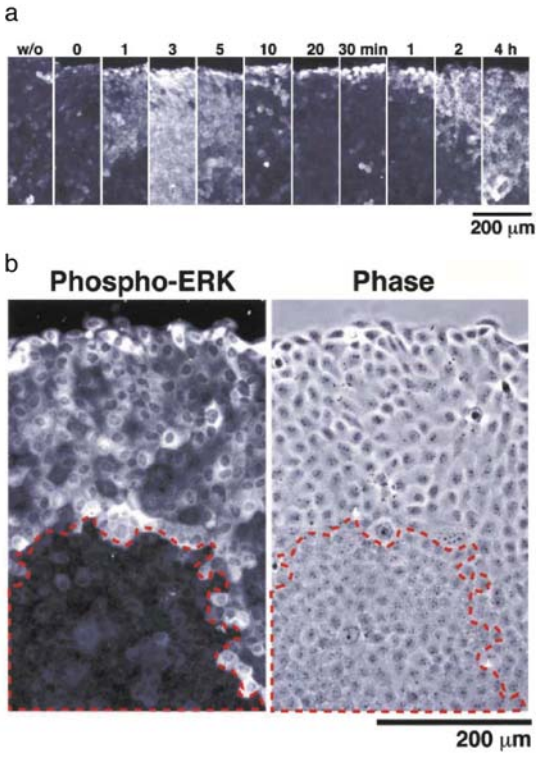

Figure 1.13. Waves of ERK Activation in MDCK cell sheets. (a) Anti-phospho ERK1/2 immunostaining of MDCK cells at the specified time points after wounding. **(b)** Correlation of ERK1/2 activation and cell shape change 2 hours after wounding. From (Matsubayashi et al., 2004).

How do cells in a group know where to migrate? The guidance mechanisms described for single cell migration are also used in the case of cells migrating collectively. However, cell-cell interaction in a migrating group adds a new level of regulation, affecting the above-mentioned mechanisms or directly providing new physico-chemical ones. 60 years ago, Abercrombie and Heaysman described for the first time that fibroblast migration *in vitro* was affected by the interaction with other cells (Abercrombie and Heaysman, 1953), causing cells to stop moving. They termed this phenomenon *contact inhibition of locomotion* (CIL). The idea was proposed as an explanation for epithelial cell activation after a wound (cell-cell contacts lost in a wound would induce cell migration) and its defect was suggested as a cause for metastatic cancer cell behavior (reduced CIL would induce tissue invasion). Due to a lack of a detailed molecular understanding of CIL and important insights made regarding the molecular mechanisms of cell polarization and chemotaxis, the interest in CIL decreased (Mayor and Carmona-Fontaine, 2010). However, in recent years, CIL has been reassessed and it has been demonstrated that applying this concept to collective cell migration provides an explanation for collective directionality. From a general perspective, in a group of cells, CIL predicts that contact between cells leads to inhibition of cell protrusion, whereas at the free edge, there is no CIL at the cell front and this leads to cell polarization and directional migration (Figure 1.14). At a molecular level, it has been shown *in vivo* and *in vitro* that in *Xenopus* neural crest cells,

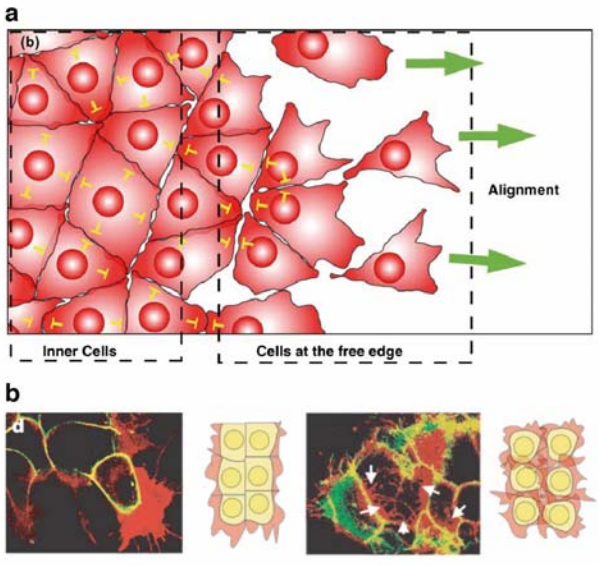

Figure 1.14. Contact inhibition of locomotion. (a) CIL in a group of cells inhibit cell protrusions at the inner cells, and directs the leader cells to polarize and migrate towards the free edge. **(b)** Xenopus neural crest cells show protrusions only at the border (left image and schematic representation), while they appear everywhere in cells with PCP inhibited(right image and schematic representation). Green = cell shape; red = cell protrusions. From (Carmona-Fontaine et al., 2008).

N-cadherin interaction at cell-cell contacts induces local inhibition of protrusion via Rho activation (Carmona-Fontaine et al., 2008) and Rac1 inhibition (Theveneau et al., 2010), whereas Rac1 is activated and new protrusions are induced at the free edge (Theveneau et al., 2010). A similar mechanisms has been proposed to act in 2D cell sheets (Rørth, 2009).

On top of this inner mechanism for polarity generation in a cell group, chemoattractants are also believed to play a role in certain cases, eventually fine-tuning the direction of collective migration. Indeed, it has been shown that the chemokine SDF-1 (Stromal cell-derived factor-1) is required for neural crest cell migration, amplifying and stabilizing directional migration determined by cell-cell contacts (Theveneau et al., 2010). The same molecule is required to define a path that will guide the movement of the lateral line primordium of zebrafish (Haas and Gilmour, 2006). Similarly, border cell migration in *Drosophila* is guided by chemoattractants presented or secreted by the surrounding germline cells, including PVF1 (platalet-derived grwoth factor (PDFG) and vascular endothelial growth factor (VEGF)-related factor 1), Spitz, Keren, and Gurken (Montell et al., 2012). Gradients of VEGF also guide endothelial tip cells during angiogenesis.

In addition to study the genes and proteins regulating cell migration, a complete understanding of the actual movement requires a detailed and quantitative description of the mechanical forces that drive cell motility. In this direction, several studies have investigated the migration of MDCK epithelial cells as a model system. Du Roure et al. (Du Roure et al., 2005) measured the forces of a migrating cell group using an array of microfabricated pillars. Their experiments showed that the highest traction forces were localized at the edge ($\approx$1.6nN/μm^2 within 2μm from the leading edge) and centripetally oriented. However, at a greater distances from the edge, cells were also exerting forces ($\approx$0.6nN/μm^2) on the substrate (Figure 1.15). This observation is consistent with a study made by Farooqui et al. (Farooqui and Fenteany, 2005), which showed that cells hundreds of microns away from the edge of the migrating epithelia exhibited cryptic lamellipodia with the same morphology and dynamics of the ones in the cells at the edge (Figure 1.15). Taken together, these observations lead to the conclusion that not only the cells at the edge are the ones responsible for the movement of the cell group.

A posterior study by Trepat et al. (Trepat et al., 2009) reported force measurements obtained using TFM on an expanding cell island. The magnitude of the measured forces was comparable to what was found by du Roure et al. However, they also showed that cells behind the leading edge generated traction forces equivalent in magnitude to the ones at the leading edge (Figure 1.16). This controversy might be due to the different geometry of the migrating cell group, since du Roure et al., were considering only a group of a few cells, whereas Trepat et al were considering large multicellular colonies. More interestingly, they also showed that forces generated by the cell on the substrate were not locally balanced; instead, they were transmitted across cell-cell junctions, building up gradients of stress across the expanding monolayer. This observation led to two fundamental conclusions. In the first place, it rules out the possibility that each cell in the monolayer is mechanically self-propelled. If this were the case, the transmitted stress would be identically zero everywhere across the monolayer. In the second place, the transmission of stress between cells across the monolayer suggests a new possible mechanism for collective guidance. Indeed, it has

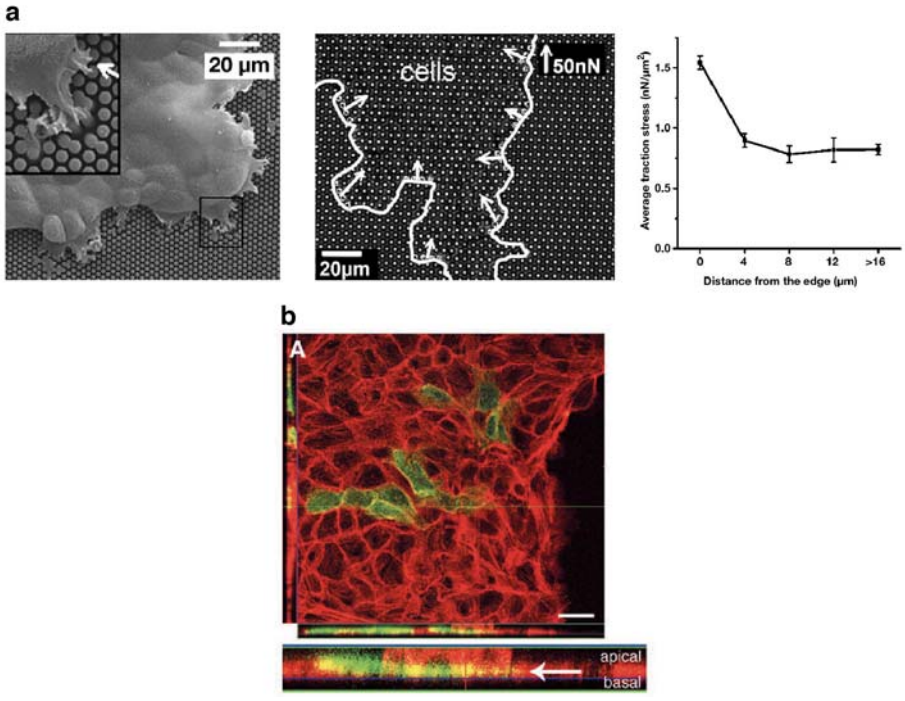

Figure 1.15. Expansion of MDCK epithelial cells. (a) Left: MDCK monolayer migrating on an array of microfabricated pillars (inset: magnified view of the area delimited by the black square). Middle: Magnitude and orientation of traction stress on a cell monolayer. The white line outlines the edge of the monolayer. The white arrows indicate the resulting force applied on four consecutive posts. Right: average traction stress versus distance from the edge. From (Du Roure et al., 2005). **(b)** Cryptic lamellipodia in submarginal cells seen in actin-GFP cells after immunostaining the monolayer with phalloidin-TRITC. The orthogonal z-stack profiles along the indicated lines in x or y are shown in the rectangular windows at the bottom or the left part of the image. A magnified region of the xz orthogonal profile is shown below. The white arrow indicates a membrane protrusion extending under the non-transfected cell in front of it. From (Farooqui and Fenteany, 2005).

been demonstrated that applying a mechanical force locally to C-cadherins on single Xenopus mesodermal cells induces polarized cell protrusion and persistent migration, typical of cells migrating collectively (figure 1.16) (Weber et al., 2012). It has been suggested that in the mesendodermal migrating epithelium this stress build-up creates an asymmetric intercellular tension that is sensed by cells, establishing a preferential direction of collective migration (Weber et al., 2012). The absence of a local force balance within a cell being part of a group of cells was again described in a later study using microfabricated pillars (Saez et al., 2010).

In order to understand precisely the role of these cell-cell transmitted forces in collective cell migration, it is fundamental to accurately map and quantify them. Moreover, studying in a systematic manner how epithelial cells adopt a migratory phenotype and the morphological and biomechanical events involved in this process has the potential to help advance our knowledge regarding the mechanisms driving partial epithelial to mesenchymal transition and collective cancer invasion. The work presented in this thesis addresses these aims.

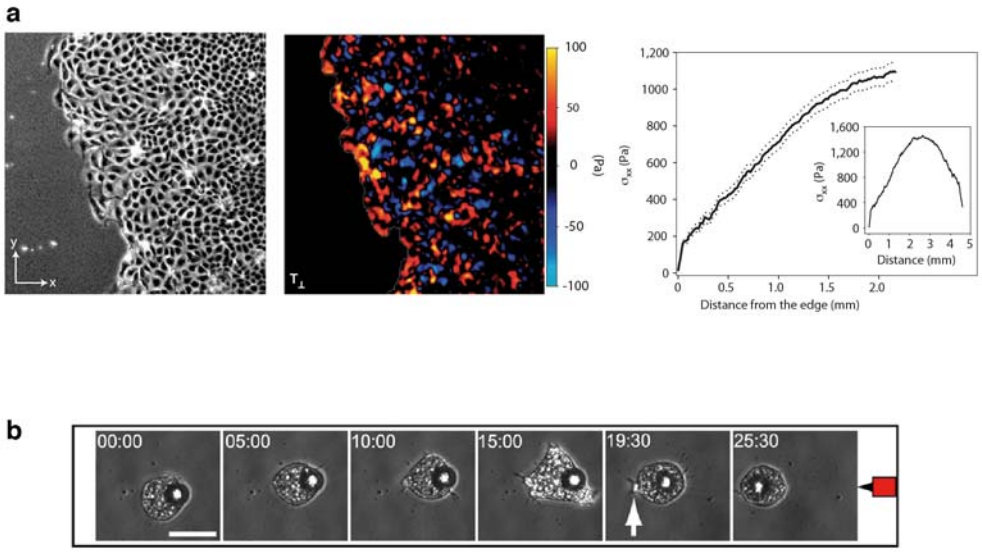

Figure 1.16. Traction forces and stress build-up. (a) Left: phase contrast image of MDCK cells migrating over a collagen-coated polyacrylamide gel. Middle: map of traction forces normal to the leading edge. Right: Cell-cell stress increases away from the leading edge (Inset: reasurement of the stress over the whole diameter of the cell colony). From (Trepat et al., 2009). **(b)** Force application to cadherin orients protrusive behavior of mesendoderm cells. A magnet pulls towards the right a cadherin-coated magnetic bead, and a lamellipodium forms (white arrow) opposite the direction of bead pull, resulting in directed cell migration. From (Weber et al., 2012).

Chapter 2 Aims of the thesis

2.1 General aim

The general aim of the thesis was to study the biomechanical mechanisms that drive the expansion of an epithelial monolayer.

2.2 Specific aims

1. To measure traction forces, cell-cell stresses, and cell morphology in an expanding colony of epithelial cells.
   1.1. To implement traction microscopy and monolayer stress microscopy in an expanding colony of epithelial cells.
   1.2. To measure cell height during colony expansion.
   1.3. To perform high-resolution imaging to study the morphological features of migratory cells.

2. To implement an experimental model for the systematic biomechanical analysis of collective epithelial migration.
   2.1. To develop an assay based on PDMS micropatterning to initially confine epithelial cells and subsequently trigger their collective migration.
   2.2. To study the evolution of cell height during monolayer expansion.
   2.3. To develop software for the automatic binarization of phase contrast images of an expanding cell sheet.

3. To provide a systematic analysis of epithelial biomechanics and morphology during collective cell migration.
   3.1. To study the morphological changes that cells undergo during monolayer expansion.
   3.2. To study changes in expression of EMT markers during monolayer expansion
   3.3. To study the contribution of cell proliferation to monolayer expansion.
   3.4. To study the evolution of cell velocity, strain rate, traction force, and intercellular stress during monolayer expansion.
   3.5. To study the effects of disrupting cell junctions and cell contractility during monolayer expansion.

Chapter 3 Papers

3.1 Collective cell guidance by cooperative intercellular forces

Tambe DT, Hardin CC, Angelini TE, Rajendran K, Park CY, Serra-Picamal X, Zhou EH, Zaman MH, Butler JP, Weitz DA, Fredberg JJ & Trepat X. Collective cell guidance by cooperative intercellular forces. *Nature Materials* 10, 469-475 (2011).

nature materials

ARTICLES

PUBLISHED ONLINE: 22 MAY 2011 | DOI: 10.1038/NMAT3025

Collective cell guidance by cooperative intercellular forces

Dhananjay T. Tambe[1†], C. Corey Hardin[2†], Thomas E. Angelini[3], Kavitha Rajendran[1], Chan Young Park[1], Xavier Serra-Picamal[4], Enhua H. Zhou[1], Muhammad H. Zaman[5], James P. Butler[1], David A. Weitz[3], Jeffrey J. Fredberg[1*] and Xavier Trepat[4*]

Cells comprising a tissue migrate as part of a collective. How collective processes are coordinated over large multi-cellular assemblies has remained unclear, however, because mechanical stresses exerted at cell–cell junctions have not been accessible experimentally. We report here maps of these stresses within and between cells comprising a monolayer. Within the cell sheet there arise unanticipated fluctuations of mechanical stress that are severe, emerge spontaneously, and ripple across the monolayer. Within that stress landscape, local cellular migrations follow local orientations of maximal principal stress. Migrations of both endothelial and epithelial monolayers conform to this behaviour, as do breast cancer cell lines before but not after the epithelial–mesenchymal transition. Collective migration in these diverse systems is seen to be governed by a simple but unifying physiological principle: neighbouring cells join forces to transmit appreciable normal stress across the cell–cell junction, but migrate along orientations of minimal intercellular shear stress.

A variety of fundamental processes in development, health, and disease depend on the coordinated motion of cell groups[1–10]. To describe coordinated cellular motions in these processes, high-throughput genomic approaches have identified molecular players and mapped their interaction into comprehensive signalling networks[11,12]. But even with detailed signalling and structural information in hand, the role of intercellular adhesion in collective migration is disputed[13,14], and our understanding of collective cellular migration lacks predictive power and remains largely descriptive. Central to these limitations is the absence of a physical picture that links cell motion to mechanical stresses exerted within the cell body and at cell–cell boundaries, for these stresses have never before been measured. Here we report high-resolution maps of these stress components everywhere within an advancing monolayer sheet, which serves as a simple experimental model system. These stress maps reveal that the local cellular trajectory follows local stress fields that are severely heterogeneous and dramatically cooperative over distances spanning many cell bodies. Together, these findings reveal an unanticipated but unifying physiological principle, namely, that each cell tends to migrate and remodel so as to maintain minimal local intercellular shear stress. Detailed knowledge of the biology of the cell–cell junction, the cryptic lamellipodium (Supplementary Information S7), or any specific molecular event could never predict such a unifying principle because it is an emergent property of a multicellular collective system. By analogy to the well-known guidance mechanisms of chemotaxis, durotaxis and haptotaxis, we call this distinct but innately collective mechanism plithotaxis, from the Greek 'plithos' denoting crowd, swarm or throng.

To measure the local state of stress within a monolayer (Fig. 1), we developed monolayer stress microscopy, MSM (Supplementary Information S1). On an inverted optical microscope, we record cell-generated displacements of fluorescent markers embedded near the surface of a collagen-coated polyacrylamide gel substrate on which the cells are adherent. We use a novel approach for stage drift compensation (Supplementary Information S1), and then use resulting dedrifted gel deformations to compute a map of the traction forces, T, exerted by the monolayer on the gel[15]. Finally, from these traction forces measured directly at the interface between the cell and its substrate (Supplementary Fig. S3), a straightforward and rigorous two-dimensional balance of forces as demanded by Newton's laws is then used to obtain the distribution of the mechanical line forces everywhere within the cell sheet (Fig. 1a); for convenience, these measured line forces (in units of force per unit length) are converted to stresses (force per unit area) using the average monolayer height, h (Fig. 1; Supplementary Fig. S4). Gradients of these line forces and stresses within the cell sheet are attributable to the pile-up of traction forces applied on the underside of the cells. At each point within the sheet the local coordinate system (Fig. 1c) can be rotated in the cell plane to find those special orientations along which the local normal stress is maximal and minimal, respectively, thus defining the two principal stress components (σ_{max} and σ_{min}) and the two corresponding, mutually perpendicular, principal orientations (Fig. 1d; Supplementary Information S1). As such, the associated MSM result displays at high resolution, and maps separately, each individual component of the in-plane stress tensor.

We consider first the average local normal stress, simply defined as $\bar{\sigma} = (\sigma_{max} + \sigma_{min})/2$, and its spatial heterogeneity. A traditional image of an advancing monolayer of rat pulmonary microvascular endothelial (RPME) cells is unremarkable (Fig. 2a). The underlying distribution of local normal stress, by contrast, is

[1]Program in Molecular and Integrative Physiological Sciences, School of Public Health, Harvard University, Boston, Massachusetts 02115, USA, [2]Division of Pulmonary and Critical Care Medicine, Massachusetts General Hospital, Boston, Massachusetts 02114, USA, [3]School of Engineering and Applied Sciences, Harvard University, Cambridge, Massachusetts 02138, USA, [4]Institute for Bioengineering of Catalonia, Universitat de Barcelona, Ciber Enfermedades Respiratorias, and Institució Catalana de Recerca i Estudis Avançats, 08036, Spain, [5]Department of Biomedical Engineering, Boston University, Boston, Massachusetts 02215, USA. [†]These authors contributed equally to this work. *e-mail: jfredber@hsph.harvard.edu; xtrepat@ub.edu.

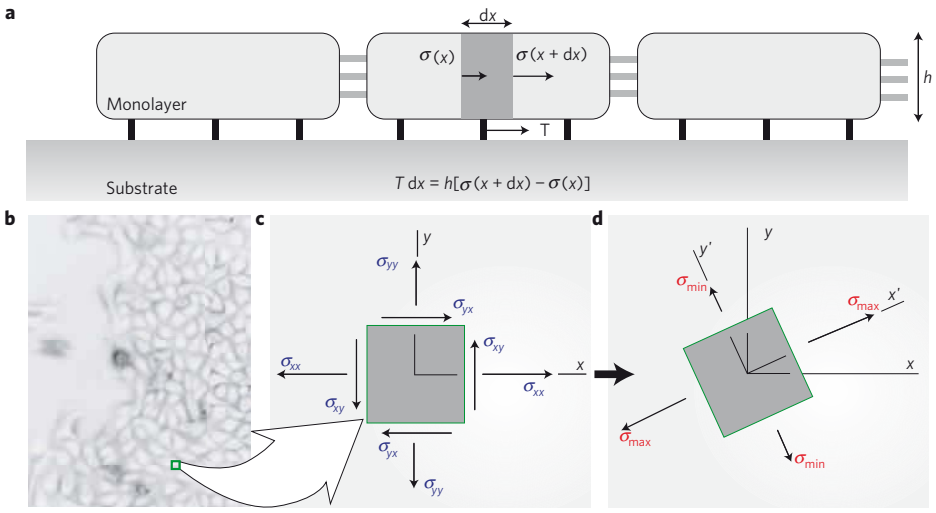

Figure 1 | Monolayer stress microscopy. a, Simplified representation of the physical relationship between cell–substrate tractions, T, which have been reported previously[15], and intercellular stresses, σ, which are reported for the first time here. Intercellular stresses arise from the accumulation of unbalanced cell–substrate tractions. At any point within the monolayer (**b**), the intercellular stresses, defined in laboratory frame (x, y), (**c**), have shear (σ_{xy}, and σ_{yx}) and normal (σ_{xx}, and σ_{yy}) components. This frame can be rotated locally to obtain the principal frame (x', y'), (**d**), where shear stresses vanish and the resulting normal stresses are called principal stresses (σ_{max} and σ_{min}). The corresponding axes are called maximum, aligned with x', and minimum, aligned with y', principal orientations.

severely heterogeneous; normal stresses are mostly positive (tensile) with values exceeding 300 Pa in regions spanning tens of cells. These regions of predominantly tensile stresses alternate with regions of weakly negative (compressive) stresses (Fig. 2c). These fluctuations occur steadily over distances spanning multiple cell widths and define a stress landscape that is rugged (Fig. 2c,i), by which we mean that the spatial fluctuations over these relatively short distances are comparable in magnitude to the spatial mean values. We consider next the distribution of the intercellular shear stress (Supplementary Fig. S1), which is not to be confused with any additional shear stress that might be imposed by flow over the monolayer surface[16], which in this case is everywhere zero. As in the case of the normal stress, the shear stress at a point within a material varies with orientation and attains its maximal value, $\mu = (\sigma_{max} - \sigma_{min})/2$, at 45° from the principal orientations (Fig. 1d). The local maximal shear stress was systematically smaller than the local normal stress, but was also characterized by a rugged landscape (Fig. 2e). As the monolayer advances, these respective stress landscapes evolve continuously in time (Supplementary Movie SM1). Finally, the dependence of local stresses on orientation signifies stress anisotropy. To visualize this anisotropy, we plotted ellipses for which the major axis corresponds to the local σ_{max} and the minor axis corresponds to the local σ_{min}, each aligned with the corresponding principal orientations. Where $\sigma_{max} = \sigma_{min}$ the stress field is isotropic, the ellipse becomes a circle, μ is zero, and there exists no preferred stress orientation. But where $\sigma_{max} \gg \sigma_{min}$ the local stress field is highly anisotropic, the ellipse becomes spindle-like, μ is nonzero, and there exists a strongly preferred and well-defined stress orientation. From region-to-region, we found that ellipse size, ellipse shape, and ellipse orientation varied extensively, but with strong local correlations (Fig. 2g).

As cells extend cryptic lamellipodia[17] (Supplementary Fig. S7) and advance within the monolayer, stresses at every point and at every instant of time must be in mechanical balance. Nonetheless, no mechanistic framework or physical picture yet exists that might link these stresses to cellular orientation, remodelling, or migration. Here we ask, to what extent are these intercellular stresses meaningful biologically and useful predictively? The answer to this question is suggested by two pieces of experimental evidence. First, because phase-contrast images and stress maps are mutually independent measurements, the coincidence between the orientation of the cell body versus the orientation of the maximal principal stress is striking (Fig. 2g and Supplementary Fig. S5). Further, because the maximal principal orientation corresponds to the local axis of highest normal stresses and zero shear stress, this result suggests that the cell–cell junction, as well as the cell body, supports high normal stresses, which are overwhelmingly tensile, but only minimal shear stresses. One would predict, therefore, that major organized actin structures that span the cell, as would be imaged at low resolution, might align with maximal principal orientations, and for the spindle-like RPME cells this is in fact seen to be the case (Fig. 2g and Supplementary Fig. S6). Second, cells not only align with the maximal principal orientation, but also migrate along that orientation (Fig. 2g, red arrows; Supplementary Movie SM2). Appreciable portions of the stress field are approximately isotropic, however, and therefore the local orientation of cell motion would not be expected to correlate with a stress field possessing no preferred orientation.

As such, these observations lead naturally to the following prediction: regions of higher stress anisotropy will exhibit stronger alignment between the direction of local maximal principal stress and that of local cellular migration velocity. To test this prediction, we reasoned as follows. As the maximum local shear stress is given by $\mu = (\sigma_{max} - \sigma_{min})/2$, we took μ as a direct and quantitative index of stress anisotropy. We then rank-ordered this stress anisotropy by quintiles. For each point within the cellular monolayer falling within any given quintile, we measured the alignment angle ϕ between the orientation of the local maximal principal stress and the orientation of the local cellular migration velocity vector (Fig. 2j, inset). The greater was the local shear stress, the narrower was the distribution of ϕ (Fig. 2j–l). We then constructed the cumulative probability distribution function, $\bar{P}(\phi)$, reasoning that if there were perfect alignment between the orientation of local cellular migration velocity and that of local maximal principal stress, then all angles ϕ would be 0° and the cumulative probability distribution would be a step function from

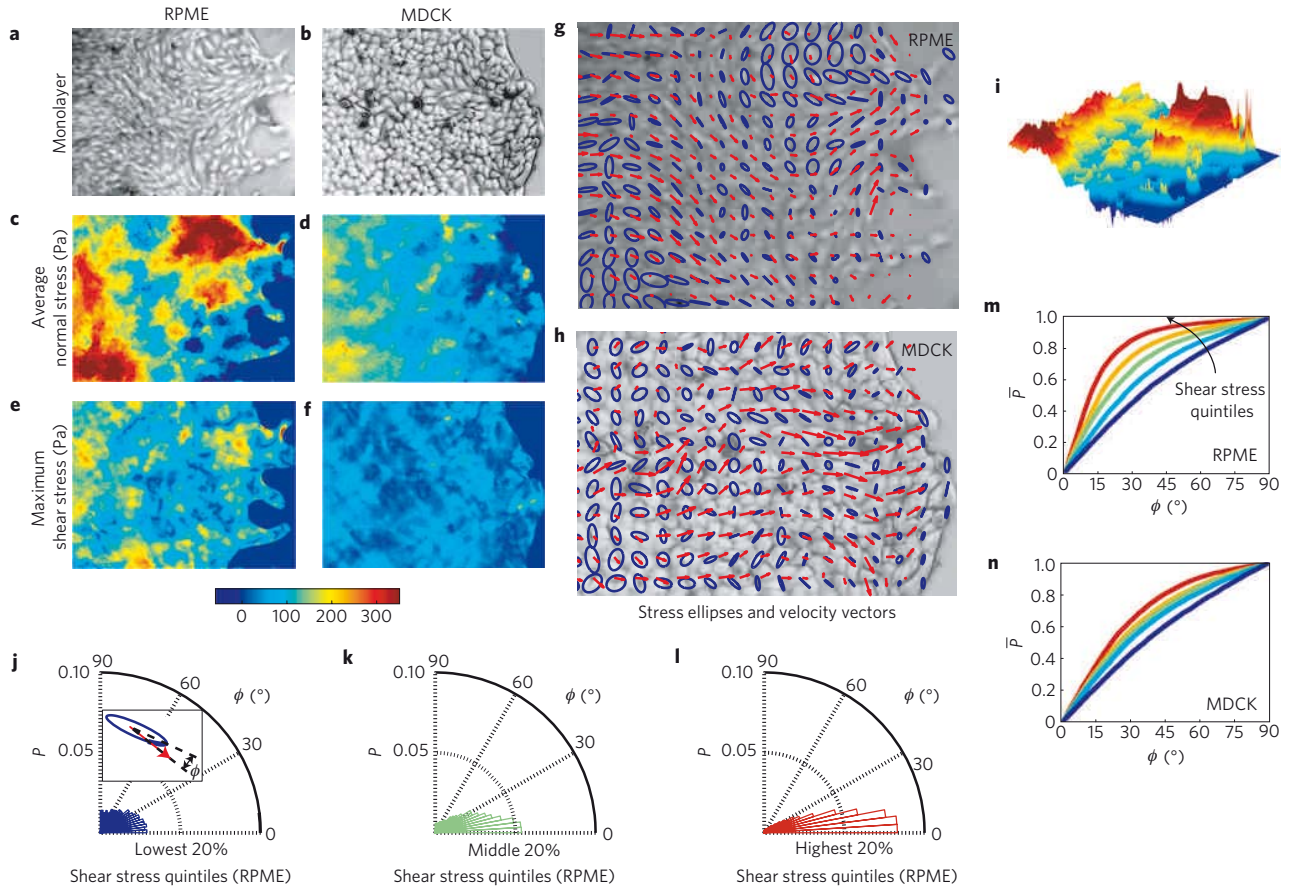

Figure 2 | Intercellular stress maps and mechanical guidance of collectively migrating monolayers. Transmitted light image of the RPME cell monolayer (**a**) and the MDCK cell monolayer (**b**). Corresponding to these images are the maps of average normal stress (**c**,**d**), maximum shear stress (**e**,**f**) and principal stress ellipses (blue) and cell velocity vectors (red) (**g**,**h**). Note that for the MDCK cell monolayer, the average tensile stress (**d**) increased systematically with increasing distance from the advancing front, thus contributing to the state of global tug-of-war[15]. The map of average normal stress for the RPME cell monolayer is predominately tensile, but forms a rugged stress landscape (**i**). The alignment angle, ϕ, between the major axis of the principal stress ellipse and the direction of the cellular motion (**j**, inset) shows that the greater the local maximum shear stress the narrower is the distribution of ϕ (**j**–**l**). The cumulative probability distribution $\bar{P}(\phi)$ varied strongly and systematically with stress anisotropy (**m**); curves, from blue to red, are in the order of higher quintiles. The cumulative probability distribution for the MDCK cell monolayer is also shown (**n**). Vertical size of the images of cell monolayers: RPME-545 μm, MDCK-410 μm. Each curve in **m** and **n**, and distributions in **j**, **k** and **l** have more than 8,000 observations.

probability 0 to probability 1 occurring at 0° (Fig. 2m). If there were no alignment, however, then all angles between 0° and 90° would be equally likely, and the cumulative probability function would be a straight line from probability 0 at 0° to probability 1 at 90°. In the regions with lowest stress anisotropy (blue), the angular distribution was broad but not uniform. In regions with highest stress anisotropy (red), the angular distribution was quite narrow; the orientation of cellular velocity and the orientation of maximal principal stress were coupled strongly, but were unrelated to the magnitude of local average stress (Supplementary Fig. S8). The stronger was the stress anisotropy the greater was the overall degree of alignment.

To assess the generality of this finding, we then examined monolayers comprising Madin–Darby canine kidney (MDCK) cells (Fig. 2b), which are of particular interest because they are epithelial, not endothelial, and because they are rounded in the plane, not spindle-shaped as are RPME cells. Despite these differences in cell type and cell morphology, the stresses were dramatically heterogeneous (Fig. 2d,f) and the local orientation of cellular migration was also found to follow the local orientation of maximal principal stress (Fig. 2h,n). Remarkably, local cell motions tended to follow local principal stress orientations even when local cell geometry displayed no preferred orientation. To assess further the generality of this finding, we next examined the behaviour of monolayers of well-established breast-cancer model systems: MCF10A cells (control or vector) (Fig. 3a), MCF10A cells overexpressing ErbB2/HER-2/neu (Fig. 3b), and MCF10A cells overexpressing 14-3-3ζ (Fig. 3c). We chose these cell lines because each exhibits pronounced morphological differences as well as diverse levels of transforming potential, expression of cell–cell junction proteins, and cell proliferation[18,19]. Much as in the case of endothelial cells and control epithelial cells, ErbB2 cells moved in alignment with the direction of maximum principal stress (Fig. 3m). By contrast, 14-3-3ζ cells, which have decreased expression of cell–cell junctional markers[18,19], were seen to move nearly independently of the orientation of the maximum principal stress (Fig. 3m). To assess further the importance of cell–cell adhesion, we weakened the cell–cell contacts of MCF10A vector cells by calcium chelation (Fig. 4g,i). As expected, the alignment between the orientations of local stress and the orientations of local cellular motions was lessened (Fig. 4s, magenta), but was restored on returning to the normal growth medium (Fig. 4i,s, blue). However, this reversibility was blocked in the presence of E-cadherin antibodies (Fig. 4r,s, red). Together, these observations

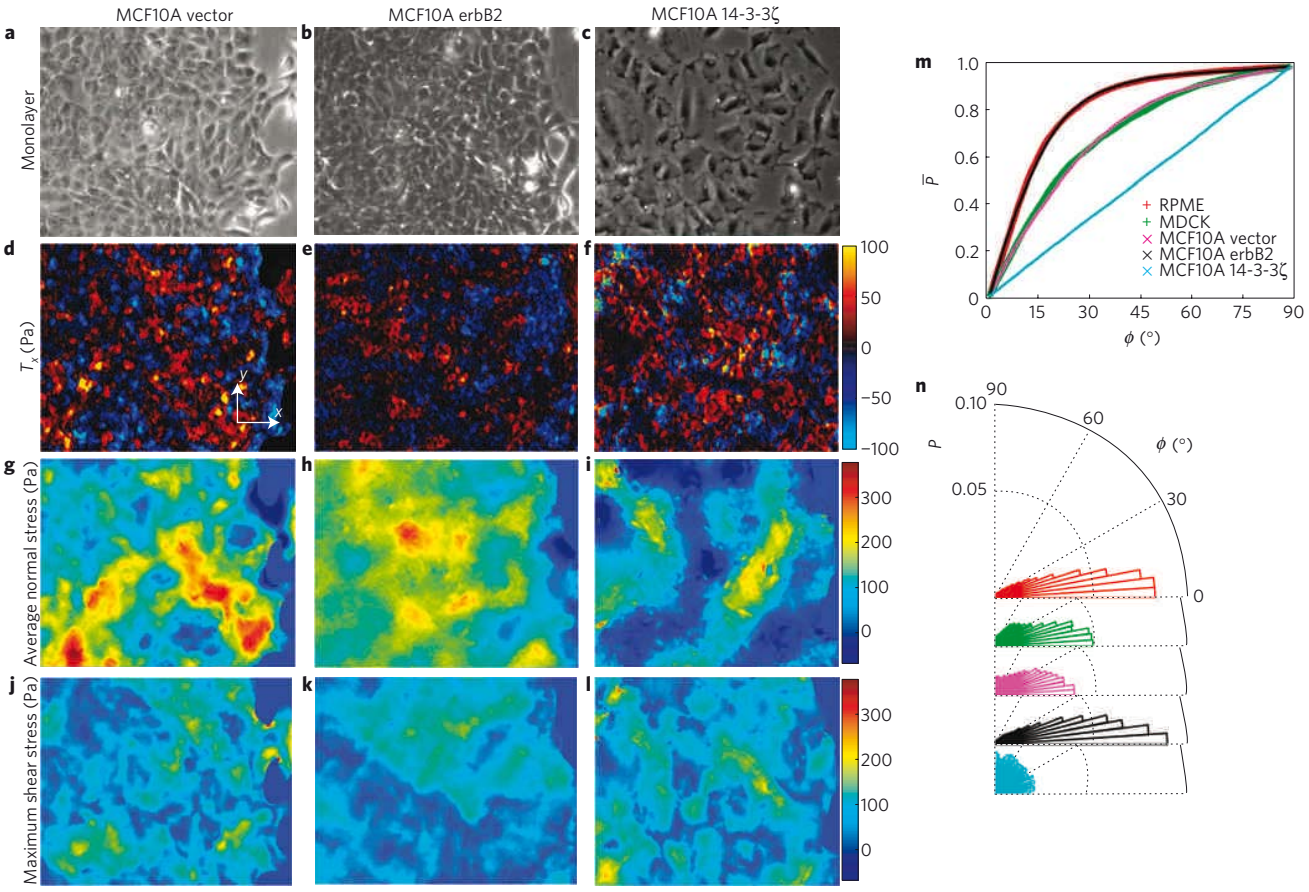

Figure 3 | Stress maps and migration in monolayers of breast-cancer model systems. Phase contrast image of nontransformed human mammary epithelial cell line, MCF10A, control or vector (**a**), cells overexpressing ErbB2 (**b**), and 14-3-3ζ (**c**). Maps of cell–substrate tractions, T_x, (**d**–**f**), normal stress (**g**–**i**), and maximum shear stress (**j**–**l**) corresponding to each of these three mammary epithelial cell lines. **m**, Cumulative probability distribution of ϕ for the regions corresponding to the highest quintile of the shear stress for five different cell sheets. **n**, Distributions corresponding to the curves in **m**. Vertical size of the images of monolayers: 410 μm. Each curve in **m** has more than 8,000 observations.

establish that transmission of mechanical stresses from cell-to-cell across many cells is necessary for plithotaxis, that is, for each individual cell to follow the local orientation of the maximal principal stress.

For collective migration to be coordinated across many cells, intercellular stresses might be expected to be cooperative over comparable distances; cooperativity of cell motions has been recently established[20,21], but cooperativity of cellular stresses has not. To quantify the spatial extent of any such stress cooperativity, we first examined the spatial autocorrelation function of the average normal stress:

$$C(R) = \frac{1}{N\mathrm{var}(\bar{\sigma})^2} \sum_{i,j=1}^{N} \sum_{|\mathbf{r}_i - \mathbf{r}_j| = R} \delta\bar{\sigma}_i \cdot \delta\bar{\sigma}_j$$

where $\delta\bar{\sigma}_i$ is the local departure of the average normal stress at position $\mathbf{r}_i$ from its spatial mean $\langle\bar{\sigma}_i\rangle$, $\mathrm{var}(\bar{\sigma})$ is the variance of those departures, and the notation $|\mathbf{r}_i - \mathbf{r}_j| = R$ means equality within a uniform bin width of 5 μm. Confining the attention to regions many cell lengths from the leading edge of an MDCK monolayer (Fig. 5a), fluctuations in normal stress (Fig. 5c) were found to be correlated over a length scale of approximately 10–15 cell diameters (Fig. 5e, blue). Cooperativity of normal stresses over 10–15 cell diameters might be attributable to alignment of principal stresses end-to-end, as in a tug-of war, or side-by-side, as police who lock arms during crowd control. To assess whether normal stresses are aligned according to either of these configurations, we decomposed the maximum principal stress into end-to-end and side-by-side contributions,

$$C_{\mathrm{end}}(R) = \frac{1}{N\|F\|^2} \sum_{i,j=1}^{N} \sum_{|\mathbf{r}_i - \mathbf{r}_j| = R} \mathbf{F}_i \cdot \mathbf{F}_j \cos^2\theta_{ij}$$

$$C_{\mathrm{side}}(R) = \frac{1}{N\|F\|^2} \sum_{i,j=1}^{N} \sum_{|\mathbf{r}_i - \mathbf{r}_j| = R} \mathbf{F}_i \cdot \mathbf{F}_j \sin^2\theta_{ij}$$

where $\|\cdots\|$ denotes L^2 norm, F_i is the local maximal principal stress considered as a vector quantity (such that the angle between the maximal and minimal principal stress orientations is taken modulo π) and θ_{ij} is the angle between adjacent vector pairs. The two components were found to contribute almost equally to force cooperativity, thus indicating the coexistence of both end-to-end and side-by-side force correlations (Fig. 5f). Simply put, to move cooperatively, neighbouring cells join forces.

Cooperative motions emerge naturally in inert particulate systems that exhibit close-packing, structural disorder, and glassy dynamics, such as colloidal glasses[22]. A central feature that identifies these systems as being glassy is the slowing of internal structural rearrangement as system density is increased; with

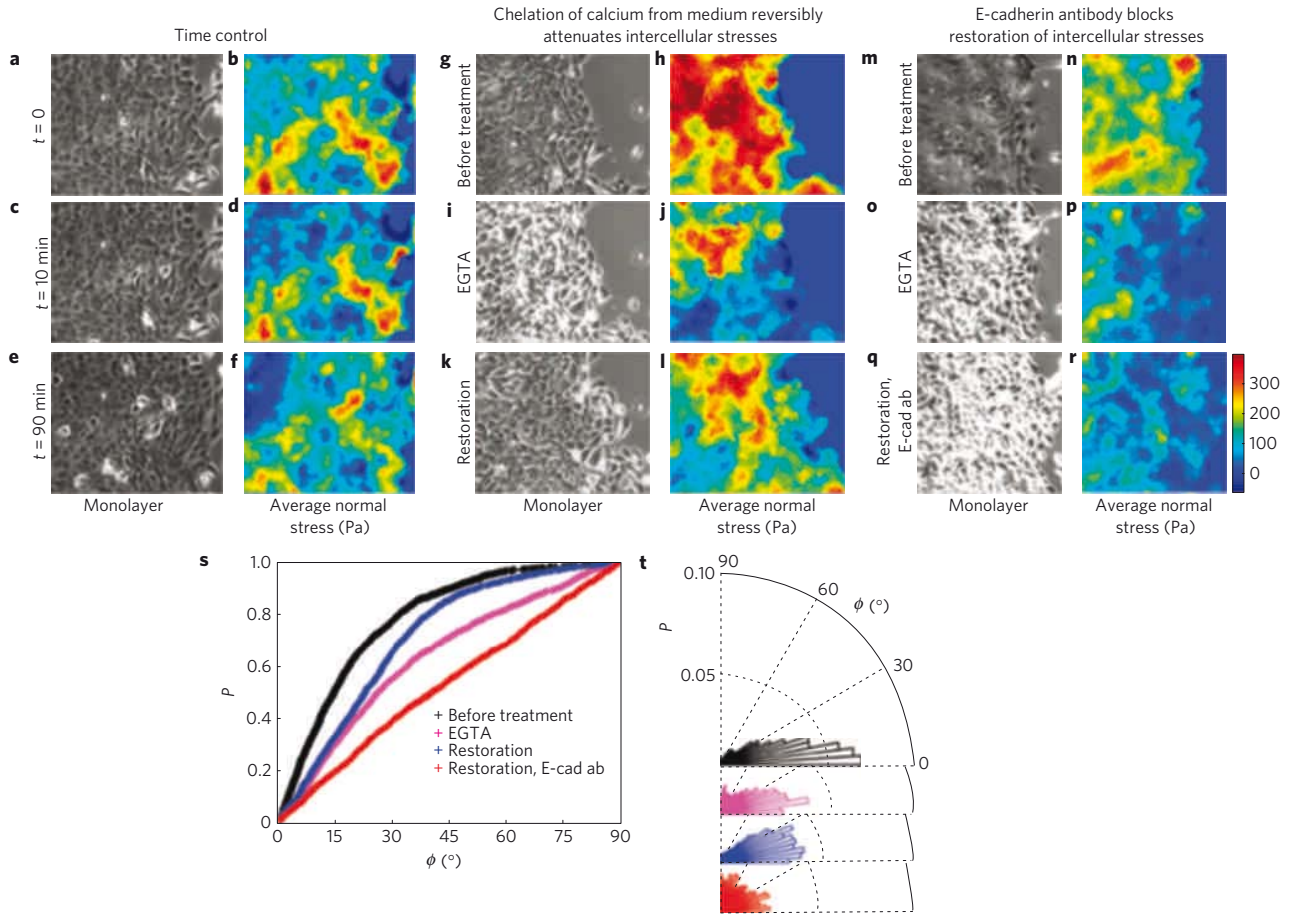

Figure 4 | Local cell guidance requires force transmission from cell-to-cell. Time-controls of intercellular stress maps of MCF10A-vector cell monolayers (**a**–**f**). The stress patterns do not change appreciably over a period of 80 min. After 10 min in the presence of the calcium chelator ethylene glycol tetraacetic acid (EGTA) (4mM), however, cells lose contacts with their neighbours (**g**,**i** and **m**,**o**). These changes lead to attenuation of intercellular average normal stress (**h**,**j** and **n**,**p**). After returning to the normal growth medium for 80 min, the stresses and cell–cell contacts are largely restored (**k**,**l**), but if the growth medium is supplemented with E-cadherin antibody (7 μg ml^{-1}) recovery of the stresses and cell–cell contacts is blocked (**q**,**r**). EGTA treatment widens the distribution of angle (ϕ) between the local cellular velocity and the local maximum principal orientation corresponding to highest of the maximum shear stress quintiles (**s**,**t**). The distribution of ϕ is narrowed if calcium is restored (**s**,**t**, blue), but widened further if the restoration medium is supplemented with E-cadherin antibody (**s** and **t**, red). Together, these data show that local cell guidance along the orientation of maximal principal stress (plithotaxis) requires force transmission across cell–cell junctions. These preferred orientations correspond to those engendering minimal intercellular shear stresses. Increased intensity at cell boundaries in phase contrast images (**i**,**o**, and **q**) reveals disruption of cell–cell junctions. Vertical size of the images of monolayers: 410 μm. Each data set in **s** and **t** has more than 1,500 observations.

increasing system density, each particle becomes increasingly trapped by its neighbours so that, to rearrange at all, many neighbouring particles must rearrange cooperatively[23]. As such, the size of cooperative clusters increases as system density increases. Moreover, as the size of the cluster grows the number of possible structural rearrangements decreases and, as such, the time needed for cooperative rearrangements increases precipitously until, eventually, the system becomes virtually frozen, or stuck[23]. Cooperative cellular motions within the monolayer sheet exhibit these very signatures of glassy dynamics[24,25], but to what extent might cellular stresses depict a complementary physical picture? To answer this question we analysed the motion of the MDCK monolayers as cellular density increased with the passage of time[15,20]. Consistent with an expectation of glassy dynamics, the spatial decay in $C(r)$ was smaller when the density was greater (Fig. 5e, red curve with corresponding monolayer and force map Fig. 5b,d), indicating that force cooperativity extended to greater distances. As a direct measure of slowing of structural rearrangements we turned to metrics commonly used in soft condensed matter systems. We consider the average number of cells which change position between two points in time, which defines an overlap function q_s:

$$q_s = \frac{1}{N}\sum_{1}^{N} w(|\mathbf{r}_i(t) - \mathbf{r}_i(t=0)|)$$

where the weight function w is equal to one if the distance between cell positions at sequential times is less than half a cell diameter, and zero otherwise. The variance of q_s is then a measure of the rate of overall structural rearrangement[26] and is related to the so-called four-point susceptibility χ^{ss}. The peak in χ^{ss} occurs at the overall structural relaxation time, and the height of that peak is related to the size of rearranging regions[27,28]. If the system is glassy, the peak in χ^{ss} is expected to shift towards longer times as system density is increased, and a clear shift of the peak in the more dense system confirms this expectation (Fig. 5g). The peak height also increases in the more dense system, confirming the presence of growing velocity clusters. Moreover,

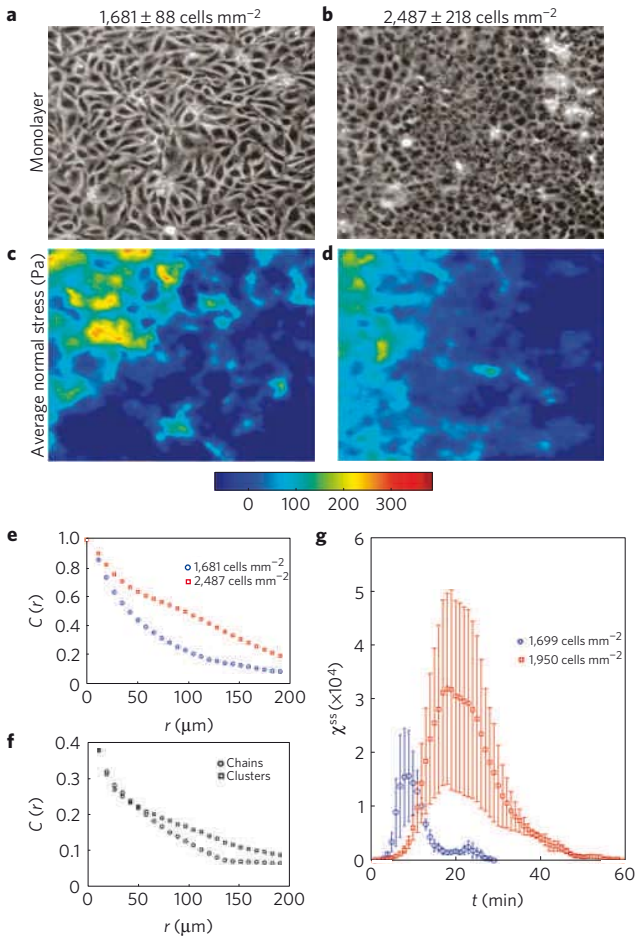

Figure 5 | Signatures of cooperativity and associated glassy dynamics. Phase contrast images of a monolayer of MDCK cells well away from the leading edge at early (**a**, $t = 196$ min, density $= 1{,}681 \pm 88$ cells mm^{-2}) and late (**b**, $t = 3{,}196$ min, density $= 2{,}487 \pm 218$ cells mm^{-2}) times. Also shown are corresponding maps of average normal stress (**c**,**d**). Note that any contribution to the stress field with a wavelength longer than the size of the field of view is not included in the calculation. Thus a stress build up extending over the entire monolayer as previously reported[15] is absent from this analysis. **e**, Time-averaged spatial autocorrelation function, $C(r)$, of average normal stress in low-density (1,681 cells mm^{-2}, blue) and high-density (2,487 cells mm^{-2}, red) regions. **f**, $C(r)$ of high-density maximal principal stress resolved into components representing force chains (circles) and force clusters (squares). **g**, Variance, χ^{ss}, of the self-overlap parameter, q_s, as a function of time, in early, low-density ($t = 1$–270 min, $1{,}699 \pm 40$ cells mm^{-2}, blue) and late, high-density ($t = 1{,}800$–$2{,}070$ min, $1{,}950 \pm 156$ cells mm^{-2}, red) intervals. Each curve represents an average over three successive 90 min windows of similar density. Error bars represent the standard deviation over the square root of the number of windows. Vertical size of the images of the monolayer: 480 μm.

these density-dependent shifts in the position and the peak height of χ^{ss}, which are indicative of slowing of structural rearrangements, occur simultaneously with growth of force clusters, as indicated by the slowing decay in the force autocorrelation function with increasing density (Fig. 5e, red). Although a mechanistic link between inter-particle forces and spatially heterogeneous dynamics in glassy systems remains unclear[29–31], the findings of Fig. 5 are consistent with an approach to a glass transition (Supplementary Information S9).

Recent advances have unravelled important features of stress transmission across specific molecular constituents of the focal adhesion and of the adherens junction, including vinculin, talin, and α-catenin for example[14,32–37], but the integrative context of these molecular events within integrated stress-bearing structures comprising highly redundant molecular pathways, or even across multi-cellular assemblies at larger scales of organization, have remained largely ambiguous. Logically, associated integrative principles have remained unstudied. Because distinct stress tensor components between contiguous cells in any complex living system have never before been measured, monolayer stress microscopy now sets the study of underlying molecular events within an integrative mechanical context that is conceptually comprehensive and experimentally rigorous. The finding that each cell comprising a monolayer tends to migrate and remodel so as to maintain minimal local intercellular shear stress complements other integrative physiological principles (Supplementary Information S10).

A central question in morphogenesis and disease is how differentiated structures emerge from homogeneous cell populations[38]. Differentiation and pattern formation in multi-cellular systems is currently explained by the existence of morphogen gradients and by local variations in the composition, topology, and stiffness of the extracellular matrix[39]. In addition, once transduced by the sensory machinery of the individual cell[40], the spontaneously emergent rugged stress landscape reported here would be expected to trigger non-uniform secretion of soluble or insoluble factors, thus altering the local cellular microenviroment, causing cytoskeletal reinforcement[41] or cytoskeletal fluidization[42,43], as well as activating in a highly non-uniform fashion stress-dependent genetic programs that give rise to differentiated tissues. These emergent stress heterogeneities are severe and persistent, but unanticipated. How they might become harnessed and regulated during morphogenesis or repair and, perhaps more importantly, how they might become unharnessed or dysregulated during disease or injury, we identify here as major open questions, but ones that are now accessible to direct experimental attack.

Received 27 November 2010; accepted 12 April 2011; published online 22 May 2011

References

1. Kumar, S. & Weaver, V. M. Mechanics, malignancy, and metastasis: The force journey of a tumor cell. *Cancer Metastasis Rev.* **28,** 113–127 (2009).
2. Butcher, D. T., Alliston, T. & Weaver, V. M. A tense situation: Forcing tumour progression. *Nat. Rev. Cancer* **9,** 108–122 (2009).
3. Discher, D. *et al.* Biomechanics: Cell research and applications for the next decade. *Ann. Biomed. Eng.* **37,** 847–859 (2009).
4. Levental, K. R. *et al.* Matrix crosslinking forces tumor progression by enhancing integrin signaling. *Cell* **139,** 891–906 (2009).
5. Paszek, M. J. & Weaver, V. M. The tension mounts: Mechanics meets morphogenesis and malignancy. *J. Mammary Gland Biol. Neoplasia* **9,** 325–342 (2004).
6. Bianco, A. *et al.* Two distinct modes of guidance signalling during collective migration of border cells. *Nature* **448,** 362–365 (2007).
7. Friedl, P. & Gilmour, D. Collective cell migration in morphogenesis, regeneration and cancer. *Nat. Rev. Mol. Cell Biol.* **10,** 445–457 (2009).
8. Giampieri, S. *et al.* Localized and reversible TGF[β] signalling switches breast cancer cells from cohesive to single cell motility. *Nature Cell Biol.* **11,** 1287–1296 (2009).
9. Montell, D. Morphogenetic cell movements: Diversity from modular mechanical properties. *Science* **322,** 1502–1505 (2008).
10. Shaw, T. J. & Martin, P. Wound repair at a glance. *J. Cell Sci.* **122,** 3209–3213 (2009).
11. Simpson, K. J. *et al.* Identification of genes that regulate epithelial cell migration using an siRNA screening approach. *Nature Cell Biol.* **10,** 1027–1038 (2008).
12. Vitorino, P. & Meyer, T. Modular control of endothelial sheet migration. *Genes Dev.* **22,** 3268–3281 (2008).
13. Bindschadler, M. & McGrath, J. L. Sheet migration by wounded monolayers as an emergent property of single-cell dynamics. *J. Cell Sci.* **120,** 876–884 (2007).

14. Liu, Z. *et al.* Mechanical tugging force regulates the size of cell–cell junctions. *Proc. Natl Acad. Sci. USA* **107,** 9944–9949 (2010).
15. Trepat, X. *et al.* Physical forces during collective cell migration. *Nature Phys.* **5,** 426–430 (2009).
16. DePaola, N., Gimbrone, M. Jr, Davies, P. & Dewey, C. Jr Vascular endothelium responds to fluid shear stress gradients. *Arteriosclerosis Thrombosis* **12,** 1254–1257 (1992).
17. Farooqui, R. & Fenteany, G. Multiple rows of cells behind an epithelial wound edge extend cryptic lamellipodia to collectively drive cell-sheet movement. *J. Cell Sci.* **118,** 51–63 (2005).
18. Lu, J. *et al.* Breast cancer metastasis: Challenges and opportunities. *Cancer Res.* **69,** 4951–4953 (2009).
19. Muthuswamy, S. K., Li, D., Lelievre, S., Bissell, M. J. & Brugge, J. S. ErbB2, but not ErbB1, reinitiates proliferation and induces luminal repopulation in epithelial acini. *Nature Cell Biol.* **3,** 785–792 (2001).
20. Angelini, T. E., Hannezo, E., Trepat, X., Fredberg, J. J. & Weitz, D. A. Cell migration driven by cooperative substrate deformation patterns. *Phys. Rev. Lett.* **104,** 168104 (2010).
21. Szabó, B. *et al.* Phase transition in the collective migration of tissue cells: Experiment and model. *Phys. Rev. E* **74,** 061908 (2006).
22. Parisi, G. & Zamponi, F. Mean-field theory of hard sphere glasses and jamming. *Rev. Mod. Phys.* **82,** 789–845 (2010).
23. Weeks, E. R., Crocker, J. C., Levitt, A. C., Schofield, A. & Weitz, D. A. Three-dimensional direct imaging of structural relaxation near the colloidal glass transition. *Science* **287,** 627–631 (2000).
24. Angelini, T. E. *et al.* Glass-like dynamics of collective cell migration. *Proc. Natl Acad. Sci. USA* **108,** 4714–4719 (2011).
25. Garrahan, J. P. Dynamic heterogeneity comes to life. *Proc. Natl Acad. Sci. USA* **108,** 4701–4702 (2011).
26. Berthier, L. *et al.* Direct experimental evidence of a growing length scale accompanying the glass transition. *Science* **310,** 1797–1800 (2005).
27. Keys, A., Abate, A., Glotzer, S. C. & Durian, D. J. Measurement of growing dynamical length scales and prediction of the jamming transition in granular material. *Nature Phys.* **3,** 260–264 (2007).
28. Toninelli, C., Wyart, M., Berthier, L., Biroli, G. & Bouchaud, J-P. Dynamical susceptibility of glass formers: Contrasting the predictions of theoretical scenarios. *Phys. Rev. E* **71,** 041505 (2005).
29. Hall, R. W. & Wolynes, P. G. Intermolecular forces and the glass transition. *J. Phys. Chem. B* **112,** 301–312 (2007).
30. Mueth, D. M., Jaeger, H. M. & Nagel, S. R. Force distribution in a granular medium. *Phys. Rev. E* **57,** 3164–3169 (1998).
31. Trappe, V., Prasad, V., Cipelletti, L., Segre, P. N. & Weitz, D. A. Jamming phase diagram for attractive particles. *Nature* **411,** 772–775 (2001).
32. del Rio, A. *et al.* Stretching single talin rod molecules activates vinculin binding. *Science* **323,** 638–641 (2009).
33. Grashoff, C. *et al.* Measuring mechanical tension across vinculin reveals regulation of focal adhesion dynamics. *Nature* **466,** 263–266 (2010).
34. Hu, K., Ji, L., Applegate, K. T., Danuser, G. & Waterman-Storer, C. M. Differential transmission of actin motion within focal adhesions. *Science* **315,** 111–115 (2007).
35. le Duc, Q. *et al.* Vinculin potentiates E-cadherin mechanosensing and is recruited to actin-anchored sites within adherens junctions in a myosin II-dependent manner. *J. Cell Biol.* **189,** 1107–1115 (2010).
36. Rajfur, Z., Roy, P., Otey, C., Romer, L. & Jacobson, K. Dissecting the link between stress fibres and focal adhesions by CALI with EGFP fusion proteins. *Nature Cell Biol.* **4,** 286–293 (2002).
37. Yonemura, S., Wada, Y., Watanabe, T., Nagafuchi, A. & Shibata, M. α-Catenin as a tension transducer that induces adherens junction development. *Nature Cell Biol.* **12,** 533–542 (2010).
38. Engler, A. J., Humbert, P. O., Wehrle-Haller, B. & Weaver, V. M. Multiscale modeling of form and function. *Science* **324,** 208–212 (2009).
39. Le Goff, L. & Lecuit, T. Gradient scaling and growth. *Science* **331,** 1141–1142 (2011).
40. Geiger, B., Spatz, J. P. & Bershadsky, A. D. Environmental sensing through focal adhesions. *Nature Rev. Mol. Cell Biol.* **10,** 21–33 (2009).
41. Roca-Cusachs, P., Gauthier, N. C., del Rio, A. & Sheetz, M. P. Clustering of α5β1 integrins determines adhesion strength whereas αvβ3 and talin enable mechanotransduction. *Proc. Natl Acad. Sci. USA* **106,** 16245–16250 (2009).
42. Krishnan, R. *et al.* Reinforcement versus fluidization in cytoskeletal mechanoresponsiveness. *PLoS ONE* **4,** e5486 (2009).
43. Trepat, X. *et al.* Universal physical responses to stretch in the living cell. *Nature* **447,** 592–595 (2007).

Acknowledgements

For their critical comments, we thank R. Hubmayr (Mayo Clinic), R. Phillips (CalTech), D. Navajas (University of Barcelona), L. B. Freund (Brown University), D. Tschumperlin (Harvard University), C. Forbes Dewey, Jr (MIT) and V. B. Shenoy (Brown University). We acknowledge the support of the European Research Council (Starting Grant FP7/ERC-242993), the Spanish Ministry of Science and Innovation (BFU2009-07595) and the National Institutes of Health (R01HL102373, R01HL107561, R01CA132633). We thank D. Yu (MDACC) for the kind gift of MCF-10A cell lines.

Author contributions

D.T.T. developed algorithms and performed stress measurements. C.C.H. analysed data pertaining to force chains and glassy dynamics. D.T.T. and T.E.A. performed measurements of cell motions. K.R. and C.Y.P. assisted in protocol design and optimization. C.Y.P. performed staining of actin cytoskeleton. X.S-P. performed additional stress measurements on MDCK cells. M.H.Z. provided cancer cell lines and assisted with related data interpretation. D.T.T. and E.H.Z. made early conceptual contributions. J.P.B., D.A.W., J.J.F. and X.T. guided data interpretation and analysis. D.T.T., C.C.H., J.P.B., X.T. and J.J.F. wrote the manuscript.

Additional information

The authors declare no competing financial interests. Supplementary information accompanies this paper on www.nature.com/naturematerials. Reprints and permissions information is available online at http://www.nature.com/reprints. Correspondence and requests for materials should be addressed to J.J.F. or X.T.

nature materials

SUPPLEMENTARY INFORMATION

DOI: 10.1038/NMAT3025

COLLECTIVE CELL GUIDANCE BY COOPERATIVE INTERCELLULAR FORCES.

Supporting Online Material

DT Tambe, CC Hardin, TE Angelini, K Rajendran, CY Park, X Serra-Picamal, EH Zhou, MH Zaman, JP Butler, DA Weitz, JJ Fredberg, X Trepat

Supplement 1. Monolayer Stress Microscopy.

Within the monolayer, physical forces are transmitted between each cell and its substrate, which are called traction forces, and between each cell and its immediate neighbors, which are called the intercellular forces (Fig. S1). The local intercellular force per unit area of contact defines the local intercellular stress, which comprises two mutually independent components: the normal stress (depicted as red arrows acting perpendicular to the local cell-cell junction) and the shear stress (depicted as a blue arrow acting parallel to the local cell-cell junction). These stresses at the cell-cell junction necessarily extend into and become supported by mechanical stresses within the cell body.

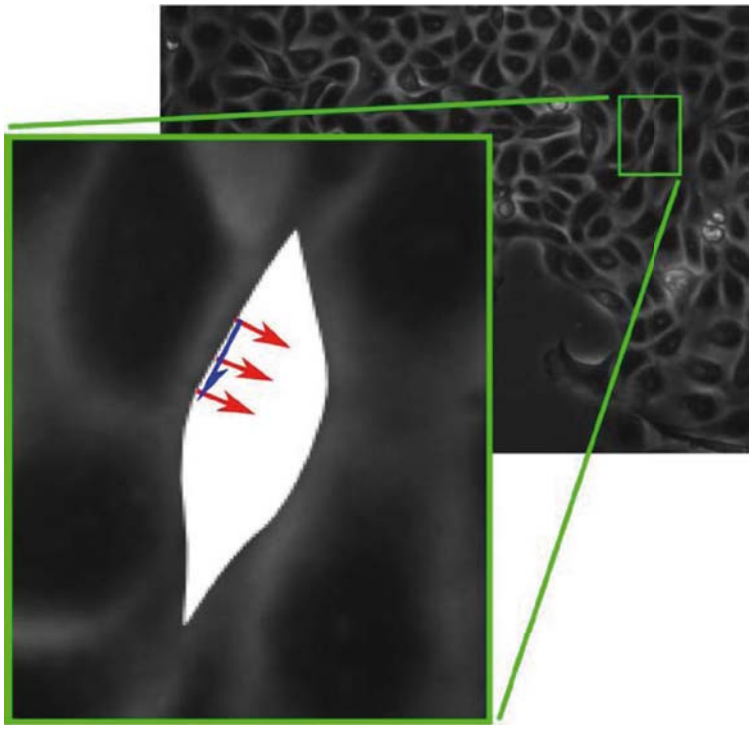

Figure S1 | Mechanical forces in sheet of migrating cells.

We have previously introduced a method to measure the distribution of traction forces that an advancing cellular monolayer exerts on its substrate.[1, 2] Here we build upon that approach in order to measure not just those traction forces, but from these data to measure the intercellular normal stresses and shear stresses that each cell exerts upon its immediate neighbors.

General approach: The intercellular stress is a local outcome of the overall balance of cell-substrate tractions across the entire monolayer as demanded by Newton's laws. Traction forces exerted locally by each cell on the substrate are balanced at distances significantly larger than the size of the cell, however.[2] Local variations in monolayer height can induce moments and out-of-plane stresses in principle, but the lateral extent of the monolayers in question here is at least three orders of magnitude greater than the thickness, and that thickness is approximately uniform (Fig. S4). Such a system therefore lends itself naturally to a formal two-dimensional balance of line tensions (force per unit length) in a system of zero thickness, and makes recovery of intercellular line tensions rigorous.

Only as a matter of computational convenience, we calculate this two-dimensional force balance within the monolayer by representing the cellular monolayer instead as a thin elastic sheet. This is permissible because, if the traction distribution is known, then the force balance itself does not depend upon cell material properties. Line tensions (in units of force per unit length) and the more familiar units of stress (force per unit area) are related through a uniform monolayer height, h (Supplement 4), but the underlying force balance itself, being two-dimensional, does not depend upon the assumption of uniform cell height. For simplicity, therefore, and without loss of generality, the remainder of the text deals solely in terms of familiar stress components.

DOI: 10.1038/NMAT3025

As such, the internal stress tensor $\sigma_{ij}(x,y)$ is treated as plane stress in the x,y plane, where i and j run over the coordinates x,y; all stress components associated with the z direction vanish. The measured local tractions $T_i(x,y)$ are the components of the shear stresses exerted *by* the cells *on* the substrate, and hence by Newton's third law, the forces exerted *by* the substrate *on* the monolayer are simply the negative of these tractions. Since at any instant there is no net force on the monolayer as a whole, these tractions must precisely balance the internal stresses generated within the monolayer. This balance of forces is formally represented by the equations of mechanical equilibrium,

$$\sigma_{ij,j} = T_i \qquad \text{(Eq. S1)}$$

where we use the Einstein convention of summation over repeated indices and $()_{,j}$ denotes $\partial / \partial x_j$. From the form of Eq. S1, it is clear that the source term on the right hand side can be thought of equivalently as a body force, although one that is nonuniform and time-varying. The internal stresses, σ_{ij}, are those required to balance the measured traction forces irrespective of whether monolayer material is active or passive, elastic or visco-elastic, linear or nonlinear. The key assumption is only that the monolayer is treated as a continuum.

Boundary conditions and boundary artifacts: Eq. S1 describes an elliptical boundary value problem. Boundary conditions on the free edge of the monolayer were taken to be homogeneous in stress, $\sigma_{ij}n_j = 0$. Boundary conditions at the edges of the field of view (shown by red lines in Fig. S2 a) were taken as zero normal displacement, $u_j n_j = 0$, where n_j denotes the components of the vector normal to the boundary. Imposition of this zero normal displacement condition is physically equivalent to continuing the monolayer outside the field of view as a mirror image, but this continuation introduces artifactual reaction forces along the boundary. Depending upon their spatial distribution, the stresses due to these reaction forces decay as $1/r$ or faster, but far from the edges the local stress field is dominated by the source term – the traction forces, T_i. As such, regions in which the boundary effects contribute appreciably to the result can be cropped out. Here we report measurements in a region that is beyond 130 μm from the field of view edges, as this inner region is largely free of boundary artifacts. To quantify associated errors we made scatter plots of average normal stresses within the inner as calculated from the maximum (actual) field of view edges against those calculated from successively smaller (cropped) fields of view. Up to a cropping distance of 60 μm from the maximum field of view, the average normal stresses within the inner region were strongly correlated ($r^2 > 0.98$, $0 <$ intercept< -20Pa, and $1 <$ slope < 0.95), thus establishing insensitivity of stresses in the inner region to the placement of the boundary.

Principal stresses and principal orientations: Eigenvalue decomposition of the stress tensor defines the principal stresses ($\sigma_{\max}$ and $\sigma_{\min}$) and the corresponding mutually perpendicular eigenvectors define the local orientation of these stresses. By definition, each of these eigenvectors also defines the orientation of zero shear stress. We also compute the scalar tension within the sheet which is local average normal stress, defined as $(\sigma_{\max} + \sigma_{\min})/2$.

Implementation by finite element analysis (FEA): Solving the equilibrium equations is equivalent to solving the boundary value problem of minimization of total potential energy per unit thickness of the monolayer defined by $\Pi = \iint_R \left(\frac{1}{2}\sigma_{ij}\varepsilon_{ij} - u_j T_j \right) dxdy$, where ε_{ij} is the planar strain tensor, and R is the bounded domain, subjected to the boundary conditions described above. We minimize this functional with respect to displacements $u_j(x,y)$ such that conditions at the domain boundaries are satisfied, as described

below. From these displacements, which are automatically compatible, we compute both strains and stresses in the monolayer.

As noted above, the specific material properties of the monolayer have no effect on the recovered distribution of intercellular forces. Without loss of generality, therefore, the monolayer is treated as an isotropic homogeneous elastic sheet with Young's modulus of 10kPa, Poisson's ratio of 0.5, and height of 5 μm. This sheet is uniformly discretized into four-node square elements (Fig S2, b, c) such that the FEA grid matches the traction grid recovered from FTTM. This grid is dense enough so that the internal stresses essentially independent of the size of elements.

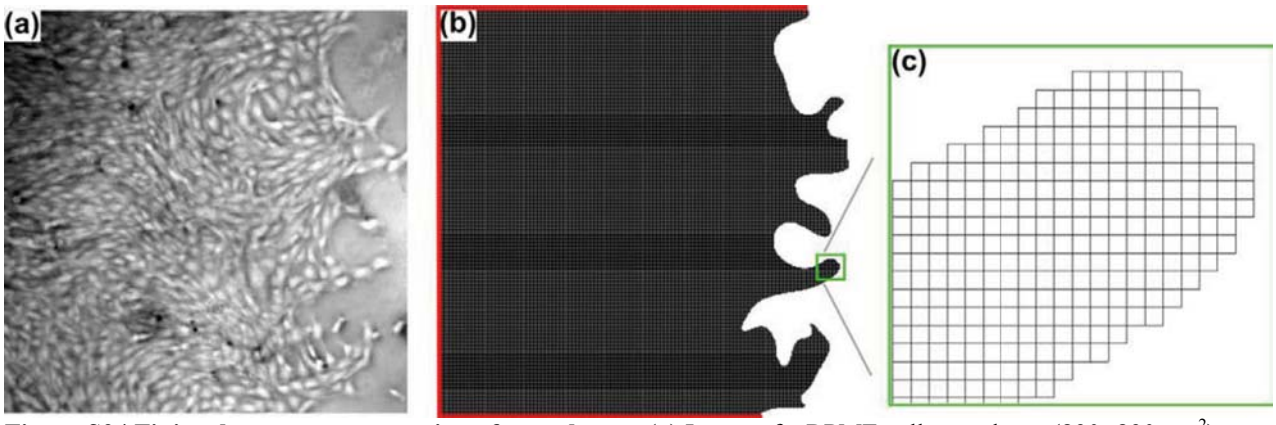

Figure S2 | Finite element representation of monolayer. (**a**) Image of a RPME cell monolayer (890×890 μm^2) bounded by a free edge on one side and edges defined by the field of view (red lines) on other three sides. (**b**) The monolayer is discretized uniformly with four node square elements. (**c**) Magnified view of a local region in (**b**) (each square is 2.61×2.61 μm^2).

This FEA scheme then transforms the boundary value problem into a system of linear equations, which are solved for the local displacements using standard Cholesky factorization. From these displacements we calculate stresses through the constitutive equation $\sigma_{ij} = \frac{2}{3} E\left(\varepsilon_{ij} + \varepsilon_{kk}\delta_{ij}\right)$ where δ_{ij} is the Kronecker delta. Explicitly, σ_{xx} and σ_{yy} are normal stresses along the laboratory $x-$ and $y-$axes, and $\sigma_{xy}(=\sigma_{yx})$ is the shear stress, also in the laboratory frame. Diagonalizing σ_{ij} amounts to a rotation, equivalent to the eigenvalue decomposition noted above, from which the principal stresses are obtained, and in this rotated system the shear stresses are zero. The entire FEA scheme is implemented using an in-house FORTRAN90 program.

Effect of isotropy and homogeneity of the material properties: Anisotropy and heterogeneity of material properties can influence the magnitude of stresses, but contribute only weakly to the recovery of orientation of planes with zero shear stress. This weak dependence is confirmed through the observation on RPME cells that the maximal principal stress orientations which are local axis of highest tension aligns with the cell orientation (Fig. 2 g and Fig S5) which, for these spindle-like cells, is largely orientation of actin stress fibers.

Measurement of gel deformation: As described previously[2], traction forces were determined from gel deformations. Gel deformations were quantified from images of embedded fluorescent markers after correcting for microscope stage drift. By contrast with our previous report [2], however, here we corrected for stage drift using an improved and simplified method. We begin with a phase contrast image of cells and a fluorescent image of markers embedded near the surface of the gel, and then acquire subsequent image pairs at 5 minute intervals for a period of 3-4 hours. To correct for stage drift, in these subsequent fluorescent

DOI: 10.1038/NMAT3025

images we matched embedded markers in an unstrained region of the gel with the same markers from the first fluorescent image. This drift correction was achieved with the help of an in-house image acquisition program developed using MATLAB. This technique of recording gel deformation provides highly reproducible and precise measurements. At the end of the experiment, cells were detached from the gel surface with isotonic 10X trypsin for 1 h followed by acquisition of drift corrected reference image of the fluorescent markers. All experiments were conducted in culture environment (37^{o}C, and 5% CO_2) on an inverted optical microscope at magnification 7.5X for RPME cells and 10X for other cells.

Measurement of cellular velocities: The cellular velocity field within the monolayer is measured by particle imaging velocimetry (PIV). Specifically, an image from sequence of phase contrast images recorded at an interval Δt is compared with the succeeding image. And window pairs, one to each image, are examined for cross correlation as a function of shifting window position. The shift of one window relative to the reference (window from image at earlier time) that maximizes the cross correlation function is taken as the displacement of the center of that window. Together with Δt, this determines the velocity of the central point of the reference window. This procedure is then repeated across the entire field, and a velocity map is constructed at each grid point in the pixelated plane. There is sufficient phase contrast between the cell interiors and the cell-cell boundary junctions such that this is a robust procedure within the sheet.

Fourier-transform traction microscopy: Algorithm used for traction mapping is same as reported by Trepat et al [2].

Supplement 2. Cell Culture.

Cell culture: All the cells were cultured on plastic flasks and incubated at 37ºC with 5% CO_2.

Cells	**Medium**
Madin-Darby canine kidney cells (MDCK) (strain II)	Modified Eagle's medium (MEM) with Earle's salts supplemented with 5% fetal bovine serum (FBS), 2mM l-glutamine, 100U/ml penicillin, and 100 g/ml streptomycin
Rat pulmonary microvascular endothelial cells (RPMEC)	Roswell Park Memorial Institute (RPMI-1640) supplemented with 10% FBS, 100 U/ml penicillin and, 100 g/ml streptomycin, and Fungizone [3].
MCF10A with overexpressing ErbB2 MCF10A with overexpressing HA-tagged 14-3-3ζ MCF10A control (vector)	Dulbecco's modified Eagle's medium (DMEM)/F12 supplemented with 5% donor horse serum, 20 ng/ml epidermal growth factor (EGF), 10 lg/ml insulin, 0.5 lg/ml hydrocortisone, 100 ng/ml cholera toxin, and antibiotics [4]

Cell seeding: A 4µl drop of dense cell solution (8 million cells/ml) was gently suspended on the center of the gel containing 2ml media. The cells were then kept at 37^{o}C and 5% CO_2 for 48 hours to form confluent circular monolayer that migrates radially outwards.

Preparation of polyacrylamide gel substrates: Polyacrylamide substrate preparation was similar to published protocol [2].

Supplement 3. Tractions exerted by the cells on its substrate.

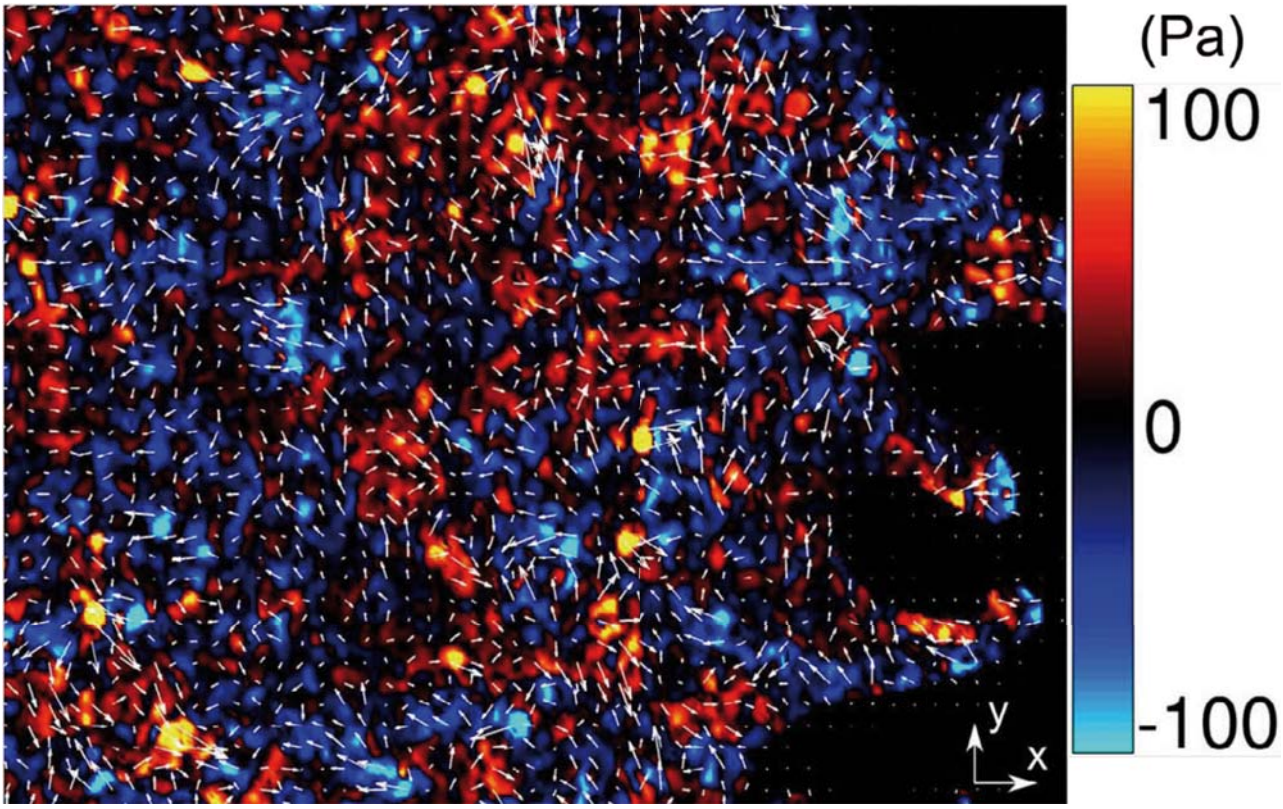

Figure S3 | Traction forces exerted by the RPME monolayer upon its substrate. Color-coded map of x-component of the traction force (corresponding to the monolayer shown in Fig. 2 a). Overlain upon this map are white arrows depicting complete traction vectors (both x and y components). Fluctuations of these tractions forces vary over length scales small compared with fluctuations of intercellular stresses (compare Fig. 2 c) because traction forces correspond to the gradient of those intercellular stresses (Eq. S1). Equivalently, Eq. S1 requires the rugged landscape of intercellular stress (Fig. 2 i) to arise from the pile-up (accumulation) of these tractions forces.

DOI: 10.1038/NMAT3025

Supplement 4. Monolayer height and its variations.

MSM is based upon nothing more than a rigorous two-dimensional force balance enforced in the cell plane. Since monolayer breadth greatly exceeds its height, a resulting state of plane stress provides computational convenience to the stress recovery procedure. Using confocal imaging of the monolayer we observe that, the first two cell rows excepted, monolayer height is roughly constant (Fig. S4). The recovered stress maps engenders errors in proportional to the ratio between the real and the assumed local monolayer height. As such, for regions greater than 20μm from the leading edge these errors would be smaller than 20%. Therefore, the profound ruggedness of the stress landscape and the associated long-range correlations of the maximum principal orientations cannot be attributed to these small variations in monolayer height.

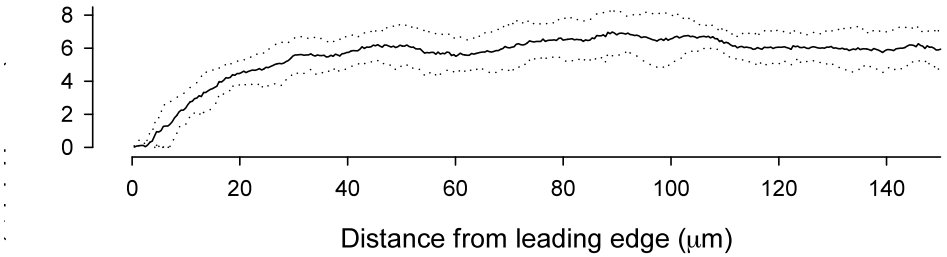

Figure S4 | Height of an MDCK monolayer expressing GFP-actin. Cell height measured using confocal microscopy (60X). The coefficient of variation is close to 20%. The solid line is the mean height and the dotted lines are mean ± standard deviation.

Supplement 5. In the endothelial monolayer, the long axis of the cell tends to align with the orientation of local maximum principal stress.

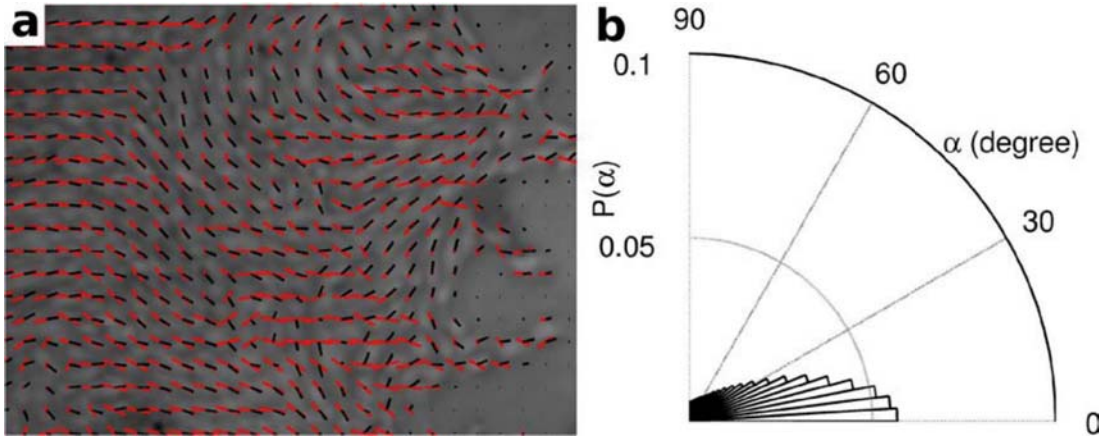

Figure S5 | Cells in RPME monolayers align with the local orientation of maximum principal stress. (**a**) Image of the RPME cell monolayer from Fig. 2 a. Shown here is an overlapped image of the orientation of long axis of the cells (black lines) and the orientation of maximum principal stresses (red lines). The local cellular orientation is the orientation of major axis of an ellipse that has same second-moments of 20x20 μm^2 region of the transmitted light image of the monolayer. The map of cell orientation is generated using image processing toolbox of MATLAB. (**b**) Distribution of angle, α, between the cell orientation and maximum principal stress orientation. The distribution is composed of more than 8000 observations. Vertical size of (**a**) is 545 μm.

Supplement 6. In the endothelial monolayer, the coarse actin structure tends to be aligned with the orientation of cell body.

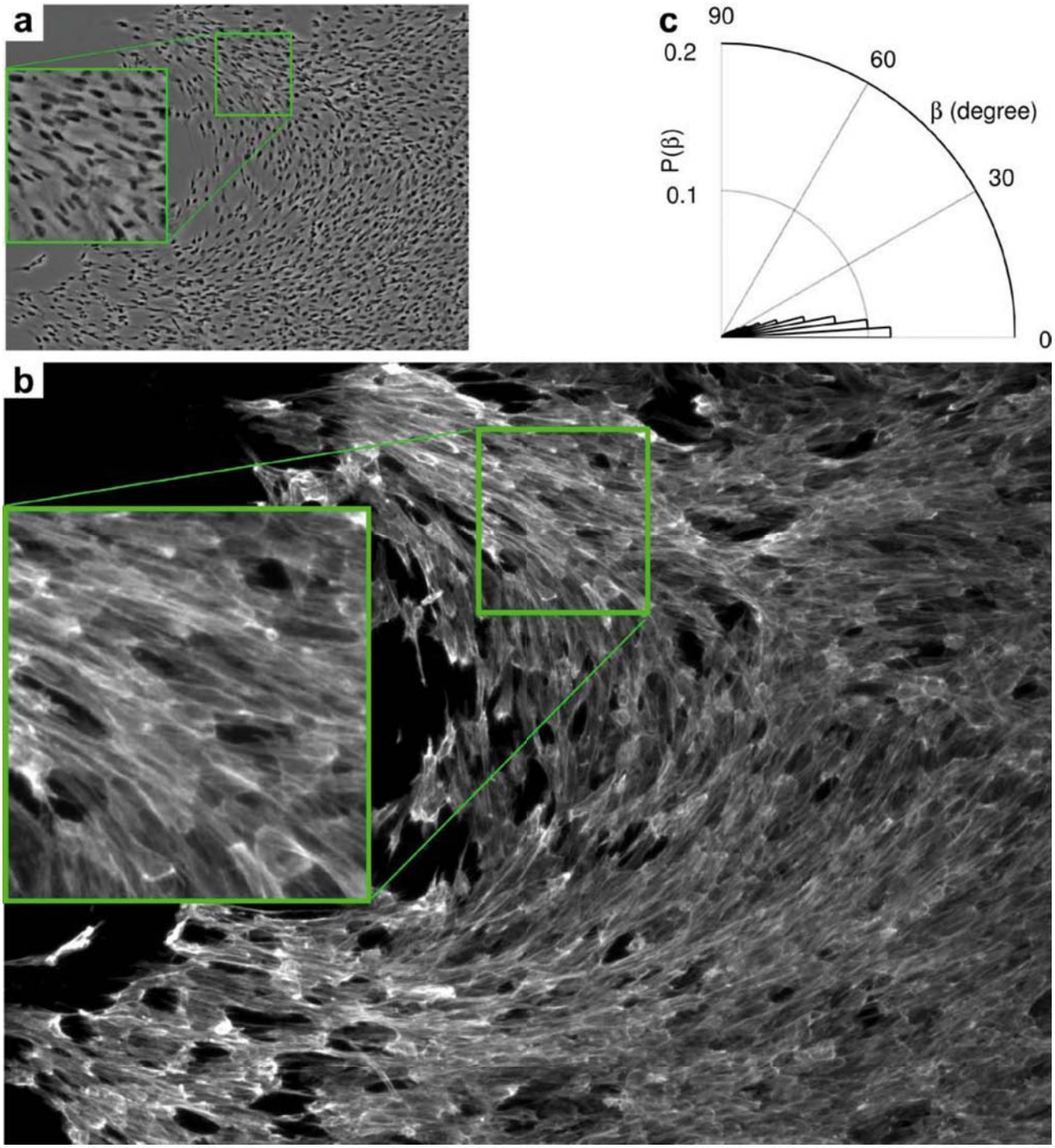

Figure S6 | In RPME cell monolayers, the orientation of the cell body and the orientation of coarse actin structures tend to be aligned. (**a**) Image of a RPME cell monolayer at 4X magnification. (**b**) Fluorescence image of actin structures (rhodamine phalloidin, Molecular Probes) [5]. (**c**) Distribution of angle, β, between the cell orientation from (**a**) and actin fiber orientation from (**b**). Local orientation of actin fibers is calculated using the same procedure used in calculating orientation of cells in (**a**) and in Fig. S5. Vertical size of (**a**) is 1700 μm.

DOI: 10.1038/NMAT3025

Supplement 7. Cells deep within the monolayer have cryptic lamellipodia.

Using a wound/scratch assay, Farooqui and Fenteany [6] reported that cells located many rows behind the leading edge protrude underneath their neighbors. They called these protrusions "cryptic lamellidopia". To test whether submarginal cells within an expanding MDCK monolayer also extend cryptic lamellipodia we seeded an epithelial colony containing MDCK cells stably expressing either actin-GFP or α-actinin-RFP (Nelson Lab, Stanford). Using confocal microscopy during expansion of the colony we observed abundant cryptic lamellipodia at least 20 rows behind the leading edge (Fig. S7). Therefore wounding is not required for the existence of cryptic lamellipodia in submarginal cells.

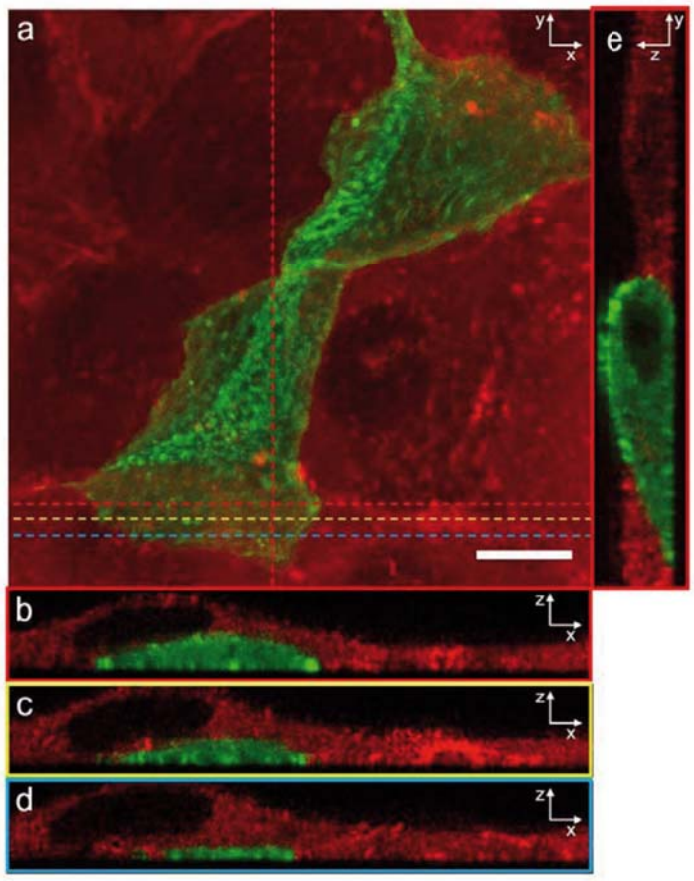

Figure S7 | Observation of lamellipodial protrusion by the submarginal cells within an expanding MDCK cell monolayer. (**a**) z-projection of submarginal cells (~20 cells away from the leading edge) in an expanding colony of MDCK cells expressing either actin-GFP or α-actinin-RFP. The bottom actin-GFP cell extends a cryptic lamellipodium under the neighboring α-actinin-RFP cell. The crytic lamellipodium is clearly visualized in panels (**b**), (**c**), and (**d**), which are xz sections (constant y) along the red, yellow, and blue dashed lines respectively. (**e**) yz section along the vertical red dashed line (constant x) shows the actin-GFP cell protruding under the α-actinin-RFP cell. Magnification 100X, resolution 1024×1024, scale bar 10 μm.

Supplement 8. Local average normal stress does not account for local cell guidance.

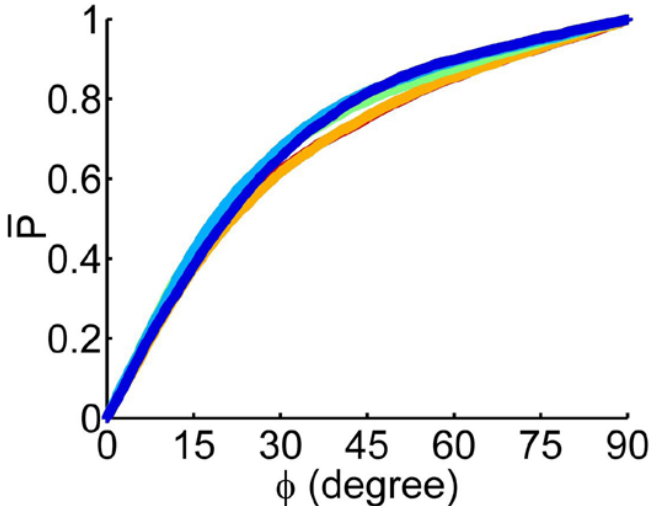

Figure S8 | Cumulative probability distribution is independent of magnitude of local average normal stress. For RPME cell monolayers, cumulative probability distribution of the alignment angle, ϕ, is plotted as a function of quintiles of local average normal stress, curves from blue, to red are in the order of higher quintiles. Unlike the magnitude of local stress anisotropy shown in Fig. 2 m, the magnitude of local average normal stress is unrelated to the shape of $\overline{P}(\phi)$. Each curve has more than 8,000 observations.

Supplement 9. Fluctuations, correlations, and the glass transition.

When a force is applied to an elastic medium, its effects decay ideally as $1/r$. But this decay is not to be confused with force fluctuations and the decay in their correlation function. To fix this latter idea, we consider the correlation decay in systems that might be considered as standards. We consider two examples that are not only instructive but also may bear parallels to the physics at play in the cellular monolayer.

We consider first the ideal and well-known case of the 2-D Ising model[7] of spin glasses above the glass transition temperature, T_c. In such systems the local spin interacts only with that of nearest neighbors. All interactions are strictly local. Even though all interactions are local the spin-spin correlation decays in space exponentially. [7] As the temperature decreases to approach T_c, moreover, successive local alignments of nearest neighbors causes long range order to emerge and the spin-spin correlation length to diverge.

We consider next an experimental model system for jamming in soft granular matter, namely, the 2-D assembly of soft, photoelastic disks. [8] When subjected to isotropic compression, force correlation length is as little as one disk diameter and the correlation function has close to a single exponential decay. But when subjected to mechanical shear, disk-disk contact forces line up into force chains, and as the jamming transition is approached the correlation length grows to span the full breadth of the system.

With these models in mind we now return to force correlation data in the monolayer (Fig. 5), which show evidence not only of force chains but also increase in the correlation length as cellular density increases. Taken together with previous observations of dramatic slowing of the cellular dynamics with increasing cellular crowding[9, 10], one is led to the hypothesis that these monolayers operate physiologically in the neighborhood of a glass transition.

DOI: 10.1038/NMAT3025

Supplement 10. Mechanically guided motion as an integrative physiological principle.

Although we have learned a great deal from recent studies of the standard model of the solitary cell crawling in isolation [11-15], in that system the physical constraints imposed by neighboring cells are not present and the innately cooperative mechanism at issue here is silenced. Consideration of the mechanical nature of the cell-cell interaction has led us to the observation that the orientation of local migration velocity aligns strongly with orientation of the maximal principal stress. This finding implies that each cell within the migrating epithelial or endothelial monolayer remodels itself locally so as to minimize shear stresses between itself and its immediate neighbors. This unanticipated finding complements other integrative physiological principles including Wolff's law of bone remodeling [16], Murray's law of vascular remodeling [17, 18], Kleiber's law of metabolic scaling[19-21], and McMahon's law of elastic similarity.[22, 23] In addition, this finding is closely related but complementary to Steinberg's hypothesis of differential adhesion for cell sorting and segregation.[24-42]

Movie SM1 | Maps of cell-substrate and cell-cell stresses. Time lapsed sequence of physical forces in the rat pulmonary microvascular endothelial (RPME) cell monolayer. As seen in the top left panel, the spindly cells move largely along long axis. During this motion, the cells apply on their substrate tractions that have dramatic spatio-temporal fluctuations (top right panel). The cells transfer the mechanically unbalanced part of the local traction to their neighbors, and on contrary to the tractions, the resulting average normal stresses have less frequent spatial fluctuations (bottom right panel). The intercellular stresses are highly anisotropic as the local maximum shear stresses are comparable to the average normal stress (bottom left panel). Cells in regions with higher stress anisotropy display stronger alignment between maximal principal stress and cell velocity. The sequence is 90 minutes long and 725x545 μm^2 in spatial extent.

Movie SM2 | Collective migration occurs along local axis of highest normal stress. Time lapsed sequence of rat pulmonary microvascular endothelial (RPME) cell monolayer overlapped with cell velocity vectors (red) and stress ellipses (blue). Long axis of the stress ellipse defines the local axis of highest normal stress, and the cell motion is locally aligned with this axis. The sequence is 90 minutes long and 725x545 μm^2 in spatial extent.

Supplement References.

1. **Ladoux, B. Cells guided on their journey. *Nature Physics* 5, 377-378 (2009).**
2. **Trepat, X. *et al.* Physical forces during collective cell migration. *Nature Physics* 5, 426-430 (2009).**
3. **An, S.S. *et al.* Hypoxia alters biophysical properties of endothelial cells via p38 MAPK- and Rho kinase-dependent pathways. *American Journal of Physiology - Cell Physiology* 289, C521-530 (2005).**
4. **Soule, H.D. *et al.* Isolation and Characterization of a Spontaneously Immortalized Human Breast Epithelial Cell Line, MCF-10. *Cancer Research* 50, 6075-6086 (1990).**
5. **J.-Victor Small, Klemens Rottner, Penelope Hahne & Anderson, K.I. Visualising the actin cytoskeleton. *Microscopy Research Technique* 47, 14 (1999).**
6. **Farooqui, R. & Fenteany, G. Multiple rows of cells behind an epithelial wound edge extend cryptic lamellipodia to collectively drive cell-sheet movement. *J Cell Sci* 118, 51-63 (2005).**
7. **McCoy, B. & Wu, T.T. *The Two-Dimensional Ising Model*, Edn. 1. (Harvard University Press, 1973).**

8. Majmudar, T.S. & Behringer, R.P. Contact force measurements and stress-induced anisotropy in granular materials. *Nature* 435, 1079-1082 (2005).
9. Angelini, T.E. *et al.* Glass-like dynamics of collective cell migration. *Proc Natl Acad Sci U S A* 108, 4714-4719 (2011).
10. Garrahan, J.P. Dynamic heterogeneity comes to life. *Proc Natl Acad Sci U S A* 108, 4701-4702 (2011).
11. Rubinstein, B., Fournier, M.F., Jacobson, K., Verkhovsky, A.B. & Mogilner, A. Actin-myosin viscoelastic flow in the keratocyte lamellipod. *Biophys J* 97, 1853-1863 (2009).
12. Mogilner, A. & Keren, K. The shape of motile cells. *Curr Biol* 19, R762-771 (2009).
13. Mogilner, A. Mathematics of cell motility: have we got its number? *J Math Biol* 58, 105-134 (2009).
14. Keren, K. *et al.* Mechanism of shape determination in motile cells. *Nature* 453, 475-480 (2008).
15. Lacayo, C.I. *et al.* Emergence of large-scale cell morphology and movement from local actin filament growth dynamics. *PLoS Biol* 5, e233 (2007).
16. Wolff, J. *The Law of Bone Remodeling*, Vol. (translation of the German 1892 edition). (Springer, 1986, Berlin Heidelberg New York; 1896).
17. Murray, C. The physiological principle of minimum work. I. The vascular system and the cost of blood volume. *Proceedings of the National Academy of Sciences USA* 12, 207-214 (1926).
18. Murray, C.D. The Physiological Principle of Minimum Work : A Reply. *J Gen Physiol* 14, 445 (1931).
19. Kleiber, M. Body size and metabolic rate. *Physiological Reviews* 27, 511–541. (1947).
20. White, C.R. Physiology: There is no single p. *Nature* 464, 691-693.
21. Kolokotrones, T., Van, S., Deeds, E.J. & Fontana, W. Curvature in metabolic scaling. *Nature* 464, 753-756.
22. McMahon, T. & Bonner, J. *On Size and Life*. (Scientific American Library, 1983).
23. McMahon, T.A. *Muscles, reflexes, and locomotion*. (Princeton University Press, Princeton, NJ; 1984).
24. Burdick, M.L. & Steinberg, M.S. Embryonic cell adhesiveness: do species differences exist among warm-blooded vertebrates? *Proc Natl Acad Sci U S A* 63, 1169-1173 (1969).
25. Gordon, R., Goel, N.S., Steinberg, M.S. & Wiseman, L.L. A rheological mechanism sufficient to explain the kinetics of cell sorting. *J Theor Biol* 37, 43-73 (1972).
26. Steinberg, M.S. On the Mechanism of Tissue Reconstruction by Dissociated Cells, Iii. Free Energy Relations and the Reorganization of Fused, Heteronomic Tissue Fragments. *Proc Natl Acad Sci U S A* 48, 1769-1776 (1962).
27. Steinberg, M.S. On the mechanism of tissue reconstruction by dissociated cells. I. Population kinetics, differential adhesiveness. and the absence of directed migration. *Proc Natl Acad Sci U S A* 48, 1577-1582 (1962).
28. Steinberg, M.S. Mechanism of tissue reconstruction by dissociated cells. II. Time-course of events. *Science* 137, 762-763 (1962).
29. Steinberg, M.S. Reconstruction of tissues by dissociated cells. Some morphogenetic tissue movements and the sorting out of embryonic cells may have a common explanation. *Science* 141, 401-408 (1963).
30. Steinberg, M.S. Cell movement in confluent monolayers: a re-evaluation of the causes of 'contact inhibition'. *Ciba Found Symp* 14, 333-355 (1973).
31. Steinberg, M.S. Adhesion-guided multicellular assembly: a commentary upon the postulates, real and imagined, of the differential adhesion hypothesis, with special attention to computer simulations of cell sorting. *J Theor Biol* 55, 431-443 (1975).
32. Steinberg, M.S. & Roth, S.A. Phases in Cell Aggregation and Tissue Reconstruction an Approach to the Kinetics of Cell Aggregation. *J Exp Zool* 157, 327-338 (1964).

DOI: 10.1038/NMAT3025

33. Steinberg, M.S. & Wiseman, L.L. Do morphogenetic tissue rearrangements require active cell movements? The reversible inhibition of cell sorting and tissue spreading by cytochalasin B. *J Cell Biol* 55, 606-615 (1972).
34. Drawbridge, J. & Steinberg, M.S. Morphogenesis of the axolotl pronephric duct: a model system for the study of cell migration in vivo. *Int J Dev Biol* 40, 709-713 (1996).
35. Duguay, D., Foty, R.A. & Steinberg, M.S. Cadherin-mediated cell adhesion and tissue segregation: qualitative and quantitative determinants. *Dev Biol* 253, 309-323 (2003).
36. Foty, R.A., Pfleger, C.M., Forgacs, G. & Steinberg, M.S. Surface tensions of embryonic tissues predict their mutual envelopment behavior. *Development* 122, 1611-1620 (1996).
37. Foty, R.A. & Steinberg, M.S. Cadherin-mediated cell-cell adhesion and tissue segregation in relation to malignancy. *Int J Dev Biol* 48, 397-409 (2004).
38. Foty, R.A. & Steinberg, M.S. The differential adhesion hypothesis: a direct evaluation. *Dev Biol* 278, 255-263 (2005).
39. Poole, T.J. & Steinberg, M.S. Different modes of pronephric duct origin among vertebrates. *Scan Electron Microsc*, 475-482 (1984).
40. Steinberg, M.S. Adhesion in development: an historical overview. *Dev Biol* 180, 377-388 (1996).
41. Wiseman, L.L., Steinberg, M.S. & Phillips, H.M. Experimental modulation of intercellular cohesiveness: reversal of tissue assembly patterns. *Dev Biol* 28, 498-517 (1972).
42. Beysens, D.A., Forgacs, G. & Glazier, J.A. Cell sorting is analogous to phase ordering in fluids. *Proc Natl Acad Sci U S A* 97, 9467-9471 (2000).

3.2 Mechanical waves during tissue expansion

Serra-Picamal X, Conte V, Vincent R, Anon E, Tambe DT, Bazallieres E, Butler JP, Fredberg JJ & Trepat X. Mechanical waves during tissue expansion. *Nature Physics* 8, 628-634 (2012).

ARTICLES
PUBLISHED ONLINE: 8 JULY 2012 | DOI: 10.1038/NPHYS2355
nature physics

Mechanical waves during tissue expansion

Xavier Serra-Picamal[1,2†], Vito Conte[1†], Romaric Vincent[1], Ester Anon[1,3], Dhananjay T. Tambe[4], Elsa Bazellieres[1], James P. Butler[4,5], Jeffrey J. Fredberg[4] and Xavier Trepat[1,2,6*]

The processes by which an organism develops its shape and heals wounds involve expansion of a monolayer sheet of cells. The mechanism underpinning this epithelial expansion remains obscure, despite the fact that its failure is known to contribute to several diseases, including carcinomas, which account for about 90% of all human cancers. Here, using the micropatterned epithelial monolayer as a model system, we report the discovery of a mechanical wave that propagates slowly to span the monolayer, traverses intercellular junctions in a cooperative manner and builds up differentials of mechanical stress. Essential features of this wave generation and propagation are captured by a minimal model based on sequential fronts of cytoskeletal reinforcement and fluidization. These findings establish a mechanism of long-range cell guidance, symmetry breaking and pattern formation during monolayer expansion.

Epithelial monolayer expansion is increasingly regarded as a mechanical phenomenon in which physical forces not only drive cell motions but also trigger and feedback to signalling pathways[1–3]. Each cell in the sheet is now known to generate forces on its underlying substrate[1], to transmit forces through intercellular junctions so as to create long-ranged gradients of tension[4], and to migrate preferentially along the direction of maximum principal stress[5]. Despite such recent discoveries, the ultraslow dynamics of epithelial expansion remain poorly understood.

To study such dynamics, we developed an experimental approach that combines soft lithography[6,7], traction force microscopy[4] and monolayer stress microscopy[5]. A polydimethylsiloxane (PDMS) membrane was fabricated with a rectangular opening and deposited on a polyacrylamide gel that had been coated with collagen I. We then seeded Madin–Darby Canine Kidney (MDCK) epithelial cells and allowed them to adhere and proliferate (Fig. 1a). On reaching confluence and a relatively high cell density, the monolayer sheet exhibited features typical of a stable epithelium including apico-basal polarity and accumulation of cortical actin at cell–cell junctions (Fig. 1b,c). Moreover, the tight junction protein ZO-1 (zona occludens 1) and the adherens junction protein E-cadherin co-localized at the lateral membranes of the cells (Fig. 1c).

Sudden removal of the PDMS membrane triggered collective cellular migration towards newly available free space (Figs 1a–c, 2a–c and Supplementary Movie S1). Over the course of 600 min, the total area of the monolayer sheet more than doubled, with less than half of the total area being attributable to proliferation (Fig. 1d inset) and the rest being attributable to cell spreading and flattening (Fig. 1b and Supplementary Text S2). In this process, the actin cytoskeleton exhibited a pronounced reorganization; it formed protrusions and transverse stress fibres in cells both at the leading edge and well behind it (Fig. 1c and Supplementary Movie S2). These changes in actin organization were paralleled by pronounced changes in the size and shape of focal adhesions (Fig. 1c). Cells did not undergo a full transition to a mesenchymal state, however; although E-cadherin was partially internalized, tight junctions remained intact and the monolayer expanded as a cohesive unit (Fig. 1c). Moreover, whereas a number of genes traditionally associated with the epithelial to mesenchymal transition such as those encoding paxillin, vinculin and β-actin exhibited changes in expression, others such as those encoding E-cadherin, vimentin and ZO-1 did not (Supplementary Fig. S1).

The internal dynamics of the monolayer were remarkable, both in terms of the distribution of cellular velocities and underlying tractions exerted by each cell on its substrate. Shortly after removal of the PDMS stencil, migration outwards was limited to cells at the leading edge (Fig. 2d), whereas cells back from the leading edge remained virtually immobile. With increasing time, however, cell movement penetrated progressively deeper into the monolayer and gave rise to a pattern of velocities characterized by an outer boundary layer of outward velocities at the edges and an inner region of negligible velocities at the centre (Fig. 2e). A similar evolution of cellular velocities was recently reported after monolayer wounding, thus supporting the notion that progressive cell mobilization away from the leading edge is a general response of cell collectives to the release of physical boundaries[8]. Traction forces exerted by cells on the underlying substrate exhibited similar spatial organization, with boundary layers of large tractions at both edges and virtually no traction at the centre. Fluctuations of both velocities and tractions increased with time and progressively expanded towards the monolayer midline (Fig. 2f,i).

If each cell in the monolayer has the capability to exert tractions on its substrate across focal or fibrillar adhesions, it also has the capability to exert stresses on its immediate neighbours across cell–cell junctions[5,9,10]. Using monolayer stress microscopy[5] (Methods and Supplementary Texts S1 and S2), we measured corresponding inter- and intra-cellular stresses, which we refer to together simply as monolayer stresses. Shortly after the stencil was lifted, the average normal stress ($\bar{\sigma}$) was largely tensile (positive) but was restricted to thin boundary layers at the leading edges, whereas the centre of the monolayer remained relaxed (Fig. 2j).

[1]Institute for Bioengineering of Catalonia, Barcelona 08028, Spain, [2]Facultat de Medicina, Universitat de Barcelona, and Ciber Enfermedades Respiratorias, Barcelona 08036, Spain, [3]Laboratoire Matière et Systèmes Complexes (MSC), Université Paris Diderot, and Unité Mixte de Recherche 7057 CNRS, F-75205 Paris Cedex 13, Paris, France, [4]School of Public Health, Harvard University, Boston, Massachusetts 02115, USA, [5]Brigham and Women's Hospital, Harvard Medical School, Boston, Massachusetts 02115, USA, [6]Institució Catalana de Recerca i Estudis Avançats (ICREA), Barcelona 08010, Spain. †These authors contributed equally to this work. *e-mail: xtrepat@ibecbarcelona.eu.

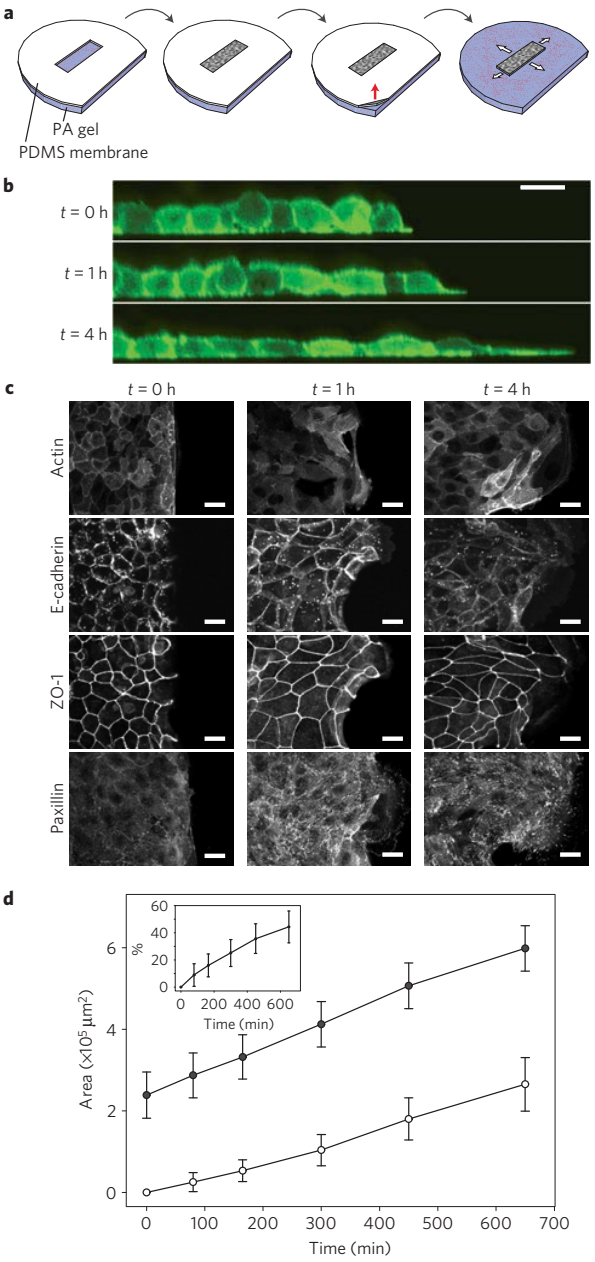

Figure 1 | Experimental model. a, A PDMS membrane is deposited on a collagen-coated polyacrylamide (PA) gel. Cells are seeded and allowed to attach only over the gap defined by the PDMS membrane. When confluent cells reach a relatively high confluence, the PDMS membrane is peeled off and cells start invading the surrounding space. **b**, Transversal view of LifeAct MDCK cells at the specified time points after the PDMS membrane was removed; scale bar, 20 μm. **c**, Basal actin (LifeAct-GFP), E-cadherin, ZO-1 and paxillin immunofluorescence micrographs before, 1 h after and 4 h after removing the membranes. Scale bars, 15 μm. **d**, Cell sheet area (filled circles) and cell sheet area due to proliferation (white circles) at different time points. The area due to proliferation was calculated by counting the number of cells in the monolayer at distinct time points and then multiplying the number of new cells by the average cell area. Data are mean ± s.d. ($n = 5$). Inset: relative contribution of cell proliferation to cell sheet area.

With time, these boundary layers became markedly heterogeneous but systematically grew to encompass increasing numbers of cells; cell–cell tension transmission exhibited a growing scale of length (Fig. 2k), and the maximum intercellular shear stress ($\bar{\mu}$) followed a similar pattern (Fig. 2m,n). Taken together, these findings demonstrate that force transmission from cell-to-cell, and cellular migration across the epithelial sheet, are initiated at the leading edge and progressively penetrate towards the centre (Supplementary Movie S3).

Moreover, these stress fields were anisotropic. At each position in the monolayer plane, the maximum (σ_{max}) and minimum (σ_{min}) principal stresses[5] were represented as an ellipse aligned with corresponding principal orientations (Fig. 2p). Throughout epithelial expansion, stress ellipses tended to be spindle-shaped and thus revealed pronounced stress anisotropy. The maximum principal stress orientation tended to be perpendicular to the leading edge and thus roughly parallel to local cell motion (Fig. 2q). As described previously, this mode of local cell guidance defines plithotaxis[2,5].

Superposed on systematic monolayer spreading were large-scale spatio-temporal fluctuations of tractions, monolayer stresses and cellular velocities (Fig. 2f,i,l,o). To better characterize the systematic evolution of mechanical patterns, we averaged these variables over the observable monolayer length (corresponding to the y coordinate), thereby reducing the dimensionality of the system to only one spatial dimension and one temporal dimension. All data could then be represented as kymographs in the x–t plane (Methods). Kymographs of cellular velocity (v_x) revealed motility patterns that were not restricted to the initial phase of inward mobilization (Fig. 3a). To the contrary, after reaching the monolayer midline at ∼150 min, the two fronts of cell motility coalesced and then continued towards the leading edges. When cells are cohesive and mass is conserved, cellular velocities must be linked to the rate of cell deformation (strain rate, $\dot{\varepsilon}_{xx}$; ref. 11) through the expression $\dot{\varepsilon}_{xx} = \partial v_x/\partial x$. Remarkably, kymographs of $\dot{\varepsilon}_{xx}$ revealed clear evidence of wave-like crests of strain rate that were launched at each leading edge, propagated away from and back to the leading edge at roughly twice the speed of the advancing front edge, and spanned the entire monolayer (Fig. 3b). To distinguish these mechanical waves from other known types of mechanical wave, and because they inscribe an X-shape on the kymograph, we call them X-waves.

To study the physical origin of the X-wave, we next focused on traction generation and stress transmission in the monolayer. Whereas traction kymographs demonstrated extrema at the leading edge, monolayer stresses were highest at the monolayer midline, indicating that local force generation was globally integrated and transmitted through cell–cell junctions to give rise to a stress build-up (Fig. 3c,d). Importantly, monolayer stress at the midline oscillated in time (Fig. 3g,h and Supplementary Movie S4); these oscillations were in phase with fluctuations of cell area (Fig. 3f,h) and demonstrated phase quadrature with strain rate (Fig. 3e). Contrary to long-held assumptions (reviewed in ref. 12), these observations establish that on the ultraslow timescales of cellular migration the dominant cellular stresses in the monolayer are elastic, not viscous.

In the absence of appreciable inertia, there can exist no exchange between kinetic and potential energy storage as is usually associated with propagation of passive mechanical waves, thus suggesting that the mechanism underlying the observed propagation might be active. To investigate this possibility, we inhibited myosin using blebbistatin. Blebbistatin prevented the formation of stress fibres (Supplementary Fig. S2) and had little effect on the velocity of the leading edge, thus confirming previous reports in wound scratch assays[8]. Blebbistatin caused traction forces and intercellular stresses to be abrogated, however (Supplementary Fig. S2 and Movie S5). A well-defined front of strain rate could be clearly identified nonetheless, but this front was stationary, did not propagate

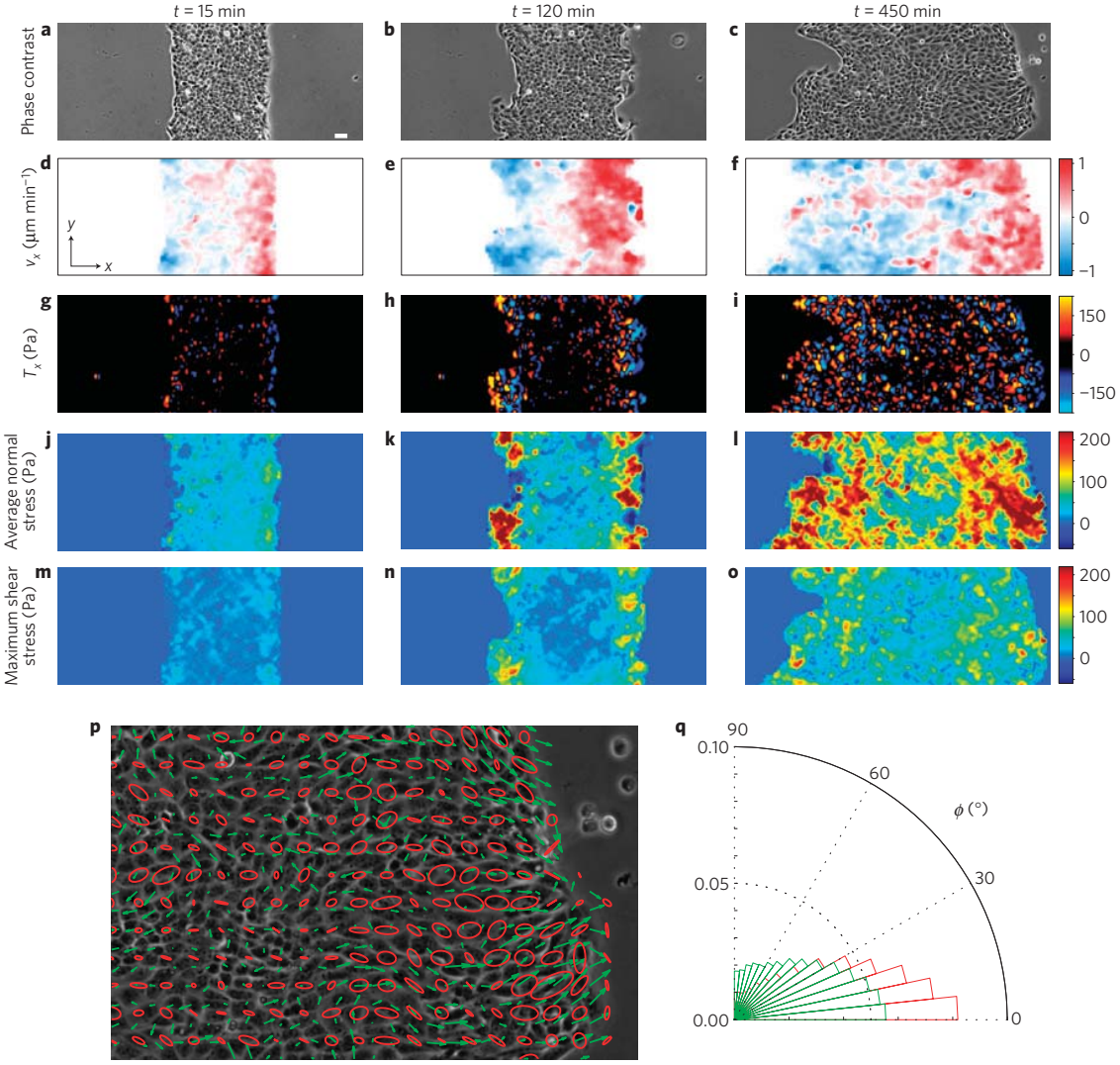

Figure 2 | Maps of cell velocity, cell substrate tractions and monolayer stresses. a–o, Phase-contrast images (**a–c**), velocity v_x (**d–f**), tractions T_x (**g–i**), average normal stress $\bar{\sigma}$ (**j–l**) and maximum shear stress $\bar{\mu}$ (**m–o**) at 15 min (**a**,**d**,**g**,**j**,**m**), 120 min (**b**,**e**,**h**,**k**,**n**) and 450 min (**c**,**f**,**i**,**l**,**o**) after removing the PDMS membrane. **p**, Principal stress ellipses (red) and velocity vectors (green) of a magnified region from **c**. **q**, Probability distribution of the major axis of the principal stress ellipse (red) and the velocities (green), where 0° represents alignment with the *x* axis and 90° represents alignment to the *y* axis. Scale bar, 50 μm.

and dispersed or attenuated after about 450 min. Together, these findings indicate that the propagating mechanical wave involves a contractile component.

To study the role of intercellular adhesion in monolayer stress transmission and wave propagation, we disrupted cell–cell junctions by chelation of extracellular calcium[5] after 280 min of monolayer expansion (Supplementary Fig. S3 and Movie S6). Within 20 min of calcium chelation, the monolayer lost its structural integrity and isolated cells were seen to escape from the leading edge. Monolayer stress exhibited a sharp drop and wave crests vanished (Supplementary Fig. S3). Restoration of calcium levels 45 min later rescued monolayer stresses and wave propagation but, remarkably, wave propagation restarted at the very edge the monolayer. These data highlight a central role for cell–cell junctions in the generation and propagation of X-waves. They show, further, that these waves are not restricted to the case of sudden release of a physical constraint.

Across experiments, monolayer expansion exhibited various levels of symmetry breaking (Supplementary Fig. S4). As in the symmetric case (Fig. 3), experiments in which symmetry was spontaneously broken showed propagation of velocity fronts back from each leading edge but, on collision, one of the two fronts penetrated past the midline into the opposite side of the monolayer before propagating back towards the leading edge (Supplementary Fig. S4a,b). As such, the characteristic time for the velocity front to complete one cycle of inward and outward propagation was longer than in the symmetric case. Symmetry breaking in multicellular systems is a widespread process that remains poorly understood[13–15]. Our findings suggest that symmetry breaking during monolayer expansion originates at the very edge of the monolayer boundaries at the very onset of migration (Supplementary Fig. S4 and Movie S7), with the highest stresses restricted to the first few rows of the fastest leading edge.

Waves in chemical systems, as in the Belousov–Zhabotinsky reaction, rely on temporal competition between reaction times and diffusion times, and a generalization of this idea to non-equilibrium mechano-chemical systems was recently proposed[16].

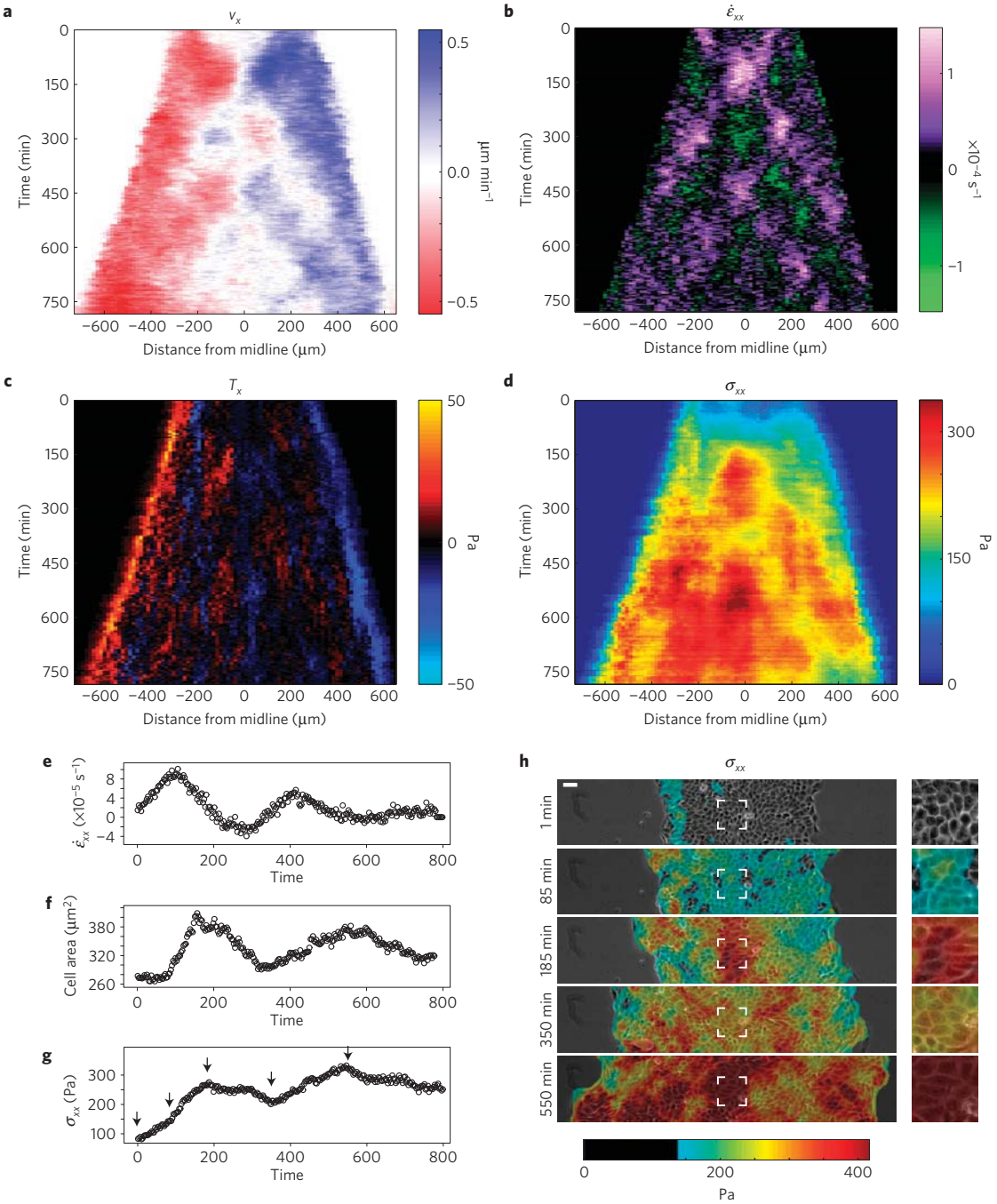

Figure 3 | Dynamic behaviour of a cell sheet expanding nearly symmetrically. a–d, Kymographs of velocity v_x (**a**), strain rate $\dot{\varepsilon}_{xx}$ (**b**), tractions T_x (**c**) and monolayer stress component σ_{xx} (**d**). Boundary artefacts attributable to particle image velocimetry have been suppressed from **b** (Supplementary Fig. S5). **e–g**, Average value of $\dot{\varepsilon}_{xx}$ (**e**), cell area (**f**) and σ_{xx} (**g**) at the monolayer midline (average over a strip of width 125 μm centred at the midline). **h**, Overlay of monolayer stress component σ_{xx} on phase-contrast images. The right square panels are a magnification of the highlighted region in the left panels. Scale bar, 50 μm.

Alternatively, wave propagation can also originate from threshold phenomena that are rapid, coupled with refractory phenomena that are slow, as in propagation of the action potential[17]. Although it remains unclear how comparable mechanisms might account for the mechanical waves reported here, a minimal one-dimensional mechanical model captures the observed phenomenology without invoking chemical factors or their associated reaction, diffusion and advection. The model treats the monolayer as a collection of springs (cells) of elastic constant k connected in series (Fig. 4a). Each cell is allowed to generate a self-propelling force $\mathbf{F}_i$. This propelling force can be transmitted through elastic forces to neighbouring cells and by frictional forces to the underlying gel substrate. The position x_i of a generic node (cell–cell junction) is affected by the force $\mathbf{F}_i$, by the elastic responses $\mathbf{f}_i^e$ and $\mathbf{f}_{i+1}^e$ of the two cells joined at that node, and by the viscous friction $\mathbf{f}_i^v$ between those two cells and the gel substrate (Fig. 4b), represented as a dashpot of constant viscosity η

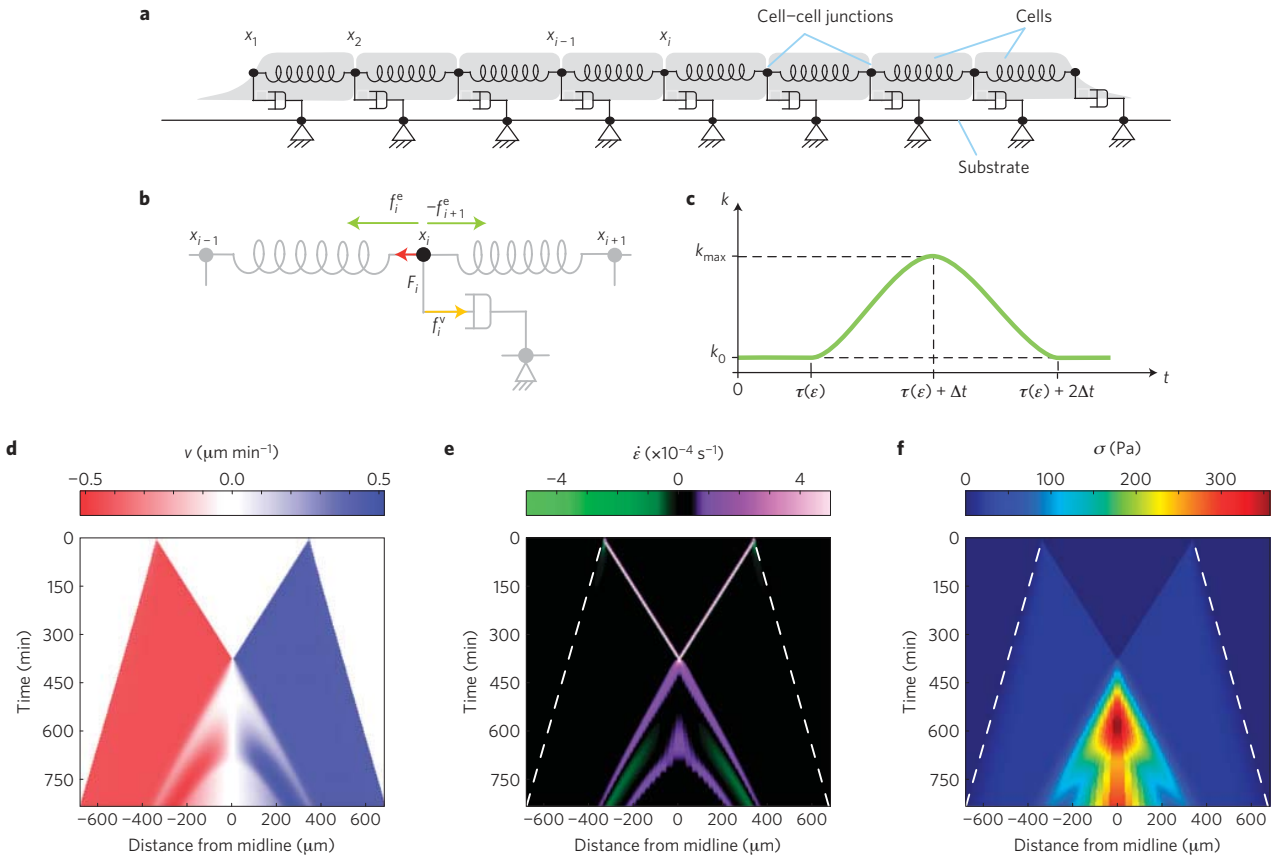

Figure 4 | Essential features of wave generation and propagation are captured by a minimal model based on sequential fronts of cytoskeletal reinforcement and fluidization. a, Schematic of the one-dimensional *in silico* model for a line of elastic epithelial cells sliding viscously on a rigid substrate in response to self-propelling forces. **b**, Schematic of the nodal force balance. Forces are represented through arrows and all act at the generic node x_i (for the sake of the clarity, they have been drawn as acting at points in the proximity of node x_i). Self-propelling force $\mathbf{F}_i$ is in red; viscous force $\mathbf{f}_i^v$ is in yellow; elastic forces $\mathbf{f}_i^e$ and $\mathbf{f}_{i+1}^e$ are in green. **c**, Dependence of the spring constant k on strain and time. When a spring reaches a strain threshold ε_{th}, it undergoes one phase of reinforcement (stiffening) followed by one phase of fluidization (softening). **d**, *In silico* velocity kymograph. **e**, *In silico* strain rate kymograph. **f**, *In silico* stress kymograph.

(Fig. 4a). Thus, force balance at each node x_i reads

$$F_i + k\varepsilon_i - k\varepsilon_{i+1} - \eta\dot{x}_i = 0$$

where ε_i denotes the strain undergone by the spring connecting nodes x_{i-1} and x_i, and $\dot{x}_i$ denotes the velocity of node x_i.

In the context of this model we first considered the two most widely invoked mechanisms for monolayer expansion, namely, that force generation is restricted to the first few leading cell rows, or that each cell in the monolayer is mechanically self-propelled. Simulation of each of these scenarios results in monolayer expansion but fails to account for the generation and propagation of X-waves (Supplementary Text S3). In contrast, such waves are captured with only two assumptions. The first is that a cell acquires a motile phenotype only when an adjacent cell either creates space[18] or pulls on the shared intercellular junction[19], either of which would promote local cell unjamming[5,20,21] and lead naturally to the propagation of a strain-rate front followed by a stress build-up (Supplementary Text S3). If, second, the cell is assumed to possess a threshold of strain beyond which the cytoskeleton first reinforces[22] but then fluidizes[23], then strain rate fronts and stress differentials become reiterated in time. As they elicit effects on cellular mechanical properties that are nonlinear in character but opposite in sign, and, importantly, as they act over disparate scales of time[23,24], reinforcement and fluidization taken together are shown to be sufficient to sustain a propagating mechanical wave with many of the same features as the X-waves demonstrated experimentally (Fig. 4d–f and Supplementary Movie S8). A role for reaction–diffusion–advection mechanisms or for gene oscillators cannot be ruled out, but to explain these mechanical waves, such mechanisms need not be invoked.

In view of this relationship, pattern formation during development is widely attributed to cellular sensing of local chemical differentials that become reiterated over the span of a great many cells. Although there is little doubt that such reiterated chemical differentials are necessary to explain patterning, it remains unclear whether they are sufficient. For example, large multicellular systems are typically heterogeneous, dynamic and noisy. In such systems, can the reaction, diffusion and advection of chemical factors act with sufficient precision to transmit requisite information over distances spanning a great many cells? This question and others have led to the hypothesis that pattern formation requires another feedback mechanism, and that such a mechanism is provided by physical forces[2,16,25–28]. It is now well established that local physical forces can be transduced into local intracellular signals to activate local regulatory protein networks[29–32], but patterns of stress and strain reiterated in time and over space across a multicellular tissue have never before been observed. Our finding of a slow mechanical wave constitutes the first direct evidence of such reiterated mechanical patterns and thus provides a natural candidate to trigger mechanotransduction

pathways during wound healing, morphogenesis and collective cellular invasion in cancer.

Methods

Cell culture. MDCK strain II cells were cultured in minimum essential media with Earle's Salts and L-glutamine (Gibco) supplemented with 10% fetal bovine serum (FBS; Gibco), 100 U ml^{-1} penicillin and 100 μg ml^{-1} streptomycin.

Microfabrication of the PDMS membranes. PDMS membranes were fabricated according to procedures described previously[7,33]. Briefly, SU8-50 masters containing rectangles of 300 × 2,500 μm were raised using conventional photolithography. Uncured PDMS was spin-coated on the masters to a thickness lower than the height of the SU8 feature (35 μm) and cured for 2 h at 60 °C. A thicker border of PDMS was applied at the edges of the membranes for handling purposes. PDMS was then peeled off from the master and kept in ethanol at 4 °C until use.

Preparation of polyacrylamide gels. Polyacrylamide gel preparation was adapted from protocols described in refs 34,35. Glass-bottom dishes were activated by using a 1:1:14 solution of acetic acid/bind-silane/ethanol. The dishes were washed twice with ethanol and air-dried for 10 min. For 3 kPa gels, a stock solution containing a concentration of 5.5% acrylamide, 0.09% bisacrylamide, 0.5% ammonium persulphate, 0.05% tetramethylethylenediamine, 0.4% of 200-nm-diameter red fluorescent carboxylate-modified beads (Fluospheres, Invitrogen) and 2 mg ml^{-1} NH-acrylate was prepared. A drop of 10 μl was added to the centre of the glass-bottom dishes, and the solution was covered with 12-mm-diameter glass coverslips. After polymerization, gels were washed with PBS and incubated with 100 μl of a collagen I solution (0.1 mg ml^{-1}, Millipore) overnight at 4 °C. Gels were washed afterwards with PBS and incubated with cell culture media with 10% FBS for 6 h.

Cell patterning on soft substrates. One hour before seeding the cells, the PDMS membranes were air dried and incubated in a solution of 2% Pluronic F-127 (Sigma-Aldrich) in PBS to avoid damage of the gel coating due to the PDMS membrane. The membranes were then washed twice with PBS and air dried for 20 min, and they were deposited on the surface of the polyacrylamide gel. A small volume (8 μl) containing 15,000 cells was placed on the exposed region of the polyacrylamide gel defined by the PDMS membrane. Once the cells were attached to the polyacrylamide gel (20 min), the unattached cells were washed away and 200 μl of medium was added. Twelve hours after seeding the cells, 2 ml of medium was added and the PDMS membranes were carefully removed with tweezers before the beginning of the experiment.

Time-lapse microscopy. Multidimensional acquisition routines were performed on an automated inverted microscope (Nikon Eclipse Ti) equipped with thermal, CO_2 and humidity control, using MetaMorph (Universal Imaging) software. Time-lapse recording started approximately 30 min after removing the PDMS membrane. The interval between image acquisition was 1 min and a typical experiment lasted for 20 h. To capture the full width of the expanding cell sheet, two images were acquired at ×10 for every time point, approximately overlapping laterally by 10%. The two images were accurately stitched with subpixel resolution using custom-made MatLab software.

Fluorescence microscopy. Immunofluorescence microscopy experiments were carried out by fixing the cells with 3% paraformaldehyde (Sigma-Aldrich) in PBS, permeabilizing with 0.5% Triton X-100 (Sigma-Aldrich) in PBS, and blocking with 10% FBS (Sigma-Aldrich) in PBS.

Primary antibodies mouse anti-E-cadherin (BD Transduction Laboratories), rabbit anti-ZO-1 (Zymed, Invitrogen) and mouse anti-paxillin (BD Transduction Laboratories) diluted at 1:1,000, 1:500 and 1:100, respectively, in 10% FBS in PBS were incubated for 1 h at room temperature, and were detected using secondary antibodies goat anti-mouse and donkey anti-rabbit (Invitrogen). A spectral confocal microscope (Nikon Eclipse C1si) was used for high-resolution image acquisition.

Cell area measurements. The contour of each cell was determined using a segmentation algorithm (Greylevel Watershed for ImageJ, D. Sage, Biomedical Image Group, EPFL). Phase-contrast images were pre-processed by contrast enhancement followed by a Gaussian blur. To limit the over-sampling inherent to water-shedding algorithms, we set up the appropriate limits for the cell area and eccentricity.

Velocity measurements. Velocity fields were computed using custom-made particle image velocimetry software on the phase-contrast images. The interrogation window was either 64 × 64 pixels or 96 × 96 pixels, and the time interval between consecutive analysed images was 1 min. Monolayer boundaries were computed using a home-made algorithm based on the standard deviation of each interrogation window in the phase-contrast images.

Traction microscopy. Traction forces were computed using Fourier transform traction microscopy with a finite gel thickness[4]. Gel displacements between any experimental time point and a reference image obtained after monolayer trypsinization were computed using home-made particle imaging velocimetry software. To reduce systematic biases in subpixel resolution and peak-locking effects, we implemented an iterative process ($n = 4$ iterations) based on a continuous window shift technique.

Monolayer stress microscopy. Monolayer stresses were computed using monolayer stress microscopy[5]. Monolayer stress microscopy uses traction forces and straightforward force balance demanded by Newton's laws to map the two-dimensional stress tensor σ in the monolayer:

$$\sigma = \begin{pmatrix} \sigma_{xx} & \sigma_{xy} \\ \sigma_{yx} & \sigma_{yy} \end{pmatrix}$$

By rotating these stress components at each point in the cell sheet, we computed the magnitude of the two principal stress components σ_{max} and σ_{min} and their corresponding, mutually perpendicular, principal orientations. For each point in the monolayer, we then computed the average normal stress within and between cells defined as $\bar{\sigma} = (\sigma_{max} + \sigma_{min})/2$ and the maximum intercellular shear stress defined as $\bar{\mu} = (\sigma_{max} - \sigma_{min})/2$.

Kymographs. For each pixel in the monolayer, we computed the distance to the closest leading edge. Next we computed the median values of velocities, tractions, monolayer stresses and strain rates of all pixels located at a given distance from the leading edge. These median values were then represented on a unidimensional segment whose width was the mean width of the monolayer. This operation was repeated for each experimental time point.

Quantification of gene expression. MDCK monolayers were collected at 0, 3, and 7 h of monolayer expansion. The total RNA was extracted using the PARIS kit (Applied Biosystems) according to the manufacturer's instructions. RNA was quantified by the absorbance at 260 nm, and reverse transcribed into complementary DNA using the high-capacity RNA-to-cDNA master mix (Applied Biosystems). Quantitative PCR was performed with the 7500 fast real-time PCR system and software (Applied Biosystems). TaqMan gene expression assays Cf02668852_g1, Cf02651495_m1, Cf02628470_m1, Cf02624268_m1, Cf02667774_m1, Cf02645536_m1, and Cf03023880_g1 were used to detect vimentin, paxillin, ZO-1, E-cadherin, β-catenin, vinculin and β-actin, respectively. Quantitative real-time PCR values were normalized to an internal control s18 (TaqMan probe Cf02624915_g1), averaged and expressed relative to gene expression before cell migration (0 h).

Received 31 January 2012; accepted 30 May 2012; published online 8 July 2012

References

1. Du Roure, O. *et al.* Force mapping in epithelial cell migration. *Proc. Natl Acad. Sci. USA* **102,** 2390–2395 (2005).
2. Trepat, X. & Fredberg, J. J. Plithotaxis and emergent dynamics in collective cellular migration. *Trends Cell Biol.* **21,** 638–646 (2011).
3. Leckband, D. E., le Duc, Q., Wang, N. & de Rooij, J. Mechanotransduction at cadherin-mediated adhesions. *Curr. Opin. Cell Biol.* **23,** 523–530 (2011).
4. Trepat, X. *et al.* Physical forces during collective cell migration. *Nature Phys.* **5,** 426–430 (2009).
5. Tambe, D. T. *et al.* Collective cell guidance by cooperative intercellular forces. *Nature Mater.* **10,** 469–475 (2011).
6. Nikolic, D. L., Boettiger, A. N., Bar-Sagi, D., Carbeck, J. D. & Shvartsman, S. Y. Role of boundary conditions in an experimental model of epithelial wound healing. *Am. J. Physiol. Cell Physiol.* **291,** C68–C75 (2006).
7. Poujade, M. *et al.* Collective migration of an epithelial monolayer in response to a model wound. *Proc. Natl Acad. Sci. USA* **104,** 15988–15993 (2007).
8. Matsubayashi, Y., Razzell, W. & Martin, P. 'White wave' analysis of epithelial scratch wound healing reveals how cells mobilise back from the leading edge in a myosin-II-dependent fashion. *J. Cell Sci.* **124,** 1017–1021 (2011).
9. Maruthamuthu, V., Sabass, B., Schwarz, U. S. & Gardel, M. L. Cell-ECM traction force modulates endogenous tension at cell–cell contacts. *Proc. Natl Acad. Sci. USA* **108,** 4708–4713 (2011).
10. Liu, Z. *et al.* Mechanical tugging force regulates the size of cell–cell junctions. *Proc. Natl Acad. Sci. USA* **107,** 9944–9949 (2010).
11. Blanchard, G. B. *et al.* Tissue tectonics: Morphogenetic strain rates, cell shape change and intercalation. *Nature Methods* **6,** 458–464 (2009).
12. Chen, X. & Brodland, G. W. Multi-scale finite element modeling allows the mechanics of amphibian neurulation to be elucidated. *Phys. Biol.* **5,** 015003 (2008).
13. Gros, J., Feistel, K., Viebahn, C., Blum, M. & Tabin, C. J. Cell movements at Hensen's node establish left/right asymmetric gene expression in the chick. *Science* **324,** 941–944 (2009).

14. Wan, L. Q. *et al.* Micropatterned mammalian cells exhibit phenotype-specific left-right asymmetry. *Proc. Natl Acad. Sci. USA* **108,** 12295–12300 (2010).
15. Brangwynne, C., Huang, S., Parker, K. K., Ingber, D. E. & Ostuni, E. Symmetry breaking in cultured mammalian cells. *In Vitro Cell Dev. Biol. Anim.* **36,** 563–565 (2000).
16. Bois, J. S., Julicher, F. & Grill, S. W. Pattern formation in active fluids. *Phys. Rev. Lett.* **106,** 028103 (2011).
17. Hodgkin, A. L. & Huxley, A. F. A quantitative description of membrane current and its application to conduction and excitation in nerve. *J. Physiol.* **117,** 500–544 (1952).
18. Carmona-Fontaine, C. *et al.* Contact inhibition of locomotion in vivo controls neural crest directional migration. *Nature* **456,** 957–961 (2008).
19. Weber, G. F., Bjerke, M. A. & Desimone, D. W. A mechanoresponsive Cadherin-Keratin complex directs polarized protrusive behavior and collective cell migration. *Dev. Cell* **22,** 104–115 (2012).
20. Angelini, T. E. *et al.* From the cover: Glass-like dynamics of collective cell migration. *Proc. Natl Acad. Sci. USA* **108,** 4714–4719 (2011).
21. Garrahan, J. P. Dynamic heterogeneity comes to life. *Proc. Natl Acad. Sci. USA* **108,** 4701–4702 (2011).
22. Riveline, D. *et al.* Focal contacts as mechanosensors: Externally applied local mechanical force induces growth of focal contacts by an mDia1-dependent and ROCK-independent mechanism. *J. Cell Biol.* **153,** 1175–1186 (2001).
23. Trepat, X. *et al.* Universal physical responses to stretch in the living cell. *Nature* **447,** 592–595 (2007).
24. Bursac, P. *et al.* Cytoskeletal remodelling and slow dynamics in the living cell. *Nature Mater.* **4,** 557–561 (2005).
25. Eyckmans, J., Boudou, T., Yu, X. & Chen, C. S. A Hitchhiker's guide to mechanobiology. *Dev. Cell* **21,** 35–47 (2011).
26. Mammoto, T. & Ingber, D. E. Mechanical control of tissue and organ development. *Development* **137,** 1407–1420 (2010).
27. Shraiman, B. I. Mechanical feedback as a possible regulator of tissue growth. *Proc. Natl Acad. Sci. USA* **102,** 3318–3323 (2005).
28. Montell, D. J. Morphogenetic cell movements: Diversity from modular mechanical properties. *Science* **322,** 1502–1505 (2008).
29. del Rio, A. *et al.* Stretching single talin rod molecules activates vinculin binding. *Science* **323,** 638–641 (2009).
30. Hoffman, B. D., Grashoff, C. & Schwartz, M. A. Dynamic molecular processes mediate cellular mechanotransduction. *Nature* **475,** 316–323 (2011).
31. Johnson, C. P., Tang, H-Y., Carag, C., Speicher, D. W. & Discher, D. E. Forced unfolding of proteins within cells. *Science* **317,** 663–666 (2007).
32. Zhang, H. *et al.* A tension-induced mechanotransduction pathway promotes epithelial morphogenesis. *Nature* **471,** 99–103 (2011).
33. Ostuni, E., Kane, R., Chen, C. S., Ingber, D. E. & Whitesides, G. M. Patterning mammalian cells using elastomeric membranes. *Langmuir* **16,** 7811–7819 (2000).
34. Kandow, C. E., Georges, P. C., Janmey, P. A. & Beningo, K. A. in *Methods in Cell Biology* Vol. 83 (eds Wang Yu-Li, E. & Discher, Dennis) 29–46 (Academic, 2007).
35. Yeung, T. *et al.* Effects of substrate stiffness on cell morphology, cytoskeletal structure, and adhesion. *Cell Motil. Cytoskeleton* **60,** 24–34 (2005).

Acknowledgements

We thank M. Bintanel for technical assistance, S. Garcia and A. Carreras for help with polyacrylamide gels and micropatterning, the Nanotechnology Platform from Barcelona Science Park, J. J. Munoz for help with the numerical implementation of the model, and P. Roca-Cusachs, D.G. Miguez, D. Navajas, R. Farre and J. Alcaraz for discussions. This research was supported by the Spanish Ministry for Science and Innovation (BFU2009-07595 and FPU fellowship XS), the European Research Council (Grant Agreement 242993) and the National Institutes of Health (R01HL102373, R01HL107561).

Author contributions

X.S-P. and X.T. designed experiments; X.S-P. performed all experiments. E.B. and X.S-P. performed gene expression experiments; X.S-P., R.V., V.C. and X.T. analysed data; D.T.T. contributed software; V.C. built the computer model and performed simulations; X.S-P., V.C., J.J.F. and X.T. wrote the manuscript; all authors discussed and interpreted results and commented on the manuscript; X.T. supervised the project.

Additional information

The authors declare no competing financial interests. Supplementary information accompanies this paper on www.nature.com/naturephysics. Reprints and permissions information is available online at www.nature.com/reprints. Correspondence and requests for materials should be addressed to X.T.

nature physics

SUPPLEMENTARY INFORMATION

DOI: 10.1038/NPHYS2355

Mechanical waves during tissue expansion

Supplementary movies

Supplementary movie 1: expansion of a micropatterned monolayer of MDCK cells (10×, phase contrast microscopy).

Supplementary movie 2: leading edge region of and expanding monolayer of MDCK cells stably expressing LifeAct-GFP (60×, confocal microsocopy).

Supplementary movie 3: dynamics of an expanding MDCK monolayer. Top: phase contrast image (10×). Center: Cell-substrate Tractions T_x (Pa). Bottom: Average normal stress (Pa).

Supplementary movie 4: monolayer stress component σ_{xx} overlaid on phase contrast images for the case of nearly symmetric monolayer expansion.

Supplementary movie 5: expansion of a micropatterned monolayer of MDCK cells treated with myosin inhibitor Blebbistatin (10×, phase contrast microscopy).

Supplementary movie 6: monolayer stress component σ_{xx} overlaid on phase contrast images. EGTA was added at 280 min, and replaced by control medium at 325 min.

Supplementary movie 7: monolayer stress component σ_{xx} overlaid on phase contrast images for the case of markedly asymmetric monolayer expansion.

Supplementary movie 8: simulation of the 1D expanding monolayer in the case in which cells undergo cycles of reinforcement and fluidization. Each dot represents a cell-cell junction.

Supplementary movie 9: simulation of the 1D expanding monolayer in the case where only the two front cells (one on each side of the monolayer) generate self-propelling forces. Each dot represents a cell-cell junction.

Supplementary movie 10: simulation of the 1D expanding monolayer in the case in which all cells have the capacity of generating self-propelling forces simultaneously. Each dot represents a cell-cell junction.

Supplementary movie 11: simulation of the 1D expanding monolayer in the case in which a cell is able to generate a self-propelling force only if its immediate front neighbor has deformed more than a given strain threshold. Each dot represents a cell-cell junction.

nature physics

SUPPLEMENTARY INFORMATION

DOI: 10.1038/NPHYS2355

Mechanical waves during tissue expansion

Supplementary Figures

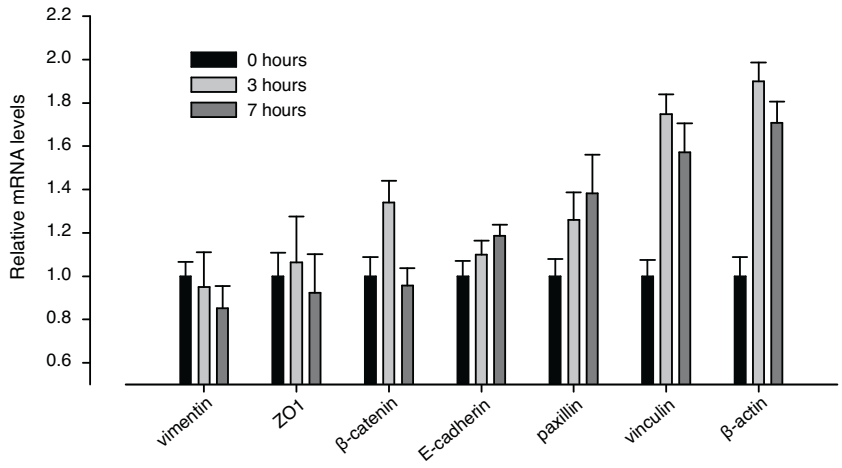

Fig. S1. Relative changes in mRNA levels during monolayer expansion. Results are plotted as mean ± SD of two independent experiments, each performed in triplicate. For each independent experiment, the cells from 5 independent cell sheets were collected.

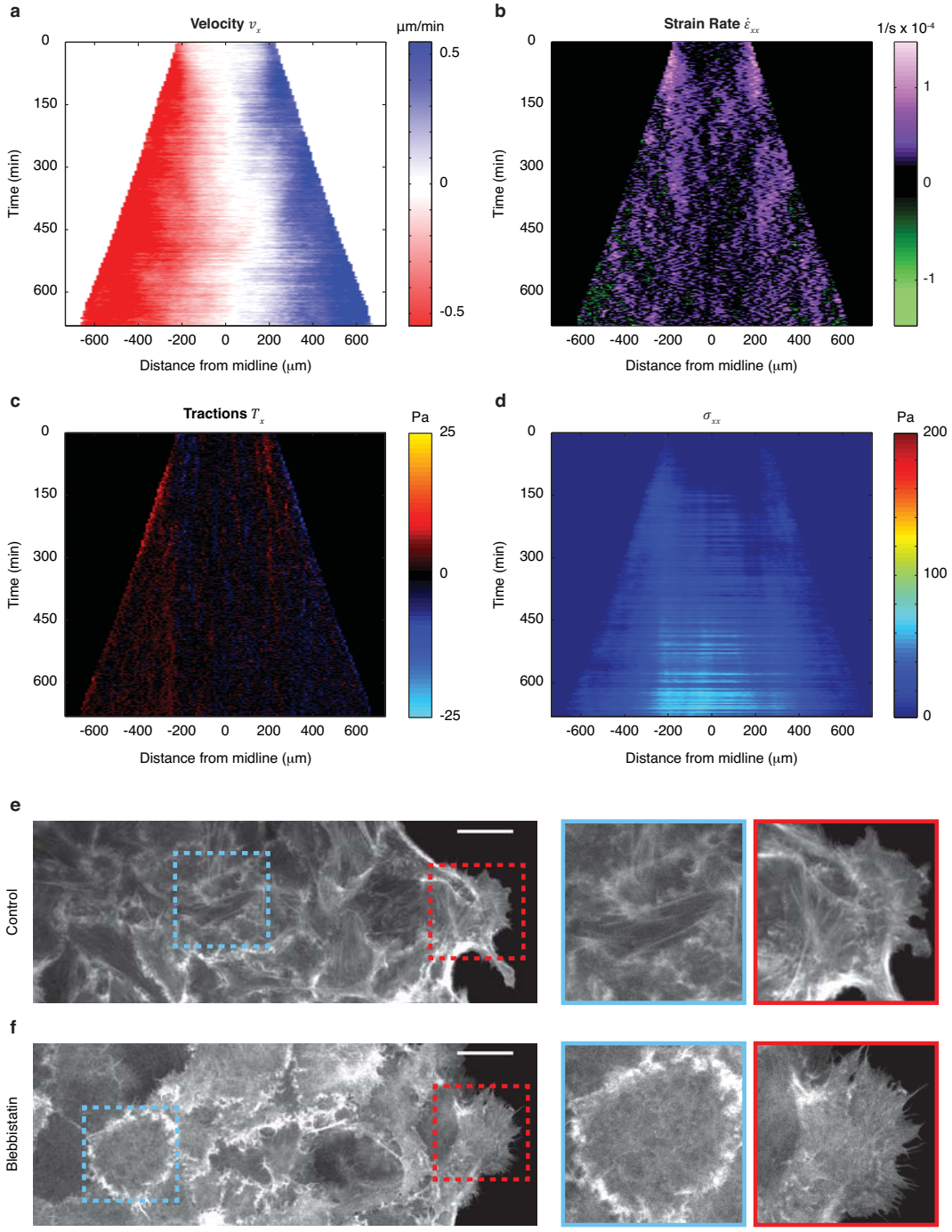

Fig. S2. Blebbistatin increases velocity of monolayer expansion but abrogates traction generation, monolayer stress transmission and wave propagation. Kymographs of velocity v_x (a), strain rate $\dot{\varepsilon}_{xx}$ (b), tractions T_x (c), and monolayer stress component σ_{xx} (d). Blebbistatin prevented stress fiber formation. (e) Control. (f) Blebbistatin treatment. Scale bar = 20 μm.

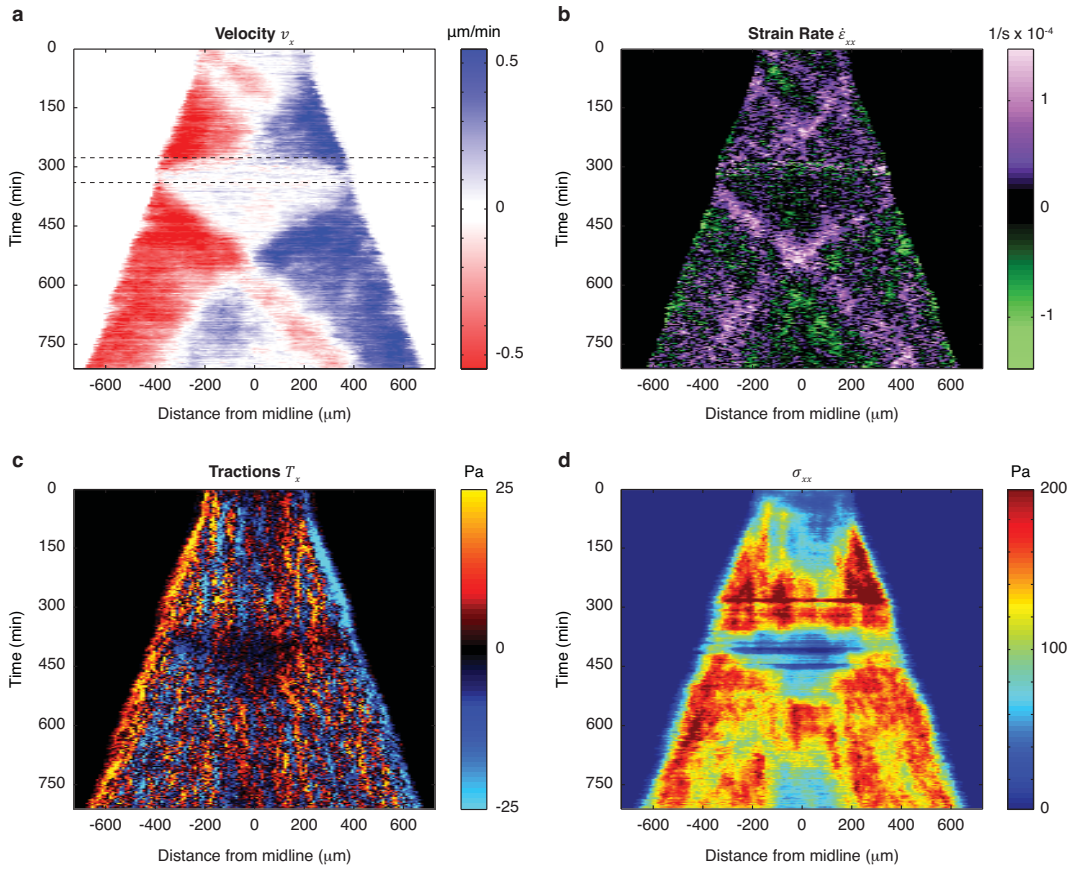

Fig. S3. Effect of a sudden disruption of cell-cell junctions with EGTA during monolayer expansion. Kymographs of velocity v_x (a), strain rate $\dot{\varepsilon}_{xx}$ (b), tractions T_x (c), and monolayer stress component σ_{xx} (d). EGTA was added at 280 min and removed at 325 min (dashed lines).

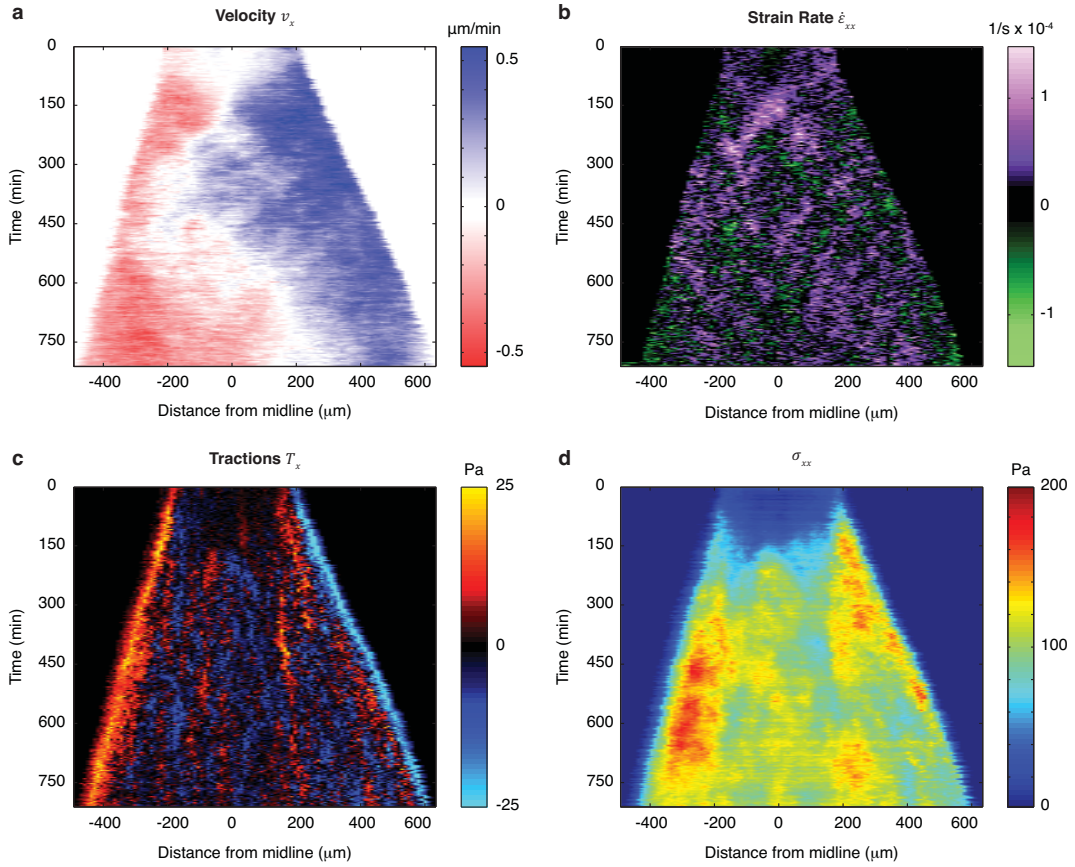

Fig. S4. Dynamic behavior of an asymmetrically expanding cell sheet. Kymographs of velocity v_x (a), strain rate $\dot{\varepsilon}_{xx}$ (b), tractions T_x (c), and monolayer stress component σ_{xx} (d).

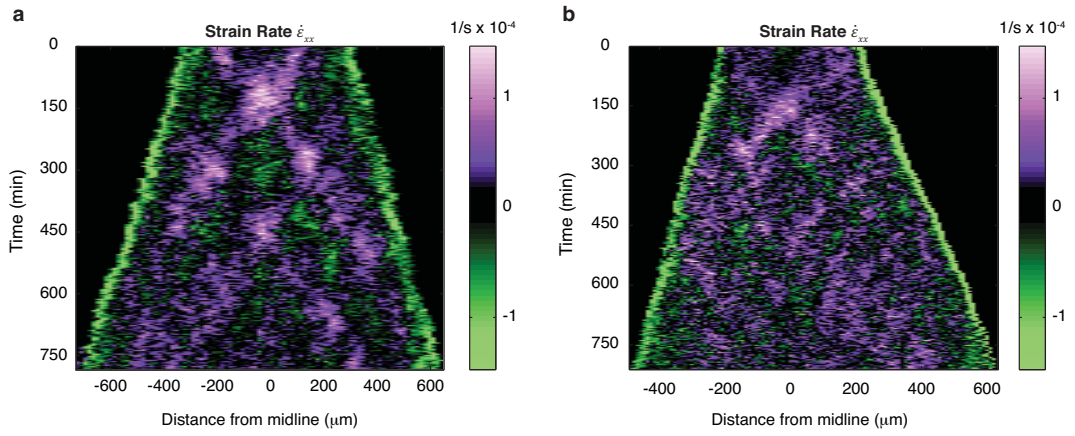

Fig. S5. Boundary effects of PIV. When PIV is applied to the monolayer boundaries, cells only occupy a fraction of the interrogation window. The velocity vector corresponding to that interrogation window has one contribution from the motile monolayer and another contribution from the immobile substrate. As a consequence, the resulting velocity is smaller than the real monolayer velocity. This effect leads to a systematic gradient of velocity at the very edge of the monolayer and, as such, to an artifactual negative strain rate. We have suppressed this artifactual data from Fig. 3b and Supplementary Fig. S4b. (a) and (b) show the unedited data corresponding to Fig. 3b and Supplementary Fig. S4b, respectively.

Supplement 1: Monolayer Stress Microscopy and material properties of the cell monolayer.

To obtain the distribution of stresses throughout the monolayer, MSM uses the map of traction forces together with the two-dimensional balance of forces that is demanded by Newton's laws[1]. Because this force balance must be obeyed at every instant, the computation of monolayer stresses from traction forces does not depend on whether the monolayer is elastic, viscous, or viscoelastic. Without loss of generality, we thus chose to treat the monolayer as a 2D elastic homogeneous material with Young's modulus E and Poisson's ratio ν. In our previous report[1] we used precisely the same approach with ν assigned to be 0.5, but in that report we asserted - incorrectly - that if the traction forces are specified then recovered stress distribution within the monolayer is independent of constitutive properties of the monolayer. While that statement is rigorously true in one-dimensional systems, it is not true in two-dimensional systems, wherein there are two degrees of freedom in the external tractions (T_x and T_y) but three components to the stress tensor (σ_{xx}, σ_{yy}, σ_{xy}). In that case, the coupling between tractions and stresses does not depend on the Young's modulus but does depend on the Poisson's ratio ν.

That being the case, we assessed the sensitivity of stress maps to the assumed value of ν by computing σ_{xx}, σ_{yy}, and σ_{xy} from a set of experimental traction fields T_x and T_y with ν ranging from 0 to 0.5 (Fig. S6). These results demonstrate that variations in ν have negligible effects on σ_{xx} and σ_{xy} but substantial effects on σ_{yy} as ν approached zero. This coupling between σ_{yy} and ν has its origin in the boundary conditions of zero normal displacement at the top and bottom edges of the field of view, but has little influence when ν > 0.4. Moreover, our findings of wave propagation and pattern formation during monolayer growth are restricted to the direction of expansion (x) and are thus largely independent of the choice of ν. Therefore, throughout this report we assume incompressibility (ν=0.5).

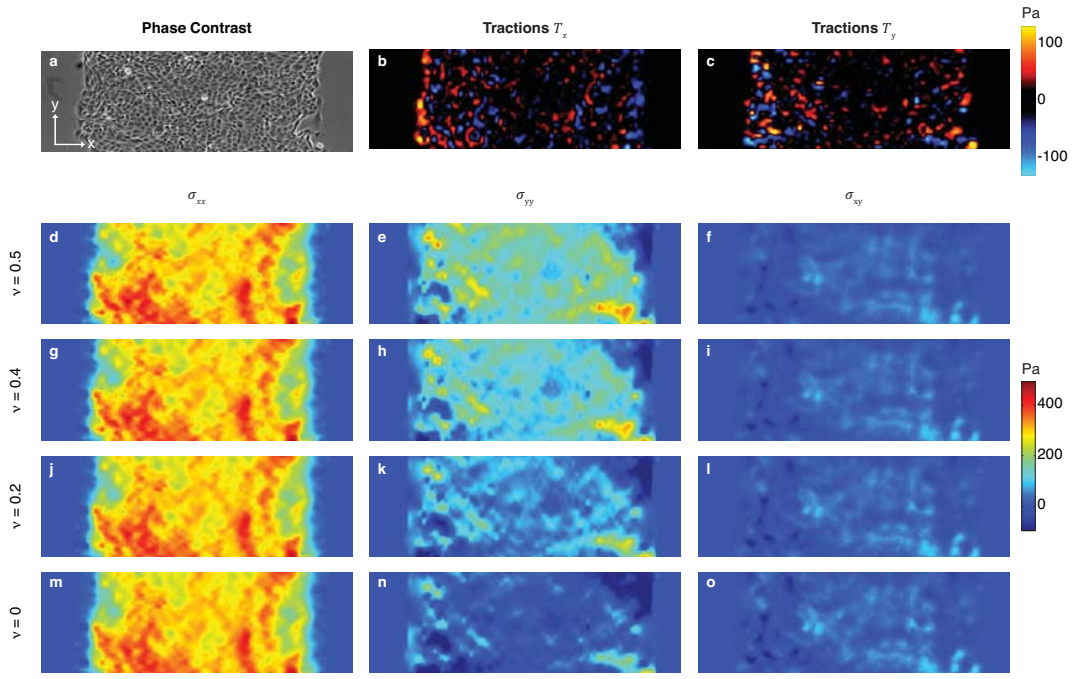

Fig. S6. Dependence of computed monolayer stresses on assumed Poisson's ratio. Phase contrast image (a), traction maps (b, c), and monolayer stress maps (d-o) for different values of Poisson's ratio.

Supplement 2: Monolayer Stress Microscopy and cell height

Monolayer Stress Microscopy performs a formal two-dimensional balance of line tension that is converted to familiar units of stress by using the average height (h) of the monolayer. To account for changes in h during monolayer expansion we used confocal microscopy. We performed z-stack confocal imaging on MDCK cells stably expressing LifeAct-GFP and computed the average fluorescence intensity $< I_{(z,t)} >$ for each time point and for each z plane, where brackets denote average over x and y within the monolayer. We calculated h as the characteristic height obtained from fitting an exponential decay to the tail of $< I_{(z,t)} >$. The average cell height was roughly homogeneous across the direction of expansion (Fig. S7b) and exhibited a sharp decrease with time that stabilized at ~8 μm (Fig. S7a).

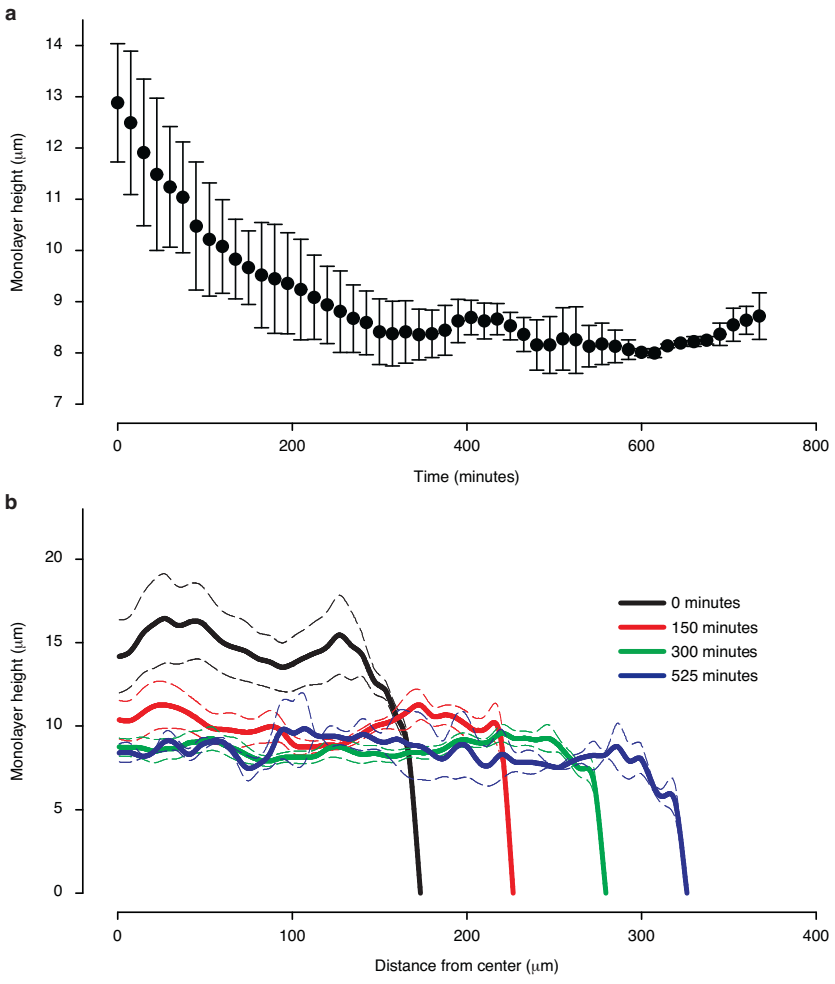

Fig. S7. Monolayer height. (a) Average cell height during monolayer expansion. Error bars represent the SD. (b) Average cell height as a function of the distance from the monolayer midline at different time points. Dashed lines are mean±SD.

Supplement 3: one-dimensional model of monolayer expansion

Using the model described in Fig. 4, we consider here four distinct loading scenarios and analyze the extent to which each of these scenarios captures the central features of our observations including 1) constant velocity of the monolayer leading edge, 2) propagation of a strain rate front, 3) monolayer stress buildup, and 4) temporal reiteration of both strain-rate propagation and stress buildup.

In every case, a numerical solution was obtained by using Newton-Raphson reiterations. In each node, residual force contributions from loads $\boldsymbol{F}_i$ along with forces of discrete elements that join at that node (springs and dashpot) were required to satisfy Eq. 1 (main text).

We first considered the simple case where only the two front cells (one on each side of the monolayer) generate self-propelling forces (Fig. S8, Supplementary movie 9). We simulated this scenario by applying two forces of constant magnitude and opposite sign to the front nodes of the monolayer. In response to these forces, leading cells begin stretching immediately, but viscous friction with the substrate prevents instantaneous transmission of the leading force to the follower cells (Fig. S8d). Consequently, the further a cell is from the leading edge, the longer that cell takes to begin stretching. This delay translates into a pulse of strain rate that penetrates the monolayer and attenuates progressively (Fig. S8c). The system tends asymptotically to a state in which stress and strain of each cell are equal across the monolayer. Accordingly, the system never displays a stress buildup nor constant velocity of the leading edges of the monolayer, thus showing that an active leader/passive follower scenario does not capture the experimental features we observed.

We next considered the case in which all cells have the capacity of generating self-propelling forces simultaneously. (Fig. S9, Supplementary movie 10). We simulated this scenario by applying outward pointing forces of constant magnitude at each node of the monolayer at the same instant of time. Under these circumstances, each half of the monolayer begins moving outwards uniformly and cohesively (Fig. S9b). The elastic stress is highest at the center of the monolayer and decreases towards its edges (Fig. S9d), thus causing a progressive decrease of cell velocities away from the monolayer midline (Fig. S9b). When the model was run in such a configuration we could simulate constant velocity at the leading edges (Fig. S9b), stress buildup in its

central regions (Fig. S9d), and outward propagation of a strain rate pulse (Fig. S9c), all features we observed experimentally. Nevertheless, the model is not able in such circumstances to reproduce an initial phase where stress and strain rate propagate inward from the leading edges towards monolayer midline.

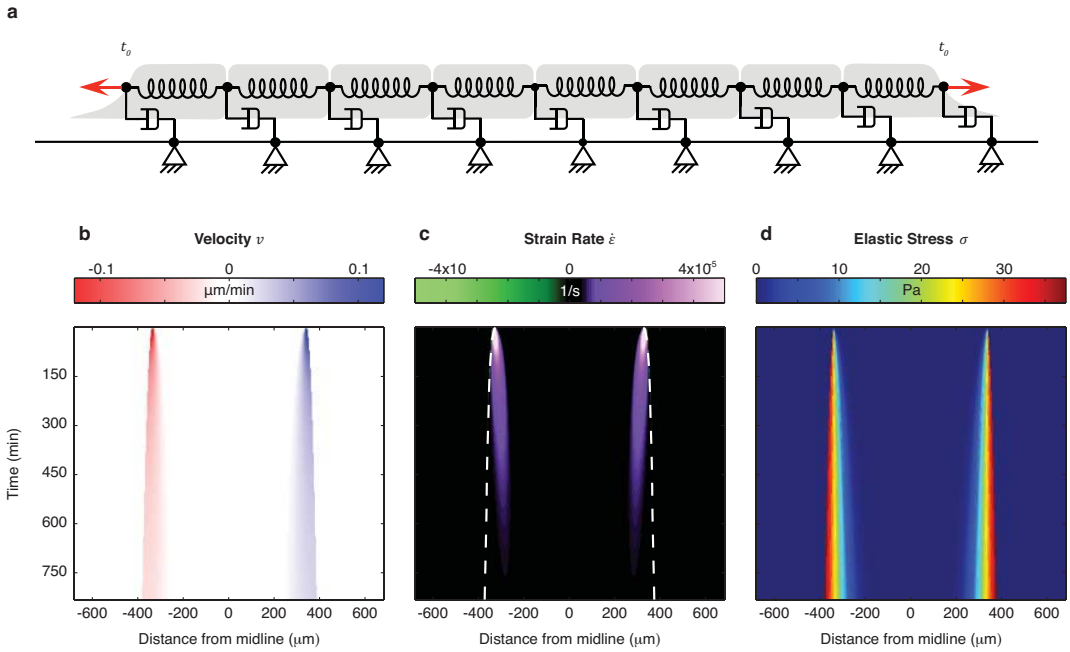

Fig. S8: (a) Cartoon illustrating epithelial dynamics induced by migrating cells located at the leading edges only. At instant $t = t_0$ the two front cells are subject to self-propelling forces of same modulus and opposite direction. (b) Kymograph of epithelial velocity field *vs.* time; (c) kymograph of epithelial strain rate field *vs.* time; (d) kymograph of epithelial elastic stress field *vs.* time.

We next considered a third case in which a cell is able to generate a self-propelling force only if its immediate front neighbor has deformed more than a given strain ε_s (Fig. S10, Supplementary movie 11). This is equivalent to assume that each cell can only acquire a motile phenotype if it senses a force larger than $k\varepsilon_s$ on its front intercellular junction. This type of mechanism has been recently invoked to explain the collective migration of cell clusters[2,3] and the underlying physics can be understood in analogy to "unjamming" phenomena[4-6]. Under such an assumption, the monolayer achieves its initial expansion by successive spreading of each cell row, which results in a strain rate pulse propagating away from the leading edge (Fig. S10c). Once the strain rate pulse reaches the monolayer midline, the system tends to its equilibrium configuration in which stress decreases away from the monolayer midline (Fig. S10d). However, the rate at which every cell tends to its equilibrium

length also decreases with the distance from the midline, thus giving rise to outward propagation of a strain rate pulse (Fig. S10c).

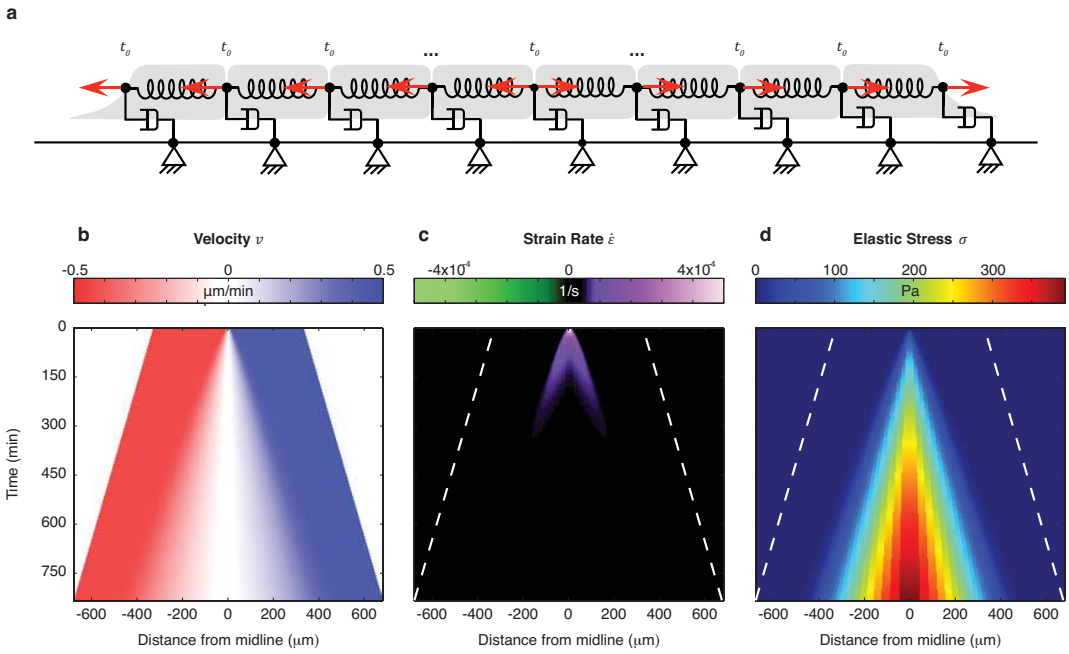

Fig. S9: (a) Cartoon illustrating epithelial dynamics induced by cells that migrate by generating outward self-propelling forces simultaneously at the initial instant t_o. (b) Kymograph of epithelial velocity field *vs.* time; (c) kymograph of epithelial strain rate field *vs.* time; (d) kymograph of epithelial elastic stress field *vs.* time.

Unjamming by itself captures central features of monolayer expansion including propagation of a strain rate pulse away from and back to the leading edge, stress buildup, and linear leading edge velocity, but it does not exhibit spatiotemporal reiteration of local differentials of stress and strain rate. Instead, the system tends asymptotically to an equilibrium state in which the length of each cell decreases with the distance from the leading edge. Spatiotemporal reiteration of local differentials in mathematical models of tissue patterning is typically obtained by considering two competing phenomena coupled through a time delay. In traditional reaction-diffusion models, the competing phenomena are activation and inhibition of morphogens and the time delay originates from their distinct diffusion and reaction rates[7,8]. This idea was recently generalized to the case of mechanochemical systems, where the competing phenomena are diffusion and contractile advection and the time delay originates in their distinct rates [9,10].

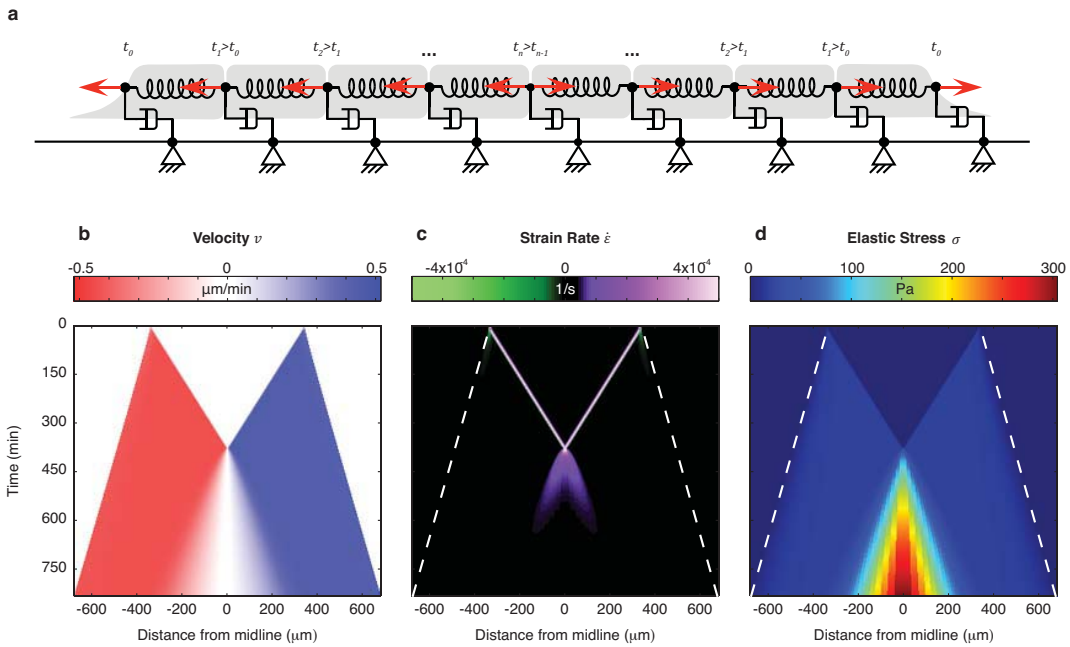

Fig. S10: (a) Cartoon illustrating epithelial dynamics induced by cells that migrate by generating outward self-propelling forces only when their immediate front neighbor has deformed more than a given threshold strain ε_s. (b) Kymograph of epithelial velocity field *vs.* time; (c) kymograph of epithelial strain rate field *vs.* time; (d) kymograph of epithelial elastic stress field *vs.* time.

Here we propose an alternative mechanism in which the two competing phenomena are two recently described non-linear responses of the cytoskeleton to stretch[11]: reinforcement, which causes increases of stiffness[12], and fluidization, which causes decreases of stiffness[13,14]. While both phenomena remain poorly understood, they have been shown to coexist but play out over different time scales. For example, after a single stretch-unstretch cycle cells fluidize suddenly, but hundreds of seconds later they reinforce slowly[13,14]. In order to introduce reinforcement and fluidization in our simple 1D model, we build upon the "unjamming" scenario previously analyzed (Fig. S10), now allowing k to vary with time. Specifically, we assume that stiffness k of each spring is constant only for strains ε_i below an arbitrary threshold $\varepsilon_{th} > \varepsilon_s$. As soon as ε_{th} is reached, a period of reinforcement begins in which k increases with time for a duration Δt. This reinforcement phase is followed by a fluidization phase during which k decreases with time for a duration Δt (Fig. 4c).

Simulations show that for the first ~400 min no cell reaches ε_{th} and thus the evolution of the monolayer (Fig. 4, Supplementary movie S8) is identical to the case described previously (Fig. S10). Progressively from the monolayer midline towards the leading

edge, cells begin to undergo strains greater than ε_{th} and thus elicit an outward wave of reinforcement. As this wave propagates outwards, it causes a progressive stalling paralleled by buildup of stress, as in a tug-of-war, toward the center. The reinforcement wave is followed by a fluidization wave with a delay Δt. This second wave enables further cell stretching and thus causes a second pulse of positive strain rate to propagate outwards and a second peak of stress at the monolayer midline. These simulations establish that cycles of reinforcement and fluidization triggered by a strain threshold result in reiterated propagation of strain rate fronts through the monolayer and oscillations of intercellular stress at the monolayer midline.

Simulation parameters

The values of F, k, and η were chosen to capture the experimental kymographs of velocity, stress, and strain-rate while remaining within the order of magnitude reported in the literature. Specifically, we chose F=4 nN, k= 4 nN, and η=9.2 nN.min/μm. Variables with units of force were transformed to more familiar units of stress by assuming a cross-sectional area of 100 μm^2. Strain thresholds were chosen to be $\varepsilon_s = 0.5$ and $\varepsilon_{th} = 1$. We note that as long as $\varepsilon_s < \varepsilon_{th}$ the model captures the generation and propagation of waves. During a reinforcement/fluidization cycle, the maximum stiffness was set to 3 times its baseline value.

References

1 Tambe, D. T. *et al.* Collective cell guidance by cooperative intercellular forces. *Nat Mater* **10**, 469-475 (2011).

2 Carmona-Fontaine, C. *et al.* Contact inhibition of locomotion in vivo controls neural crest directional migration. *Nature* **456**, 957-961 (2008).

3 Weber, G. F., Bjerke, M. A. & Desimone, D. W. A Mechanoresponsive Cadherin-Keratin Complex Directs Polarized Protrusive Behavior and Collective Cell Migration. *Developmental cell* (2011).

4 Angelini, T. E. *et al.* From the Cover: Glass-like dynamics of collective cell migration. *Proceedings of the National Academy of Sciences of the United States of America* **108**, 4714-4719 (2011).

5 Keys, A. S., Abate, A. R., Glotzer, S. C. & Durian, D. J. Measurement of growing dynamical length scales and prediction of the jamming transition in a granular material. *Nat Phys* **3**, 260-264 (2007).

6 Trappe, V., Prasad, V., Cipelletti, L., Segre, P. N. & Weitz, D. A. Jamming phase diagram for attractive particles. *Nature* **411**, 772-775 (2001).

7 Kondo, S. & Miura, T. Reaction-diffusion model as a framework for understanding biological pattern formation. *Science (New York, N.Y* **329**, 1616-1620 (2010).
8 Turing, A. M. The Chemical Basis of Morphogenesis. *Philosophical Transactions of the Royal Society of London. Series B, Biological Sciences* **237**, 37-72 (1952).
9 Bois, J. S., Julicher, F. & Grill, S. W. Pattern formation in active fluids. *Physical review letters* **106**, 028103 (2011).
10 Howard, J., Grill, S. W. & Bois, J. S. Turing's next steps: the mechanochemical basis of morphogenesis. *Nature reviews* **12**, 392-398 (2011).
11 Kroy, K. & Glaser, J. The glassy wormlike chain. *New J. Phys.*, 416 (2007).
12 Riveline, D. *et al.* Focal contacts as mechanosensors: externally applied local mechanical force induces growth of focal contacts by an mDia1-dependent and ROCK-independent mechanism. *The Journal of cell biology* **153**, 1175-1186 (2001).
13 Trepat, X. *et al.* Universal physical responses to stretch in the living cell. *Nature* **447**, 592-595 (2007).
14 Bursac, P. *et al.* Cytoskeletal remodelling and slow dynamics in the living cell. *Nat Mater* **4**, 557-561 (2005).

Chapter 4 Summary of the results and discussion

Cells exert and withstand forces, not only at the interface between the cells and the extra cellular matrix but also at cell-cell junctions. Different methods have been developed to quantify epithelial cell traction forces (Du Roure et al., 2005; Trepat et al., 2009; Saez et al., 2010), and it has been demonstrated that traction forces exerted locally by each cell on its substrate can be ultimately balanced at distances significantly larger than the size of the cell (Trepat et al., 2009). Intercellular stresses arise from the accumulation of unbalanced cell-substrate tractions. However, measurements of the forces at cell-cell junctions had never been performed.

In the first paper we presented a new method to map and quantify the stresses within a monolayer (monolayer stress microscopy, MSM), and showed their importance in guiding collective cell migration. MSM was conceived and developed by other researchers (Tambe et al., 2011). I collaborated in the study by performing measurements in epithelial cells, quantifying the monolayer height in a migrating monolayer (needed for MSM), and studying at high-resolution cell morphological migratory features inside the monolayer.

MSM uses the maps of traction force of a migrating cell sheet to compute the distribution of the physical forces at every point within the monolayer. Traction forces were computed using traction force microscopy as described previously (Trepat et al., 2009). Using finite element analysis, the intracellular stresses arising from the accumulation of unbalanced cell-substrate tractions are calculated. The analysis is restricted to the interior regions of the optical field of view, where the influences of cell-generated forces in distant regions (outside the optical field of view) are minimal. At any point within the monolayer, a stress tensor with the normal stresses along the laboratory frame axis x and y (σ_{xx} and σ_{yy}) and the shear stress (σ_{xy} and σ_{yx}) is obtained. Eigenvalue decomposition of this stress tensor defines the principal stresses (σ_{max} and σ_{min}) and the corresponding, mutually perpendicular, principal orientations. The average local normal stress, then, can be defined as $\bar{\sigma} = (\sigma_{max} + \sigma_{min})/2$. It describes the magnitude of the stress at each point within the monolayer.

Maps of average normal stress on endothelial (rat pulmonary microvascular endothelial cells) and epithelial (MDCK) cells show that stresses are mostly positive, exceeding 300 Pa in regions spanning tens of cells. At each point within the cell monolayer, the stress field can be isotropic (where $\sigma_{max} = \sigma_{min}$) or anisotropic (where $\sigma_{max} > \sigma_{min}$). Interestingly, cells were found to align and migrate along the orientation of the

maximal principal stress. Indeed, the higher the stress anisotropy, the smaller the alignment angle between the orientation of local cellular migration and that of local maximal principal stress. This emergent guidance mechanism of collective cell migration was termed plithotaxis, from the Greek 'plithos', denoting crowd, swarm, or throng.

In order to test the implication of this finding in cancer research, stress measurements were performed in cells with different metastatic potential. MCF-10A control cells (normal breast epithelial cells), MCF-10A overexpressing ErbB2 (increased invasiveness), or 14-3-3ζ (increased invasiveness and reduced cell-cell junction markers) were tested. MCF-10A control and ErbB2 cells moved in alignment with the direction of maximum principal stress, as previously observed in endothelial and epithelial cells. However, 14-3-3ζ cells migrated independently of principal stress directions. The relevance of cell-cell adhesions was further demonstrated by weakening cell-cell contacts using calcium chelation. This treatment lessened the alignment between local cellular migration and local stress orientation. Placing the cells again to normal growth medium conditions restored plithotaxis, but this reversibility was blocked in the presence of E-cadherin antibodies in the medium.

Monolayer Stress Microscopy requires the average height of the monolayer to convert the two-dimensional balance of line tension to familiar units of stress. Z-stack images of MDCK actin-GFP cells were acquired and cell height was measured according to GFP intensity. Average monolayer height increased smoothly over the first two cells of the leading edge (approximately 20 μm), and thereafter was roughly constant at approximately 6 μm, with a coefficient of variation close to 20%. As such, the errors on the stress computations for regions more than 20 μm away from the leading edge would be smaller than 20%.

Using a wound scratch assay, Farooqui et al. reported previously that MDCK cells located many rows behind the leading edge formed cryptic lamellipodia that extended underneath their neighbors (Farooqui and Fenteany, 2005). By mixing MDCK actin-GFP and α-actinin-RFP cells, we observed that cryptic lamellipodia were also formed away from the leading edge in an expanding colony. This observation supports the findings that cells located away from the leading edge produce migratory structures, generating traction forces that are eventually transmitted to their neighbors.

In the second paper, I implemented a new approach to study biomechanically the expansion of an epithelial monolayer. The approach is based on PDMS micropatterning of cells in a polyacrylamide gel in order to 1) initially confine cell groups in a well-defined geometrical region and 2) trigger collective cell migration upon removal of the membrane. The approach allows the measurement of traction forces (using TFM) and cell-cell stresses (using MSM), as well as a quantification of cellular velocities during monolayer expansion. Membrane openings of 300 x 2500 μm were used. The approach permits reproducible, controllable, and systematic conditions and, therefore, has the potential to be scaled up and used in high-throughput studies.

In the first place we studied the morphological and genetic changes occurring in epithelial cells (MDCK II) switching from a static to a migratory phenotype. Cells flattened, the actin cytoskeleton reorganized forming stress fibers, and focal adhesions emerged, as seen by localized paxillin accumulation at the basal region of the cell. By using quantitative PCR, we measured the expression of different genes traditionally associated to epithelial-to-mesenchymal transition. After seven hours of collective cell migration initiation, ß-actin, vinculin, and paxillin, increased significantly their expression, whereas vimentin, zo-1, ß-catenin or E-cadherin did not.

In the second place, we studied the biomechanical features of the monolayer expansion. To do so, we analyzed cellular velocities, tractions and stresses. Removal of the PDMS membrane produced an increase in cellular velocities localized initially at the free edges. Cells in the central part were initially static and became motile progressively. Traction forces were initially low, and increased as the cells migrated. Forces generated by cells at the leading edges were opposed to the direction of cell movement. Interestingly, at the initial phase, these forces were balanced by forces of opposite sign exerted by cells two or three rows away from the leading edge, generating a local increase in cell-cell stresses within the first cell rows. However, this was a transient situation: as the cells inside the monolayer became migratory, they exerted high traction forces, equivalent in magnitude to the forces generated by leading cells, and high stress regions were found everywhere in the monolayer.

Finally, we studied the dynamic evolution of the mechanical parameters. As the monolayer expanded, temporal and spatial fluctuations of cell velocities, tractions, and stresses were observed. In order to analyze the evolution of the different parameters systematically, we computed the average value of these parameters along the monolayer (corresponding to y axis), and represented them as spatio-temporal kymographs. Patterns of inward and outward mobilizations could be clearly appreciated in cell velocity kymographs. Kymographs of strain rate, obtained from cellular velocities,

revealed clear waves launched at each leading edge propagating away from and back to the leading edge, and spanning all the expanding monolayer. At the central region of the monolayer, these waves of strain rate were translated in a clear increase in cell area, and, interestingly, with a peak of cell-cell stress. Moreover, these cell-cell stresses and cell area oscillated with time as the monolayer expanded. Both the strain rate waves and stress oscillations were perturbed when disrupting the cell contractile machinery (using the myosin II inhibitor blebbistatin) or cell-cell junctions (using calcium chelator ethylene glycol tetraacetic acid, EGTA). In the case of myosin II inhibition, the monolayer still expanded but both the strain-rate waves and stress oscillations were absent. Interestingly, a sudden disruption of cell-cell junctions using EGTA induced an immediate arrest in wave propagation, and enabling cell-cell junction formation successively reinitialized wave propagation from the edges and stress oscillations in the monolayer.

Different computational models were tested in order to investigate the mechanisms accounting for wave propagation and area and stress oscillations. Neither restricting force generation to cells at the leading edge nor allowing each cell to be mechanically self-propelled captured the experimental findings. However, they were perfectly reproduced when considering two assumptions: in the first place, cells could only acquire a motile phenotype when an adjacent cell either created space or pulled on the shared intercellular junctions. This created a local unjamming and lead to the propagation of a strain-rate front followed by a stress build-up. Secondly, if cells were assumed to have a threshold of strain beyond which the cytoskeleton first reinforced and then fluidized, the strain rate fronts and stress differentials became reiterated in time.

A new study by Ng et al. has reported the propagation of a motility wave in a wound-healing assay using MCF10A epithelial cells (Ng et al., 2012), consistent with the findings described above. By performing experiments in substrates of different compliances, they observed that the wave of motility coordination propagated faster and farther reaching on stiff substrates, suggesting collective cell migration to be mechanosensitive. Similarly to the experiments performed using MDCK cells, multicellular coordination was reduced upon myosin II inhibition or cadherin-mediated cell-cell adhesion disruption, indicating that a contractile force transmission between neighbouring cells was needed to regulate collective migration.

To what extend are these mechanical events relevant in physiological or pathophysiological conditions? It is well established that cells integrate signals and respond to their mechanical environment (DuFort et al., 2011). The reported mechanical waves constitute tissue-generated mechanical candidates to trigger mechanotransduction events during wound healing, morphogenesis, or collective cellular invasion in cancer. The precise signaling pathways involved in the migratory phenotype acquisition remain to be precisely elucidated, although it is likely they involve the MAPK/Erk signaling cascade, as reported by Matsubayashi et al. (Matsubayashi et al., 2004) in wound-healing assays. Moreover, not only migratory properties could be influenced by the described mechanical waves. Indeed, it has been demonstrated that external forces affect cell division orientation (Fernandez et al., 2011; Fink et al., 2011), which is fundamental to shape tissues properly (Gillies and Cabernard, 2011). In this direction, it is promising to explore the possible influence of the reported mechanical waves in the rate or orientation of cell divisions.

Chapter 5 Conclusions of the thesis

1. Traction microscopy and monolayer stress microscopy were implemented in order to measure the traction forces and cell-cell stresses of an expanding colony of MDCK epithelial cells. Cells were found to align and migrate along the direction of the maximal principal stress, similarly to endothelial cells (aim 1.1).

2. Local height of the expanding cell colony was measured using MDCK actin-GFP cells. Average cell height increased smoothly at the leading edge and thereafter remained constant at approximately 6 μm (aim 1.2).

3. Cryptic lamellipodia were observed in cells located away from the leading edge (aim 1.3)

4. An experimental model was implemented to study systematically the expansion of an epithelial monolayer. A PDMS membrane was used to initially confine cells in a well-defined geometrical region and to trigger collective cell migration upon its removal. The model was implemented in soft, collagen-coated polyacrylamide gels, which permitted the biomechanical study of the process (aim 2.1).

5. Local height of an expanding monolayer of MDCK cells expressing life-Act GFP was measured. Average cell height was roughly homogeneous in space but exhibited a sharp decrease with time that stabilized at ~8 μm (aim 2.2).

6. Software to automatically determine monolayer boundaries of the expanding cell monolayer was developed. The algorithm is based on computing the standard deviation of different interrogation windows on the phase contrast image (aim 2.3).

7. Morphological changes after triggering collective cell migration were studied. Actin stress fibres formed, paxillin accumulated at focal adhesions and E-cadherin was partially internalized. Zo-1 remained unaltered (aim 3.1).

8. Quantitative PCR of EMT markers was performed before and after triggering collective cell migration. ß-actin, vinculin, and paxillin increased significantly their expression, whereas vimentin, Zo-1, ß-catenin or E-cadherin did not (aim 3.2).

9. The contribution of cell proliferation to monolayer expansion was studied. Less than 50% of the total cell sheet area after 10 hours of expansion was attributable to cell proliferation (aim 3.3).

10. Traction forces and cell-cell stresses were initially low across the monolayer and increased as cells adopted a migratory phenotype (aim 3.4).

11. Wave-like crests of strain rate are propagated away from and back to the leading edge during monolayer expansion. At the central region of the expanding monolayer, oscillations of cell area were paralleled by fluctuations of cell-cell stresses. A model based on sequential fronts of cytoskeletal reinforcement and fluidization captured the experimental findings (aim 3.4).

12. The contribution of cell-cell junctions to the propagation of mechanical waves was studied. Cell-cell junction disruption halted wave propagation and mechanical oscillations (aim 3.5).

13. The contribution of cell contractility to wave propagation was studied. Cells migrated collectively after myosin inhibition, but strain rate waves and mechanical oscillations were impaired (aim 3.5).

Appendices

Appendix A

Preparation of PDMS membranes with hollow regions using SU-8 masters

REAGENTS AND MATERIALS

- SU-8 50 photoresist (MicroChem)
- SU-8 developer (MicroChem)
- Sylgard 184 silicone elastomer base and curing agent - PDMS (Dow Corning)
- 1H,1H,2H,2H-Perfluorooctyl-trichlorosilane (Sigma)
- Glass slides
- Acetone
- Ethanol
- Transparent mask containing the desired features. If the desired patterns are large (all dimensions larger than 10 μm) the design can be done using Adobe Illustrator and printed at high resolution on a transparent paper.
- Vacuum jar

CLEANROOM EQUIPMENT

Parts of this protocol must be performed at the clean room (spinning, UV exposing and development). The equipment that will be used is:

- Spinner
- UV mask aligner
- Hot plates
- Water bath sonicator

PROTOCOL

a. SU-8 spinning on glass slides

1) Clean glass slides by sonicating them for 5 minutes in acetone, ethanol, and miliQ water consecutively. Dry out the slides using a stream of compressed nitrogen.
2) Under yellow light, place the glass slide on the spinner holder and immobilize it with vacuum. Pour some SU-8 on top of the glass slides and smear it using a plastic Pasteur pipette.
3) Spin-coat for 5 seconds at 500 rpm and then for 30 seconds at 3500 rpm to obtain a thin layer of SU-8.

b. SU-8 photolitography

4) Transfer the glass slides to the hot plate and soft-bake for 6 minutes at 65 ºC and then for 20 minutes at 95 ºC.
5) Stick the transparency mask on the bottom side of the square glass of the UV aligner and
6) Place the glass slide on the UV mask stand and bring it into contact with the resist. Expose to UV light for 5 seconds.
7) Place the glass slides for 1 minute at 65 ºC and for 6 minutes at 95 ºC.

c. SU-8 development and silanization

8) Immerse the glass slide in SU-8 developer; the non-exposed regions are washed away. This process takes around 5 minutes. Rinse with isopropanol and dry out using nitrogen. Yellow light is no longer required.
9) Place the slides in a vacuum jar and add 1-2 drops of 1H,1H,2H,2H-Perfluorooctyl-trichlorosilane in a cover slip. Induce vacuum and wait 1 hour.

d. Fabrication of PDMS membranes

10) Prepare the PDMS by mixing thoroughly base and crosslinker in a 10:1 proportion for 5 minutes and remove air placing the mixture in a vacuum jar for 1 hour.
11) Place the glass slide containing the SU-8 raised features on the spinner holder and immobilize it using vacuum. Pour some PDMS on top.

12) Spin-coat the PDMS for 5 seconds at 500 rpm and then for 1 minute 15 seconds at 4200 rpm.
13) Place the slide in the hot plate for 20 minutes at 70 ºC
14) Using a plastic Pasteur pipette, place some more PDMS at the edges of the thin PDMS membrane to make handling easier.
15) Place the slide in the oven for 1 hour at 70 ºC.
16) Detach the PDMS membrane from the glass slide using tweezers and store them at 4 ºC in ethanol until use.

Appendix B

Membrane based patterning for collective cell migration

REAGENTS AND MATERIALS

- Glass-bottom petri dishes (35 mm) - Mattek, Ashland, MA
- Hepes 10 mM.
- 40% Acrylamide solution – BioRad (161-0140)
- 2% BIS solution – BioRad (161-0142)
- 200 nm diam. Red fluorescent latex beads – Molecular Probes (F-8811)
- 10 % Amonium persulfate diluted in water - BioRad (161-0700)
- TEMED – Sigma (T-9281)
- NHS acrylate - Sigma (A8060-1g)
- Rat tail collagen type I – Upstate, Lake Placid, NY (08-115)
- Silane solution of:
    - 3-(Trimethoxysilyl)propyl methacrylate - Sigma (M6514) (714 μl)
    - Acetic Acid (714 μl)
    - Absolut etanol (1ml)
- Pluronic F-127 - Sigma (P2443)
- PDMS membranes fabricated according protocol described in appendix 1

PROTOCOL

a. Glass-bottom petri dish activation

1. Add bind silane solution on the glass-bottom dishes until they are covered and incubate for 30 minutes.
2. Wash with ethanol twice.

b. Preparation of polyacrylamide gels

3. Prepare the polymerizing solution. To obtain a stiffness of 1 kPa (Shear Modulus), add:
   - 304 ml HEPES
   - 100 ml NHS solution (10 mg/ml)
   - 2 ml beads (after vortexing)
   - 68,75 ml acrylamide
   - 22,5 ml bisacrylamide
   - 2,5 ml APS
   - 0,25 ml TEMED
4. Vortex and add 10 μl to the center of the glass-bottom dish.
5. Place a 12 mm glass coverslip on top and wait at least 40 minutes until polymerization is complete.
6. Add 2 ml of distilled water and gently remove the coverslip with a surgical blade.
7. Place the gels under the hood and sterilize them with UV for 20 min.

c. Collagen coating

8. Prepare a solution of 0,1mg/ml of collagen I in PBS and add 200 μl on top of the polyacrylamide gel. Leave it overnight at 4ºC.
9. Aspirate collagen and wash the gels twice with PBS. Add 2 ml of media. Wait at least 30 min. If the gels are not used immediately, they can be stored at 4 ºC for a few days.

d. Cell seeding

10. Incubate the PDMS membranes in Pluronic for 1 hour.
11. Dry out the PDMS membranes (20 minutes).
12. Aspirate media from polyacrylamide gels and let them dry for 4 minutes.
13. Carefully place the PDMS membranes on the gels and wait 2 minutes.
14. Concentrate 40.000 cells in 8 μl of media and place them on the hollow region defined by the PDMS membrane.
15. Once the cells have attached (after 20 minutes), wash and add more media (200 μl) on top of the PDMS membrane. Keep the cells at the incubator overnight.
16. To start the experiment, add 2ml of media and remove the PDMS membrane.

Appendix C

Publications and conference communications

Publications

1. Kim JH, **Serra-Picamal X**, Tambe DT, Steward, Butler JP, Trepat X, Fredberg JJ. 2013. Propulsion and navigation modules within the advancing monolayer sheet. (Submitted).

2. **Serra-Picamal X**, Conte V, Vincent R, Anon E, Tambe DT, Bazellieres E, Butler JP, Fredberg JJ, Trepat X. 2012. Mechanical waves during tissue expansion. *Nature Physics* 8, 628–634.

3. Anon E, **Serra-Picamal X**, Hersen P, Gauthier NC, Sheetz MP, Trepat X, Ladoux B. 2012. Cell crawling mediates collective cell migration to close undamaged epithelial gaps. *Proceedings of the National Academy of Sciences* 109, 10891-10896.

4. Tambe DT, Hardin CC, Angelini TE, Rajendran K, Park CY, **Serra-Picamal X**, Zhou EH, Zaman MH, Butler JP, Weitz DA, Fredberg JJ, and Trepat X. 2011. Collective cell guidance by cooperative intercellular forces. *Nature Materials* 10, 469 - 475.

5. **Serra-Picamal X**, and Trepat X. 2011. Nanotecnologías para el estudio de la migración celular. *Revista de la Sociedad Española de Bioquímica y Biología Molecular* 168, 14 - 17.

Conference communications

1. **Serra-Picamal X**, Uroz M, Trepat X. Mechanical waves orient cell-division during monolayer growth. December 2012. *American Society for Cell Biology Meeting.* San Francisco (USA). Poster communication.

2. Bazellieres E, Vincent R, **Serra-Picamal X**, Conte V, Bintanel M, Trepat X. Regulation of collective cell migration and intercellular force transmission by cell-cell junction proteins. December 2012. *American Society for Cell Biology Meeting.* San Francisco (USA). Poster communication.

3. Vincent R, **Serra-Picamal X**, Conte V, Bazellieres E, Anon E, and Trepat X. Self-rheology of cell monolayers. September 2012. *EMBO conference "Physics of cell: from soft to living matter"*. Poster communication. *

4. **Serra-Picamal X**, Conte V, Anon E, Vincent R, and Trepat X. Mechanical waves during tissue expansion. June 2012. *5th Ibec symposium on Bioengineering and Nanomedicine*. Barcelona. Poster communication.

5. Conte V, **Serra-Picamal X**, Vincent R, and Trepat X. Modelling mechanical wave propagation in epithelial expansion. June 2012. *5th Ibec symposium on Bioengineering and Nanomedicine*. Barcelona. Oral and poster communication. **

6. Vincent R, **Serra-Picamal X**, Conte V, Anon E, and Trepat X. Self-rheology of cell monolayer. March 2012. *Meeting of The American Physical Society*. Boston (USA). Oral communication.

7. **Serra-Picamal X**, Anon E, Conte V, Vincent R, and Trepat X. Distinct regimes of mechanical propagation at the onset of collective cell migration. February 2012. *QuanTissue: Quantitative Models in Cell and Developmental Biology*. Barcelona. Poster communication.

8. **Serra-Picamal X**, Anon E, and Trepat X. Distinct regimes of mechanical propagation at the onset of collective cell migration. December 2011. *American Society for Cell Biology Meeting*. Denver (USA). Poster communication.

9. **Serra-Picamal X**, Anon E, Conte V, Vincent R, and Trepat X. Emergence Of Mechanical Patterns During Tissue Growth. October 2011. *4th IBEC Symposium on Bioengineering and Nanomedicine*. Barcelona. Oral and poster communication. *

10. Bazellieres E, **Serra-Picamal X**, Casares L, Vincent R, and Trepat X. Inter-cellular force transmission through cell-cell junctions during collective cell migration. October 2011. *4th IBEC Symposium on Bioengineering and Nanomedicine*. Barcelona. Poster communication.

11. Conte V, **Serra-Picamal X**, Vincent R, and Trepat X. Modelling mechanical pattern formation in tissue Dynamics. October 2011. *4th IBEC Symposium on Bioengineering and Nanomedicine*. Barcelona. Poster communication.

12. Anon E, **Serra-Picamal X**, Hersen P, Sheetz MP, Trepat X, and Ladoux B. Size and shape dependence of the mechanisms driving epithelial sealing. October 2011. *4th European Cell Mechanics Meeting*. Amsterdam (The Netherlands). Oral communication. **

13. **Serra-Picamal X**, Anon E, and Trepat X. Physical forces and cell cell interactions at the onset of collective cell migration. May 2011. *Frontiers in Cell Migration and Mechanotransduction*. Bethesda (USA). Poster communication.

14. Pouille PA, **Serra-Picamal X**, Martín-Blanco E, and Trepat X. Epithelium expansion dynamics on a planar substrate. May 2011. Lisbon (Portugal). Poster communication.

15. **Serra-Picamal X**, Anon E, and Trepat X. Physical forces at the onset of collective cell migration. December 2010. *50th American Society for Cell Biology Meeting. Philadelphia (USA)*. Poster communication.

16. **Serra-Picamal X**, Anon E, and Trepat X. Traction forces, cell-cell stresses, and collective cell migration. August 2010. *6th World Congress on Biomechanics*. Singapur (Singapur). Oral communication.

17. **Serra-Picamal X**, Anon E, and Trepat X. Traction forces, cell-cell stresses, and collective cell migration. June 2010. *3rd IBEC Symposium on Bioengineering and Nanomedicine*. Barcelona. Oral and poster communication. **

18. **Serra-Picamal X**, and Trepat X. Combination of traction microscopy and micropatterning technology to study collective cell migration. November 2009. *1st IRB PhD Symposium*. Barcelona. Poster communication. *

19. **Serra-Picamal X**, and Trepat X. Combination of traction microscopy and micropatterning technology to study collective cell migration. October 2009. *3rd European Meeting on Cell Mechanics*. Bad Honnef (Germany). Oral communication.

20. **Serra-Picamal X**, and Trepat X. Combination of traction microscopy and micropatterning technology to study collective cell migration. September 2009. *III Jornada de biofsica*. Barcelona. Oral communication.

21. **Serra-Picamal X**, Anon E, Mascarenas D, Navajas D, Butler JP, Fredberg JJ, and Trepat X. Wound Healing Mechanics: Moving Together Without a Leader April 2009. *2nd IBEC Symposium on Bioengineering and Nanomedicine*. Barcelona. Oral communication.

* Best poster award

** Best presentation award

Appendix D

Resum de la tesi

Introducció - La migració cel·lular és un procés fonamental en el desenvolupament i homeòstasis d'organismes multicel·lulars. La formació de teixits durant el desenvolupament embrionari, la curació de ferides, o la resposta immunitària requereixen la migració de les cèl·lules a localitzacions específiques. D'altra banda, en situacions patològiques com la invasió de cèl·lules cancerígenes, les cèl·lules del tumor primari migren a teixits distants, on poden generar tumors secundaris[1].

La migració cel·lular es pot produir de forma individual o de forma col·lectiva. En aquest darrer cas, grups de cèl·lules migren de manera cohesionada, físicament i funcionalment. Per fer-ho, formen diferents tipus d'estructures multicel·lulars, com ara monocapes que migren sobre una superfície bidimensional o agregats cel·lulars que migren a través de la matriu extracel·lular o altres cèl·lules formant estructures tridimensionals. El mecanisme que permet el moviment de cèl·lules individuals està ben establert i es basa en un procés que es repeteix cíclicament i que inclou la generació de protrusions a la part anterior de la cèl·lula, formació d'adhesions, translocació del cos cel·lular per contracció i alliberament de les adhesions a la part posterior[2]. Per contra, els mecanismes que permeten la migració col·lectiva no estan tan ben descrits. En part, això es deu al fet que és necessari comprendre amb detall la interacció entre els mecanismes de senyalització bioquímica i la mecànica cel·lular, a través de la qual es generen les forces que permeten, en última instància, el moviment de la cèl·lula. En aquest sentit, s'han desenvolupat diferents mètodes per quantificar les forces que teixits epitelials exerceixen sobre el substrat (forces de tracció)[3,4]. S'ha demostrat que, en conjunts multicel·lulars, forces exercides localment per una cèl·lula poden ser balancejades per forces exercides a distàncies significativament més grans que la mida de la cèl·lula. Això implica l'existència de forces inter-cel·lulars, que són transmeses entre cèl·lules adjacents a través de les unions cel·lulars[3]. S'ha suggerit que aquestes forces poden ser rellevants a l'hora de determinar migració cel·lular col·lectiva[5]. Aquestes forces, però, no s'han mesurat mai experimentalment.

Objectius - L'objectiu general d'aquesta tesi ha estat estudiar els mecanismes biomecànics involucrats en l'expansió d'una monocapa epitelial. Per tal de fer-ho, en primer lloc s'han mesurat les forces de tracció, els esforços cèl·lula-cèl·lula, i la morfologia cel·lular d'una colònia de cèl·lules epitelials en expansió. En segon lloc, s'ha

implementat un nou model experimental i realitzat un anàlisi sistemàtic de la migració cel·lular col·lectiva en teixits epitelials, la qual cosa n'ha permès la caracterització morfològica, genètica i biomecànica.

Resultats i discussió - Els resultats de la tesi s'han presentat en forma de dos articles.

En el primer article[6], es va presentar un nou mètode per quantificar les forces intra- i intercel·lulars en una monocapa en migració, i es va demostrar la seva importància a l'hora de definir la direcció del moviment de les cèl·lules. Es va observar que les cèl·lules en un teixit estan sotmeses a un esforç majoritàriament de tensió i que fluctua en l'espai i en el temps. A més, aquest esforç és generalment anisotròpic, i es va demostrar que les cèl·lules tendeixen a alinear-se i migrar en la direcció de l'esforç principal màxim. A aquesta comportament se'l va descriure com a 'plithotaxis', al·ludint a la paraula grega *plithos* (multitud). Es va observar que tant cèl·lules endotelials, epitelials, i cèl·lules de càncer de mama abans però no després de la transició epiteli-mesenquimal segueixen aquest comportament.

En el segon article[7], es va desenvolupar un nou model experimental basat en la utilització de membranes de polidimetilsiloxà (PDMS) per l'estudi biomecànic de l'expansió de teixits epitelials. L'aproximació va consistir en confinar inicialment grups de cèl·lules epitelials en regions geomètriques ben definides mitjançant la membrana de PDMS i induir posteriorment la migració cel·lular col·lectiu al retirar la membrana, permetent l'estudi de l'expansió epitelial d'una manera controlada i sistemàtica. Inicialment es van estudiar els canvis morfològics i genètics que cèl·lules epitelials pateixen quan canvien d'un fenotip estàtic a un fenotip migratori. A l'iniciar-se la migració cel·lular col·lectiva, les cèl·lules adopten un fenotip parcialment mesenquimal, perdent polaritat apico-basal, generant fibres d'estrès a la part basal i formant noves adhesions focals. Mitjançant la tècnica de PCR quantitativa es van mesurar els nivells d'expressió de gens tradicionalment associats a transicions epiteli-mesenquimals. Al cap de 7 hores d'iniciar-se la migració cel·lular col·lectiva, els gens que codifiquen per paxilina, vinculina, i b-actina augmentaven de forma significativa la seva expressió, mentre que d'altres (vimentina, ZO1, b-catenina i E-cadherina) no ho feien. En segon lloc, es va estudiar l'expansió de la monocapa des d'un punt de vista biomecànic. Es va observar que l'expansió de monocapes epitelials implica l'adquisició d'un fenotip migratori de forma progressiva caracteritzat per traccions i esforços cel·lulars elevats. A l'estudiar l'evolució dinàmica dels paràmetres mecànics, es va observar l'existència d'ones de deformació cel·lular que es propaguen en la monocapa durant la seva

expansió. A més, aquestes ones estan relacionades amb oscil·lacions d'esforç intercel·lular que es produeixen de forma sistemàtica durant l'expansió epitelial. Es va comprovar que ni la propagació d'aquestes ones ni les oscil·lacions d'esforç es produeixen si es suprimeix la maquinària contràctil de la cèl·lula o si es restringeixen les unions cèl·lula-cèl·lula. Aquestes ones mecàniques transmeses en el teixit poden tenir repercussions sobre cèl·lules localitzades centenars de micres més allunyades d'allà a on han estat generades inicialment, de tal manera que podrien constituir una important forma de senyalització durant la migració cel·lular col·lectiva.

Conclusions - Els resultats presentats en aquesta tesi han servit per demostrar l'existència d'un sistema de guiatge cel·lular basat en la transmissió de forces intercel·lulars durant la migració cel·lular col·lectiva. A més, s'ha estudiat l'expansió de teixits epitelials des d'un punt de vista biomecànic, i s'han descobert ones mecàniques que es propaguen durant aquest procés. Així, s'han proporcionat noves eines i coneixements sobre els esdeveniments biomecànics implicats en la migració cel·lular col·lectiva, que poden servir per obtenir una millor comprensió de determinats processos embriogènics, la curació de ferides o la invasió de certs tipus de cèl·lules cancerígenes.

Bibliografia

1 Friedl, P. & Gilmour, D. Collective cell migration in morphogenesis, regeneration and cancer. *Nature Reviews Molecular Cell Biology* **10**, 445-457 (2009).

2 Ridley, A. J. *et al.* Cell migration: integrating signals from front to back. *Science* **302**, 1704-1709 (2003).

3 Trepat, X. *et al.* Physical forces during collective cell migration. *Nature physics* **5**, 426-430 (2009).

4 Du Roure, O. *et al.* Force mapping in epithelial cell migration. *Proceedings of the National Academy of Sciences of the United States of America* **102**, 2390 (2005).

5 Weber, G. F., Bjerke, M. A. & DeSimone, D. W. A Mechanoresponsive Cadherin-Keratin Complex Directs Polarized Protrusive Behavior and Collective Cell Migration. *Developmental cell* **22**, 104-115 (2012).

6 Tambe, D. T. *et al.* Collective cell guidance by cooperative intercellular forces. *Nature materials* **10**, 469-475 (2011).

7 Serra-Picamal, X. *et al.* Mechanical waves during tissue expansion. *Nature physics* **8**, 628-634 (2012).

Appendix E

Resum dels articles

Títol: Collective cell guidance by cooperative intercellular forces. (Guiatge cel·lular col·lectiu per mitjà de forces intercel·lulars cooperatives).

Autors: Tambe DT, Hardin CC, Angelini TE, Rajendran K, Park CY, Serra-Picamal X, Zhou EH, Zaman MH, Butler JP, Weitz DA, Fredberg JJ & Trepat X.

Publicació: *Nature Materials* 10, 469-475 (2011).

Resum:

Les cèl·lules que componen un teixit migren com una part d'un col·lectiu. La coordinació de processos col·lectius en conjunts multicel·lulars, però, no és clara, ja que els esforços exercits a les unions cèl·lula-cèl·lula no han estan accessibles experimentalment. En aquest estudi es presenten mapes d'aquests esforços dins i entre les cèl·lules que componen una monocapa. Dins el teixit cel·lular apareixen fluctuacions no anticipades d'esforços mecànics que són severes, sorgeixen espontàniament i que es propaguen a través de la monocapa. En aquest context d'esforç mecànic, les cèl·lules migren seguint les orientacions locals de l'esforç principal màxim. La migració tant de cèl·lules endotelials com epitelials segueixen aquest comportament, així com cèl·lules de càncer de mama abans però no després de la transició epiteli-mesenquimal. La migració col·lectiva en aquests sistemes està governada per un principi fisiològic simple i unificador: les cèl·lules adjacents uneixen forces per transmetre esforços normals a través d'unions cèl·lula-cèl·lula, però migren al llarg de les orientacions d'un mínim d'esforç tangencial.

Títol: Mechanical waves during tissue expansion. (Ones mecàniques durant l'expansió de teixits).

Autors: Serra-Picamal X, Conte V, Vincent R, Anon E, Tambe DT, Bazallieres E, Butler JP, Fredberg JJ & Trepat X.

Publicació: *Nature Physics* 8, 628-634 (2012).

Resum:

Els processos pels quals un organisme adquireix la seva forma i cura les ferides impliquen l'expansió d'una monocapa de cèl·lules. El mecanisme que governa aquesta expansió epitelial és desconegut, tot i que la seva desregulació contribueix a diverses malalties, incloent els carcinomes, que representen al voltant del 90 % de tots els càncers. Utilitzant una monocapa de cèl·lules epitelials geomètricament ben definida com a model experimental, presentem la descoberta d'una ona mecànica que es propaga lentament i s'estén a través de la monocapa, travessant unions intercel·lulars d'una manera cooperativa i acumulant diferencials de tensió mecànica. Les característiques essencials de la generació i propagació d'aquesta ona queden capturades per un model mínim basat en fronts seqüencials de reforçament i fluïdització del citoesquelet. Aquesta descoberta estableix un mecanisme de guiatge cel·lular de llarg abast, ruptura de simetria i formació de patrons durant l'expansió d'una monocapa.

Bibliography

Abercrombie, M. and J. Heaysman (1953). "Observations on the social behaviour of cells in tissue culture. I. Speed of movement of chick heart fibroblasts in relation to their mutual contacts." Experimental cell research **5**(1): 111.

Adams, R. H. and K. Alitalo (2007). "Molecular regulation of angiogenesis and lymphangiogenesis." Nature Reviews Molecular Cell Biology **8**(6): 464-478.

Affolter, M. and E. Caussinus (2008). "Tracheal branching morphogenesis in Drosophila: new insights into cell behaviour and organ architecture." Development **135**(12): 2055-2064.

Alberts, B. (2002). Molecular Biology of the Cell, Garland Science.

Alexander, S., G. Koehl, M. Hirschberg, E. Geissler and P. Friedl (2008). "Dynamic imaging of cancer growth and invasion: a modified skin-fold chamber model." Histochemistry and Cell Biology **130**(6): 1147-1154.

Anon, E., X. Serra-Picamal, P. Hersen, N. C. Gauthier, M. P. Sheetz, X. Trepat and B. Ladoux (2012). "Cell crawling mediates collective cell migration to close undamaged epithelial gaps." Proceedings of the National Academy of Sciences **109**(27): 10891-10896.

Arboleda-Estudillo, Y., M. Krieg, J. Stühmer r, N. A. Licata, D. J. Muller and C. P. Heisenberg (2010). "Movement directionality in collective migration of germ layer progenitors." Current Biology **20**(2): 161-169.

Arnaout, M., B. Mahalingam and J. P. Xiong (2005). "Integrin structure, allostery, and bidirectional signaling." Annu. Rev. Cell Dev. Biol. **21**: 381-410.

Ballestrem, C., B. Hinz, B. A. Imhof and B. Wehrle-Haller (2001). "Marching at the front and dragging behind." The Journal of cell biology **155**(7): 1319-1332.

Bass-Zubek, A. E., L. M. Godsel, M. Delmar and K. J. Green (2009). "Plakophilins: multifunctional scaffolds for adhesion and signaling." Current Opinion in Cell Biology **21**(5): 708-716.

Beningo, K. A. and Y. L. Wang (2002). "Flexible substrata for the detection of cellular traction forces." Trends in cell biology **12**(2): 79-84.

Burton, K., J. H. Park and D. L. Taylor (1999). "Keratocytes generate traction forces in two phases." Molecular biology of the cell **10**(11): 3745-3769.

Butler, J. P., I. M. Tolić-Nørrelykke, B. Fabry and J. J. Fredberg (2002). "Traction fields, moments, and strain energy that cells exert on their surroundings." American journal of physiology-cell physiology **282**(3): C595-C605.

Campbell, I. D. and M. J. Humphries (2011). "Integrin structure, activation, and interactions." Cold Spring Harbor perspectives in biology **3**(3).

Carey, S. P., J. M. Charest and C. A. Reinhart-King (2011). "Forces during cell adhesion and spreading: Implications for cellular homeostasis." Stud Mechanobiol Tissue Eng Biomater **4**: 29-69.

Carmona-Fontaine, C., H. K. Matthews, S. Kuriyama, M. Moreno, G. A. Dunn, M. Parsons, C. D. Stern and R. Mayor (2008). "Contact inhibition of locomotion in vivo controls neural crest directional migration." Nature **456**(7224): 957-961.

Chan, C. E. and D. J. Odde (2008). "Traction Dynamics of Filopodia on Compliant Substrates." Science **322**(5908): 1687-1691.

Choi, C. K., M. Vicente-Manzanares, J. Zareno, L. A. Whitmore, A. Mogilner and A. R. Horwitz (2008). "Actin and α $\pm$-actinin orchestrate the assembly and maturation of nascent adhesions in a myosin II motor-independent manner." Nature cell biology **10**(9): 1039-1050.

Das, T., T. K. Maiti and S. Chakraborty (2008). "Traction force microscopy on-chip: shear deformation of fibroblast cells." Lab on a Chip **8**(8): 1308-1318.

del Rio, A., R. Perez-Jimenez, R. Liu, P. Roca-Cusachs, J. M. Fernandez and M. P. Sheetz (2009). "Stretching single talin rod molecules activates vinculin binding." Science **323**(5914): 638.

Delanoë-Ayari, H., J. P. Rieu and M. Sano (2010). "4D Traction Force Microscopy Reveals Asymmetric Cortical Forces in Migrating Dictyostelium Cells." Physical Review Letters **105**(24): 248103.

Dembo, M. and Y.-L. Wang (1999). "Stresses at the Cell-to-Substrate Interface during Locomotion of Fibroblasts." Biophysical Journal **76**(4): 2307-2316.

Desai, A. and T. J. Mitchison (1997). "Microtubule polymerization dynamics." Annual Review of Cell and Developmental Biology **13**(1): 83-117.

Dianqing, W. (2005). "Signaling mechanisms for regulation of chemotaxis." Cell research **15**(1): 52-56.

Drees, F., S. Pokutta, S. Yamada, W. J. Nelson and W. I. Weis (2005). " α -Catenin Is a Molecular Switch that Binds E-Cadherin- β -Catenin and Regulates Actin-Filament Assembly." Cell **123**(5): 903-915.

Druckenbrod, N. R. and M. L. Epstein (2005). "The pattern of neural crest advance in the cecum and colon." Developmental Biology **287**(1): 125-133.

Du Roure, O., A. Saez, A. Buguin, R. H. Austin, P. Chavrier, P. Siberzan and B. Ladoux (2005). "Force mapping in epithelial cell migration." Proceedings of the National Academy of Sciences of the United States of America **102**(7): 2390.

DuFort, C. C., M. J. Paszek and V. M. Weaver (2011). "Balancing forces: architectural control of mechanotransduction." Nature Reviews Molecular Cell Biology **12**(5): 308-319.

Eisenbach, M. and J. W. Lengeler (2004). Chemotaxis, Imperial College Press.

Engler, A., L. Bacakova, C. Newman, A. Hategan, M. Griffin and D. Discher (2004). "Substrate compliance versus ligand density in cell on gel responses." Biophysical Journal **86**(1): 617-628.

Engler, A. J., S. Sen, H. L. Sweeney and D. E. Discher (2006). "Matrix elasticity directs stem cell lineage specification." Cell **126**(4): 677-689.

Farooqui, R. and G. Fenteany (2005). "Multiple rows of cells behind an epithelial wound edge extend cryptic lamellipodia to collectively drive cell-sheet movement." Journal of Cell Science **118**(1): 51-63.

Fernandez, P., M. Maier, M. Lindauer, C. Kuffer, Z. Storchova and A. R. Bausch (2011). "Mitotic Spindle Orients Perpendicular to the Forces Imposed by Dynamic Shear." PLoS One **6**(12): e28965.

Fink, J., N. Carpi, T. Betz, A. Bétard, M. Chebah, A. Azioune, M. Bornens, C. Sykes, L. Fetler and D. Cuvelier (2011b). "External forces control mitotic spindle positioning." Nature cell biology **13**(7): 771-778.

Follonier, L., S. b. Schaub, J.-J. Meister and B. Hinz (2008). "Myofibroblast communication is controlled by intercellular mechanical coupling." Journal of Cell Science **121**(20): 3305-3316.

Fournier, M. F., R. Sauser, D. Ambrosi, J.-J. Meister and A. B. Verkhovsky (2010). "Force transmission in migrating cells." The Journal of cell biology **188**(2): 287-297.

Friedl, P. and D. Gilmour (2009). "Collective cell migration in morphogenesis, regeneration and cancer." Nature Reviews Molecular Cell Biology **10**(7): 445-457.

Friedl, P., Y. Hegerfeldt and M. Tusch (2004). "Collective cell migration in morphogenesis and cancer." International Journal of Developmental Biology **48**: 441-450.

Fudge, D., D. Russell, D. Beriault, W. Moore, E. B. Lane and A. W. Vogl (2008). "The intermediate filament network in cultured human keratinocytes is remarkably extensible and resilient." PLoS One **3**(6): e2327.

Gaggioli, C., S. Hooper, C. Hidalgo-Carcedo, R. Grosse, J. F. Marshall, K. Harrington and E. Sahai (2007). "Fibroblast-led collective invasion of carcinoma cells with differing roles for RhoGTPases in leading and following cells." Nature cell biology **9**(12): 1392-1400.

Gardel, M. L., I. C. Schneider, Y. Aratyn-Schaus and C. M. Waterman (2010). "Mechanical integration of actin and adhesion dynamics in cell migration." Annual Review of Cell and Developmental Biology **26**: 315-333.

Giannone, G. g., R.-M. Mège and O. Thoumine (2009). "Multi-level molecular clutches in motile cell processes." Trends in cell biology **19**(9): 475-486.

Gillies, T. E. and C. Cabernard (2011). "Cell Division Orientation in Animals." Current Biology **21**(15): R599-R609.

Green, K. J., S. Getsios, S. Troyanovsky and L. Godsel (2010). "Intercellular junction assembly, dynamics, and homeostasis." Cold Spring Harbor perspectives in biology **2**(2).

Haas, P. and D. Gilmour (2006). "Chemokine Signaling Mediates Self-Organizing Tissue Migration in the Zebrafish Lateral Line." Developmental cell **10**(5): 673-680.

Han, B., X. H. Bai, M. Lodyga, J. Xu, B. B. Yang, S. Keshavjee, M. Post and M. Liu (2004). "Conversion of mechanical force into biochemical signaling." Journal of Biological Chemistry **279**(52): 54793.

Harris, A. K., D. Stopak and P. Wild (1981). "Fibroblast traction as a mechanism for collagen morphogenesis."

Harris, A. K., P. Wild and D. Stopak (1980). "Silicone rubber substrata: a new wrinkle in the study of cell locomotion." Science **208**(4440): 177-179.

Hegerfeldt, Y., M. Tusch, E.-B. Bröcker and P. Friedl (2002). "Collective Cell Movement in Primary Melanoma Explants: Plasticity of Cell-Cell Interaction, β 1-Integrin Function, and Migration Strategies." Cancer Research **62**(7): 2125-2130.

Herrmann, H., H. Bär, L. Kreplak, S. V. Strelkov and U. Aebi (2007). "Intermediate filaments: from cell architecture to nanomechanics." Nature Reviews Molecular Cell Biology **8**(7): 562-573.

Hur, S. S., Y. Zhao, Y. S. Li, E. Botvinick and S. Chien (2009). "Live cells exert 3-dimensional traction forces on their substrata." Cellular and molecular bioengineering **2**(3): 425-436.

Indra, I., V. Undyala, C. Kandow, U. Thirumurthi, M. Dembo and K. A. Beningo (2011). "An in vitro correlation of mechanical forces and metastatic capacity." Physical Biology **8**(1): 015015.

Isenberg, B. C., P. A. DiMilla, M. Walker, S. Kim and J. Y. Wong (2009). "Vascular smooth muscle cell durotaxis depends on substrate stiffness gradient strength." Biophysical Journal **97**(5): 1313-1322.

Kaksonen, M., C. P. Toret and D. G. Drubin (2006). "Harnessing actin dynamics for clathrin-mediated endocytosis." Nature Reviews Molecular Cell Biology **7**(6): 404-414.

Kaltschmidt, J. A., N. Lawrence, V. Morel, T. Balayo, B. G. Fernández, A. Pelissier, A. Jacinto and A. Martinez Arias (2002). "Planar polarity and actin dynamics in the epidermis of Drosophila." Nature cell biology **4**(12): 937-944.

Kalluri, R. and R. A. Weinberg (2009). "The basics of epithelial-mesenchymal transition." The Journal of clinical investigation **119**(6): 1420.

Kandow, C. E., P. C. Georges, P. A. Janmey and K. A. Beningo (2007). Polyacrylamide Hydrogels for Cell Mechanics: Steps Toward Optimization and Alternative Uses. Methods in Cell Biology. W. Yu-Li and E. D. Dennis, Academic Press. **Volume 83:** 29-46.

Kawakami, T., K. Nabeshima, M. Hamasaki, A. Iwasaki, T. Shirakusa and H. Iwasaki (2009). "Small cluster invasion: a possible link between micropapillary pattern and lymph node metastasis in pT1 lung adenocarcinomas." Virchows Archiv **454**(1): 61-70.

Kirfel, G., A. Rigort, B. Borm and V. Herzog (2004). "Cell migration: mechanisms of rear detachment and the formation of migration tracks." European Journal of Cell Biology **83**(11-12): 717-724.

Kraning-Rush, C. M., J. P. Califano and C. A. Reinhart-King (2012). "Cellular Traction Stresses Increase with Increasing Metastatic Potential." PLoS One **7**(2): e32572.

Kraynov, V. S., C. Chamberlain, G. M. Bokoch, M. A. Schwartz, S. Slabaugh and K. M. Hahn (2000). "Localized Rac activation dynamics visualized in living cells." Science Signalling **290**(5490): 333.

Kreplak, L., H. Bär, J. Leterrier, H. Herrmann and U. Aebi (2005). "Exploring the mechanical behavior of single intermediate filaments." Journal of molecular biology **354**(3): 569-577.

Lämmermann, T., B. L. Bader, S. J. Monkley, T. Worbs, R. Wedlich-Söldner, K. Hirsch, M. Keller, R. Förster, D. R. Critchley, R. Fässler and S. M. (2008). "Rapid leukocyte migration by integrin-independent flowing and squeezing." Nature **453**(7191): 51-55.

Larsen, M., C. Wei and K. M. Yamada (2006). "Cell and fibronectin dynamics during branching morphogenesis." Journal of Cell Science **119**(16): 3376-3384.

le Digabel, J., N. Biais, J. Fresnais, J.-F. Berret, P. Hersen and B. Ladoux (2011). "Magnetic micropillars as a tool to govern substrate deformations." Lab on a Chip **11**(15): 2630-2636.

le Duc, Q., Q. Shi, I. Blonk, A. Sonnenberg, N. Wang, D. Leckband and J. de Rooij (2010). "Vinculin potentiates E-cadherin mechanosensing and is recruited to actin-anchored sites within adherens junctions in a myosin II,Äìdependent manner." The Journal of cell biology **189**(7): 1107-1115.

Leckband, D. E., Q. le Duc, N. Wang and J. de Rooij (2011). "Mechanotransduction at cadherin-mediated adhesions." Current Opinion in Cell Biology **23**(5): 523-530.

Li, B., F. Li, K. M. Puskar and J. H. C. Wang (2009). "Spatial patterning of cell proliferation and differentiation depends on mechanical stress magnitude." Journal of Biomechanics **42**(11): 1622-1627.

Li, B., M. Lin, Y. Tang, B. Wang and J. H. C. Wang (2008). "A novel functional assessment of the differentiation of micropatterned muscle cells." Journal of Biomechanics **41**(16): 3349-3353.

Lin, X. and B. P. Helmke (2008). "Micropatterned structural control suppresses mechanotaxis of endothelial cells." Biophysical Journal **95**(6): 3066-3078.

Liu, M., Y. Qin, J. Liu, A. K. Tanswell and M. Post (1996). "Mechanical Strain Induces pp60 Activation and Translocation to Cytoskeleton in Fetal Rat Lung Cells." Journal of Biological Chemistry **271**(12): 7066-7071.

Liu, Z., J. L. Tan, D. M. Cohen, M. T. Yang, N. J. Sniadecki, S. A. Ruiz, C. M. Nelson and C. S. Chen (2010). "Mechanical tugging force regulates the size of cell-cell junctions." Proceedings of the National Academy of Sciences **107**(22): 9944-9949.

Lo, C. M., H. B. Wang, M. Dembo and Y. Wang (2000). "Cell movement is guided by the rigidity of the substrate." Biophysical Journal **79**(1): 144-152.

Lodish, H., A. Berk, C. A. Kaiser, M. Krieger, M. P. Scott, A. Bretscher, H. Ploegh and P. Matsudaira (2007). Molecular Cell Biology, W. H. Freeman.

Luo, B. H., C. V. Carman and T. A. Springer (2007). "Structural basis of integrin regulation and signaling." Annual review of immunology **25**: 619.

Machacek, M., L. Hodgson, C. Welch, H. Elliott, O. Pertz, P. Nalbant, A. Abell, G. L. Johnson, K. M. Hahn and G. Danuser (2009). "Coordination of Rho GTPase activities during cell protrusion." Nature **461**(7260): 99-103.

Martin, A. C., M. Gelbart, R. Fernandez-Gonzalez, M. Kaschube and E. F. Wieschaus (2010). "Integration of contractile forces during tissue invagination." The Journal of cell biology **188**(5): 735-749.

Maskarinec, S. A., C. Franck, D. A. Tirrell and G. Ravichandran (2009). "Quantifying cellular traction forces in three dimensions." Proceedings of the National Academy of Sciences **106**(52): 22108-22113.

Matsubayashi, Y., M. Ebisuya, S. Honjoh and E. Nishida (2004). "ERK activation propagates in epithelial cell sheets and regulates their migration during wound healing." Current Biology **14**(8): 731-735.

Matsubayashi, Y., W. Razzell and P. Martin (2011). "'White wave' analysis of epithelial scratch wound healing reveals how cells mobilise back from the leading edge in a myosin-II-dependent fashion." Journal of Cell Science **124**(7): 1017-1021.

Mayor, R. and C. Carmona-Fontaine (2010). "Keeping in touch with contact inhibition of locomotion." Trends in cell biology **20**(6): 319-328.

Mofrad, M. R. K. and R. D. Kamm (2006). Cytoskeletal Mechanics - Models and Measurements, Cambridge University Press.

Montell, D. J., W. H. Yoon and M. Starz-Gaiano (2012). "Group choreography: mechanisms orchestrating the collective movement of border cells." Nature Reviews Molecular Cell Biology **13**(10): 631-645.

Munevar, S., Y. Wang and M. Dembo (2001). "Traction force microscopy of migrating normal and H-ras transformed 3T3 fibroblasts." Biophysical Journal **80**(4): 1744-1757.

Nabeshima, K., T. Inoue, Y. Shimao, H. Kataoka and M. Koono (1999). "Cohort migration of carcinoma cells: differentiated colorectal carcinoma cells move as coherent cell clusters or sheets." Histology and histopathology **14**(4): 1183.

Nalbant, P., L. Hodgson, V. Kraynov, A. Toutchkine and K. M. Hahn (2004). "Activation of endogenous Cdc42 visualized in living cells." Science **305**(5690): 1615-1619.

Nemethova, M., S. Auinger and J. V. Small (2008). "Building the actin cytoskeleton: filopodia contribute to the construction of contractile bundles in the lamella." The Journal of cell biology **180**(6): 1233-1244.

Ng, M. R., A. Besser, G. Danuser and J. S. Brugge (2012). "Substrate stiffness regulates cadherin-dependent collective migration through myosin-II contractility." The Journal of cell biology **199**(3): 545-563.

Nikolic, D. L., A. N. Boettiger, D. Bar-Sagi, J. D. Carbeck and S. Y. Shvartsman (2006). "Role of boundary conditions in an experimental model of epithelial wound healing." American journal of physiology-cell physiology **291**(1): C68-C75.

Ninov, N., S. Menezes-Cabral, C. Prat-Rojo, C. Manjón, A. Weiss, G. Pyrowolakis, M. Affolter and E. Martín-Blanco (2010). "Dpp Signaling Directs Cell Motility and Invasiveness during Epithelial Morphogenesis." Current Biology **20**(6): 513-520.

Pelham, R. J. and Y. Wang (1997). "Cell locomotion and focal adhesions are regulated by substrate flexibility." Proceedings of the National Academy of Sciences **94**(25): 13661.

Pellegrin, S. p. and H. Mellor (2007). "Actin stress fibres." Journal of Cell Science **120**(20): 3491-3499.

Pertz, O., L. Hodgson, R. L. Klemke and K. M. Hahn (2006). "Spatiotemporal dynamics of RhoA activity in migrating cells." Nature **440**(7087): 1069-1072.

Polio, S. R., K. E. Rothenberg, D. Stamenović and M. L. Smith (2012). "A micropatterning and image processing approach to simplify measurement of cellular traction forces." Acta biomaterialia **8**(1): 82-88.

Pollard, T. D. (2003). "The cytoskeleton, cellular motility and the reductionist agenda." Nature **422**(6933): 741-745.

Pollard, T. D., L. Blanchoin and R. D. Mullins (2000). "Molecular mechanisms controlling actin filament dynamics in nonmuscle cells." Annual review of biophysics and biomolecular structure **29**(1): 545-576.

Pollard, T. D. and G. G. Borisy (2003). "Cellular Motility Driven by Assembly and Disassembly of Actin Filaments." Cell **112**(4): 453-465.

Poujade, M., E. Grasland-Mongrain, A. Hertzog, J. Jouanneau, P. Chavrier, B. Ladoux, A. Buguin and P. Silberzan (2007). "Collective migration of an epithelial monolayer in response to a model wound." Proceedings of the National Academy of Sciences **104**(41): 15988-15993.

Revenu, C. and D. Gilmour (2009). "EMT 2.0: shaping epithelia through collective migration." Current opinion in genetics & development **19**(4): 338-342.

Ridley, A. J., M. A. Schwartz, K. Burridge, R. A. Firtel, M. H. Ginsberg, G. Borisy, J. T. Parsons and A. R. Horwitz (2003). "Cell migration: integrating signals from front to back." Science **302**(5651): 1704-1709.

Riveline, D., E. Zamir, N. Q. Balaban, U. S. Schwarz, T. Ishizaki, S. Narumiya, Z. Kam, B. Geiger and A. D. Bershadsky (2001). "Focal Contacts as Mechanosensors: Externally Applied Local Mechanical Force Induces Growth of Focal Contacts by an Mdia1-Dependent and Rock-Independent Mechanism." The Journal of cell biology **153**(6): 1175-1186.

Rørth, P. (2009). "Collective cell migration." Annual Review of Cell and Developmental **25**: 407-429.

Sabass, B., M. L. Gardel, C. M. Waterman and U. S. Schwarz (2008). "High Resolution Traction Force Microscopy Based on Experimental and Computational Advances." Biophysical Journal **94**(1): 207-220.

Saez, A., E. Anon, M. Ghibaudo, O. Du Roure, J. Di Meglio, P. Hersen, P. Silberzan, A. Buguin and B. Ladoux (2010). "Traction forces exerted by epithelial cell sheets." Journal of Physics: Condensed Matter **22**: 194119.

Sahai, E. (2005). "Mechanisms of cancer cell invasion." Current opinion in genetics & development **15**(1): 87-96.

Serra-Picamal, X. and X. Trepat (2011). "Nanotecnologías para el estudio de la migración celular." SEBBM(168): 14-17.

Shakya, R., T. Watanabe and F. Costantini (2005). "The role of GDNF/Ret signaling in ureteric bud cell fate and branching morphogenesis." Developmental cell **8**(1): 65-74.

Simpson, K. J., L. M. Selfors, J. Bui, A. Reynolds, D. Leake, A. Khvorova and J. S. Brugge (2008). "Identification of genes that regulate epithelial cell migration using an siRNA screening approach." Nature cell biology **10**(9): 1027-1038.

Simske, J. S. and J. Hardin (2000). "Getting into shape: epidermal morphogenesis in Caenorhabditis elegans embryos." Bioessays **23**(1): 12-23.

Sniadecki, N. J., A. Anguelouch, M. T. Yang, C. M. Lamb, Z. Liu, S. B. Kirschner, Y. Liu, D. H. Reich and C. S. Chen (2007). "Magnetic microposts as an approach to apply forces to living cells." Proceedings of the National Academy of Sciences **104**(37): 14553-14558.

Solon, J., A. Kaya-Copur, J. Colombelli and D. Brunner (2009). "Pulsed forces timed by a ratchet-like mechanism drive directed tissue movement during dorsal closure." Cell **137**(7): 1331-1342.

Tamada, M., T. D. Perez, W. J. Nelson and M. P. Sheetz (2007). "Two distinct modes of myosin assembly and dynamics during epithelial wound closure." The Journal of cell biology **176**(1): 27-33.

Tambe, D. T., C. C. Hardin, T. E. Angelini, K. Rajendran, C. Y. Park, X. Serra-Picamal, E. H. Zhou, M. H. Zaman, J. P. Butler and D. A. Weitz (2011). "Collective cell guidance by cooperative intercellular forces." Nature materials **10**(6): 469-475.

Tan, J. L., J. Tien, D. M. Pirone, D. S. Gray, K. Bhadriraju and C. S. Chen (2003). "Cells lying on a bed of microneedles: an approach to isolate mechanical force." Proceedings of the National Academy of Sciences **100**(4): 1484-1489.

Theveneau, E., L. Marchant, S. Kuriyama, M. Gull, B. Moepps, M. Parsons and R. Mayor (2010). "Collective chemotaxis requires contact-dependent cell polarity." Developmental cell **19**(1): 39-53.

Theveneau, E. and R. Mayor (2011). "Collective cell migration of the cephalic neural crest: The art of integrating information." Genesis **49**(4): 164-176.

Trepat, X., Z. Chen and K. Jacobson (2012). "Cell Migration." Comprehensive Physiology.

Trepat, X., M. R. Wasserman, T. E. Angelini, E. Millet, D. A. Weitz, J. P. Butler and J. J. Fredberg (2009). "Physical forces during collective cell migration." Nature physics **5**(6): 426-430.

Trichet, L., J. Le Digabel, R. J. Hawkins, S. R. K. Vedula, M. Gupta, C. Ribrault, P. Hersen, R. Voituriez and B. Ladoux (2012). "Evidence of a large-scale

mechanosensing mechanism for cellular adaptation to substrate stiffness." Proceedings of the National Academy of Sciences **109**(18): 6933-6938.

Van Haastert, P. J. M. and P. N. Devreotes (2004). "Chemotaxis: signalling the way forward." Nature Reviews Molecular Cell Biology **5**(8): 626-634.

Vicente-Manzanares, M., J. Zareno, L. Whitmore, C. K. Choi and A. F. Horwitz (2007). "Regulation of protrusion, adhesion dynamics, and polarity by myosins IIA and IIB in migrating cells." The Journal of cell biology **176**(5): 573-580.

Vitorino, P. and T. Meyer (2008). "Modular control of endothelial sheet migration." Science Signalling **22**(23): 3268.

Vogel, V. and M. Sheetz (2006). "Local force and geometry sensing regulate cell functions." Nature Reviews Molecular Cell Biology **7**(4): 265-275.

Vorotnikov, A. (2011). "Chemotaxis: Movement, direction, control." Biochemistry (Moscow) **76**(13): 1528-1555.

Wang, J. and B. Li (2009). "Application of cell traction force microscopy for cell biology research." Methods in molecular biology (Clifton, NJ) **586**: 301-313.

Wang, J. H. C. and B. Li (2010). "The principles and biological applications of cell traction force microscopy."

Wang, J. H. C. and J. S. Lin (2007). "Cell traction force and measurement methods." Biomechanics and modeling in mechanobiology **6**(6): 361-371.

Wang, N., E. Ostuni, G. M. Whitesides and D. E. Ingber (2002). "Micropatterning tractional forces in living cells." Cell motility and the cytoskeleton **52**(2): 97-106.

Wang, Y., E. L. Botvinick, Y. Zhao, M. W. Berns, S. Usami, R. Y. Tsien and S. Chien (2005). "Visualizing the mechanical activation of Src." Nature **434**(7036): 1040-1045.

Weber, G. F., M. A. Bjerke and D. W. DeSimone (2012). "A Mechanoresponsive Cadherin-Keratin Complex Directs Polarized Protrusive Behavior and Collective Cell Migration." Developmental cell **22**(1): 104-115.

Wojciak-Stothard, B. (2011). "Endothelial cell migration under flow." Methods in molecular biology (Clifton, NJ) **769**: 137.

Wolf, K., I. Mazo, H. Leung, K. Engelke, U. H. Von Andrian, E. I. Deryugina, A. Y. Strongin, B. E.B. and P. Friedl (2003). "Compensation mechanism in tumor cell migration mesenchymal-amoeboid transition after blocking of pericellular proteolysis." The Journal of cell biology **160**(2): 267-277.

Worthylake, R. A., S. Lemoine, J. M. Watson and K. Burridge (2001). "RhoA is required for monocyte tail retraction during transendothelial migration." The Journal of cell biology **154**(1): 147-160.

Wu, Y. I., D. Frey, O. I. Lungu, A. Jaehrig, I. Schlichting, B. Kuhlman and K. M. Hahn (2009). "A genetically encoded photoactivatable Rac controls the motility of living cells." Nature **461**(7260): 104-108.

Yamada, S., S. Pokutta, F. Drees, W. I. Weis and W. J. Nelson (2005). "Deconstructing the Cadherin-Catenin-Actin Complex." Cell **123**(5): 889-901.

Yamamoto, E., G.-I. Kohama, H. Sunakawa, M. Iwai and H. Hiratsuka (1983). "Mode of invasion, bleomycin sensitivity, and clinical course in squamous cell carcinoma of the oral cavity." Cancer **51**(12): 2175-2180.

Yang, Z., J. S. Lin, J. Chen and J. H. C. Wang (2006). "Determining substrate displacement and cell traction fields,Äîa new approach." Journal of theoretical biology **242**(3): 607-616.

Yonemura, S., Y. Wada, T. Watanabe, A. Nagafuchi and M. Shibata (2010). "α-Catenin as a tension transducer that induces adherens junction development." Nat Cell Biol **12**(6): 533-542.